Progress in Materials Science 92 (2018) 64–111

Contents lists available at ScienceDirect

Progress in Materials Science

journal homepage: www.elsevier.com/locate/pmatsci

Advanced catalysts for sustainable hydrogen generation and storage via hydrogen evolution and carbon dioxide/nitrogen reduction reactions

Kai-Hua Liu [a,1], Hai-Xia Zhong [b,1], Si-Jia Li [a], Yan-Xin Duan [a], Miao-Miao Shi [a], Xin-Bo Zhang [b], Jun-Min Yan [a,*], Qing Jiang [a]

[a] Key Laboratory of Automobile Materials (Jilin University), Ministry of Education, Department of Materials Science and Engineering, Jilin University, Changchun 130022, China

[b] State Key Laboratory of Rare Earth Resource Utilization, Changchun Institute of Applied Chemistry, Chinese Academy of Sciences, Changchun 130022, China

ARTICLE INFO

Article history:
Received 29 January 2017
Received in revised form 5 September 2017
Accepted 6 September 2017
Available online 13 October 2017

Keywords:
Hydrogen evolution
Carbon dioxide reduction
Nitrogen reduction
Electrocatalysts
Nanostructures

ABSTRACT

Accompanied by continuous increasing energy crisis and CO_2-induced global warming, constructing renewable energy system becomes one of the major scientific challenges. Thereinto, electrocatalysis plays a critical role in clean energy conversion, enabling a series of sustainable chemistries and processes for future technologies. Herein, we mainly discuss recent advances of heterogeneous electrocatalysts for hydrogen production and storage via several clean energy reactions such as hydrogen evolution, carbon dioxide and nitrogen reduction. Emphasis is given to the structure/composition–catalytic activity relationship and strategies of performance improvement. Certainly, several challenges and research directions toward these reactions are also discussed. The comprehensive review might provide guidance to design robust electrocatalysts that allow for the sustainable production of fuels and chemicals.

Contents

1. Introduction . . . 65
2. Catalysts for HER . . . 66
   2.1. Fundament for HER . . . 66
   2.2. Catalysts based on Pt . . . 68
      2.2.1. Construct alloy or core-shell structure . . . 69
      2.2.2. Choose special supports . . . 70
   2.3. Catalysts based on Mo and W . . . 72
      2.3.1. Zero/one-dimension nanostructure . . . 72
      2.3.2. Two-dimension nanostructure . . . 77
      2.3.3. Three-dimension nanostructure . . . 81
   2.4. Catalysts based on Fe, Co and Ni . . . 83
      2.4.1. Catalysts based on Fe . . . 83

* Corresponding author.
E-mail address: junminyan@jlu.edu.cn (J.-M. Yan).

[1] These authors are contributed equally to this review article.

https://doi.org/10.1016/j.pmatsci.2017.09.001
0079-6425/

Nomenclature

Acronyms

ALD	atomic layer deposition
CC	carbon cloth
CNTs	carbon nanotubes
CVD	chemical vapor deposition
CP	carbon paper
CV	cyclic voltammetry
DFT	density functional theory
FE	faradaic efficiency
HBE	hydrogen bonding energy
HER	hydrogen evolution reaction
MCVs	mesoporous carbon vesicles
MOF	metal organic frameworks
MPC	macroporous carbon
OER	oxygen evolution reaction
OMC	ordered mesoporous carbon
rGO	reduced graphene oxide
RHE	reversible hydrogen electrode
STM	scanning tunneling microscopy
STS	scanning tunneling spectroscopy
TMCs	transition metal carbides
TMDs	transition metal dichalcogenides
TOF	turnover frequency
XANES	X-ray absorption near-edge structure
XAS	X-ray absorption spectroscopy
0/1D	zero/one-dimension
2D	two-dimension
3D	three-dimension

Symbols

b	Tafel slope
ΔG_{H*}	Gibbs free energy for hydrogen adsorption
j_0	exchange current density
η	overpotential
η_{10}	current density of 10 mA cm^{-2}

2.4.2. Catalysts based on Co . . . 84
2.4.3. Catalysts based on Ni . . . 87
2.4.4. Compounds of Fe, Co and Ni . . . 88
2.5. Metal free catalysts based on carbon . . . 90
3. Heterogeneous catalytic decomposition of HCOOH . . . 92
4. Electrochemical CO_2 reduction to HCOOH . . . 94
4.1. Catalysts based on Sn . . . 94
4.2. Catalysts based on Co . . . 96
4.3. Catalysts based on other metals . . . 97
4.4. Catalysts based on carbon-based materials . . . 98
5. Electrochemical N_2 reduction to NH_3 . . . 98
6. Summary and outlook . . . 99
Acknowledgements . . . 100
References . . . 100

1. Introduction

Under the current background of increasing global energy demand and serious environmental issues connected with burning fossil fuels, exploiting new energy supply based on low-carbon and renewable resource is particularly significant

for the sustainable society [1–6]. Hydrogen (H_2), as a clean energy carrier, holds great promise for addressing the above issues and opening new avenue for future carbon-free energy economy by virtue of its highest energy density per unit mass and the pollution-free by-product of only water [7–9]. However, effective production and storage of H_2 are still the particular challenges of hydrogen economy. Today, among the main H_2 production pathways, producing H_2 from electricity-driven splitting of water via the hydrogen evolution reaction (HER), preferably coupled with renewable energy resources (wind or solar energy) can be more coinciding with long term consideration for future sustainable energy supply [10–14]. While for the H_2 storage, besides the storage of H_2 as a compressed gas or cryogenic liquid or using hydrogen storage materials (e.g., metal hydrides), chemical storage materials, especially formic acid (HCOOH), have attracted major concerns due to their high hydrogen content and easy recharging as a liquid. Besides, ammonia (NH_3), containing 17.6% of hydrogen by mass, is also an ideal carrier for H_2 [15].

As earth's atmosphere can provide abundant feedstock of H_2O, CO_2, and N_2, which can potentially be converted into the aforementioned products via electrochemical processes driven by renewable energy resources (wind or solar energy). Once high-efficient electrocatalysts with the required properties are developed, the possible sustainable pathways for hydrogen economy can be fabricated (Scheme 1). For instance, the water electrolysis has been regarded as a sustainable source of H_2. CO_2 captured from the atmosphere or decomposition of HCOOH could become a feedstock for fuels or HCOOH via electrochemical reduction. Likewise, N_2 can also be carried out the similar cycle process. Although these electrochemical reactions have been put forward for a long time, the overall energy efficiency is still questionable for practical application which is likely attributed to the slow kinetics of the electrochemical reactions. Thus, the current implementation of these technologies on a large scale mainly hinges on seeking efficient catalysts to accelerate the reaction and thus improve the efficiency [16]. Thereinto, precious metals have exhibited the best catalytic performance than others for many electrochemical reactions, but their widespread application is greatly constrained by the scarcity and prohibited price, as well as the limited stability [17,18]. Therefore, the development of alternative electrocatalysts composed of low-cost and earth-abundant elements has nowadays attracted much more research interests [19–25].

Considering the rapid and new development of electrocatalysts for these thriving fields, a comprehensive review may help to compare different catalysts and guide the further scientific activities. In this review, we summarize the development of heterogeneous catalysts for these reactions. Emphasis is given to the structure/composition–catalytic activity relationship and strategies of performance improvement. Some important synthetic methods and strategies are also introduced, which may apply to prepare other high-efficiency catalysts. Finally, some challenges and research directions are also discussed.

2. Catalysts for HER

2.1. Fundament for HER

Generally, the HER undergoes multi-step electrochemical reaction process occurring at the surface of electrode. Overall, two different mechanisms with three possible reactions are widely accepted (Table 1). For instance, in acidic solution, both of the two mechanisms must proceed via the first step, which is the hydrogen adsorption step, well-known as Volmer reaction. In this step, an electron is transferred to the electrode surface to capture a proton and thus form the absorbed hydrogen atom. Subsequently, difference occurs at this step of generating hydrogen. For Volmer-Heyrovsky mechanism, the formation

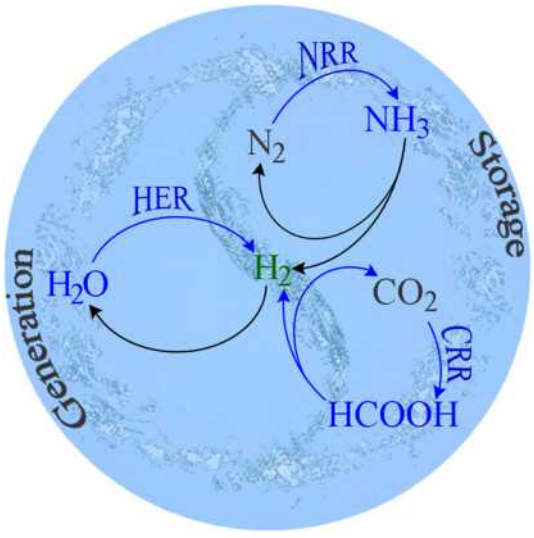

Scheme 1. Schematic illustration of possible sustainable pathways for hydrogen generation and storage.

Table 1
Reaction steps for HER in acidic and alkaline electrolytes.

Overall reaction	Reaction steps	Equations	Tafel slope (mV dec^{-1})
$2H^+ + 2e^- \rightarrow H_2$ (Acidic solution)	Volmer	$H^+ + e^- + * \rightarrow H^*$	b = 2.3RT/αF = 120
	Heyrovsky	$H^* + H^+ + e^- \rightarrow H_2$	b = 2.3RT/2 F = 30
	Tafel	$2H^* \rightarrow H_2$	b = 2.3RT/(1 + α)F = 40
$2H_2O + 2e^- \rightarrow H_2 + 2OH^-$ (Alkaline solution)	Volmer	$H_2O + e^- \rightarrow H^* + OH^-$	
	Heyrovsky	$H_2O + e^- + H^* \rightarrow H_2 + OH^-$	
	Tafel	$2H^* \rightarrow H_2$	

of hydrogen is through the transfer of one electron to the absorbed hydrogen and thus couple of one proton. For Volmer-Tafel pathway, hydrogen evolution is via the combining of two absorbed hydrogen, wherein the electrode surface must possess proximal pair of hydrogen absorbed atom sites.

To estimate the HER activity of target electrocatalysts, some important parameters are required to be calculated, mainly including overpotential (η), Tafel slope and exchange current density (j_0), faradaic efficiency (FE), turnover frequency (TOF), stability as well as the hydrogen bonding energy (HBE). Firstly, hydrogen evolution can be started at 0 V vs. reversible hydrogen electrode (RHE) at the standard condition, but actually larger potential is needed to push HER at target electrode, wherein the excess potential compared to the theoretical one is overpotential. In most case, the overpotential to reach the current density of 10 mA cm^{-2} (η_{10}) is used to compare the catalytic activity of catalysts, which is the metric relevant to solar fuel synthesis. Then, the Tafel slope and exchange current density are two important kinetic parameters which can be obtained from Tafel equation ($\eta = b \log (j/j_0)$, where b is the Tafel slope. The possible rate-determining reaction mechanism of catalyst can be deduced by Tafel slope (Table 1) and the j_0 is correlated to the rate of electron transfer under equilibrium conditions. In brief, the efficient electrocatalyst usually possesses the low overpotential, small Tafel slope and high exchange current density during the HER process. As for FE, it is the ratio between the experimental and theoretical hydrogen production. Thereinto, the theoretical production can be calculated from galvanostatic or potentiostatic electrolysis and the practical production can be obtained by gas chromatography, and most of FE loss originates from the heat loss or formation of other products. Besides, the catalytic activity of individual active site can be implied by TOF, which is defined as that a catalyst can convert to a desired product per catalytic site per unit of time. However, it is difficult to garn precise TOF as the heterogeneously electrocatalytic reaction always occurs at the surface of electrode. Therefore, the concentration of the so-called surface metal ion is calculated and thus used to estimate the TOF of electrocatalyst [26,27], but this approach is suitable for the metallic based catalysts with obvious redox peaks in the electrolyte, such as Ni, Fe and Co. Considering from practical application, the stability is another critical parameter, which can be characterized by two simple electrochemical techniques: cyclic voltammetry (CV) and galvanostatic/potentiostatic electrolysis. Finally, ideal HER electrocatalysts should have moderate HBE as the strong hydrogen bonding may block the active sites and thus fail to release hydrogen, while the weak hydrogen bonding may fail to stabilize the intermediate and then prevent any reaction from further occurring. Thus, the Gibbs free energy for hydrogen adsorption (ΔG_{H*}) is a good descriptor of the intrinsic activity of a metal for HER, and a plot of j_0 against ΔG_{H*} was acquired and showed a volcano shape (Fig. 1) [28]. Obviously, Pt group metals which have the highest activity are located at the summit of the volcano, and close to zero hydrogen absorption energy.

There are many parameters to measure the HER activity of electrocatalysts. However, comparing the performance of different catalysts is complicated because of the various measurement conditions, such as deposited substrates, electrolyte

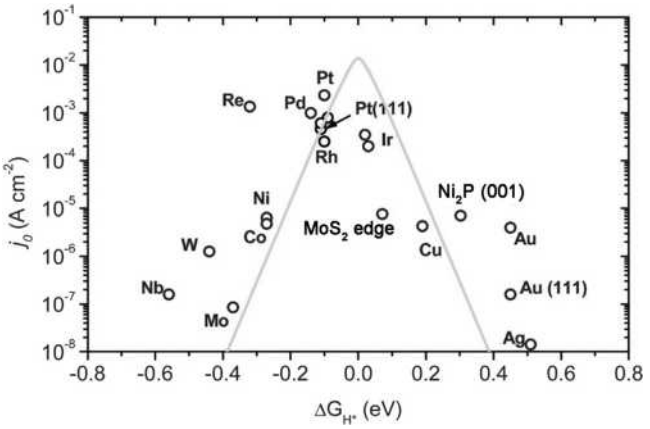

Fig. 1. A volcano plot of experimentally measured exchange current density (j_0) as a function of the DFT-calculated Gibbs free energy of adsorbed atomic hydrogen (ΔG_{H^*}).

compositions and concentrations as well as pH values. Thus, for well comparison of different catalysts, standard electrochemical tests are of great value. As a successful example, Jaramillo et al. proposed a benchmark study on HER electrocatalysts (Fig. 2), which may be greatly significant for the development of standard test techniques [29].

2.2. Catalysts based on Pt

As we all know, both theoretic and experiment researches show that precious metals, especially Pt, are the best electrocatalysts for HER. Apart from their apparent advantages, the obvious drawbacks including scarcity and prohibitive cost still plague on these precious metal catalysts, limiting their widespread commercial applications. Therefore, to reduce the usage of precious metals but keep or improve the high catalytic activity is highly essential to ensure the sustainable hydrogen production. Considering the fact that catalytic reaction occurs on the solid-liquid interface, so the most common methods are:

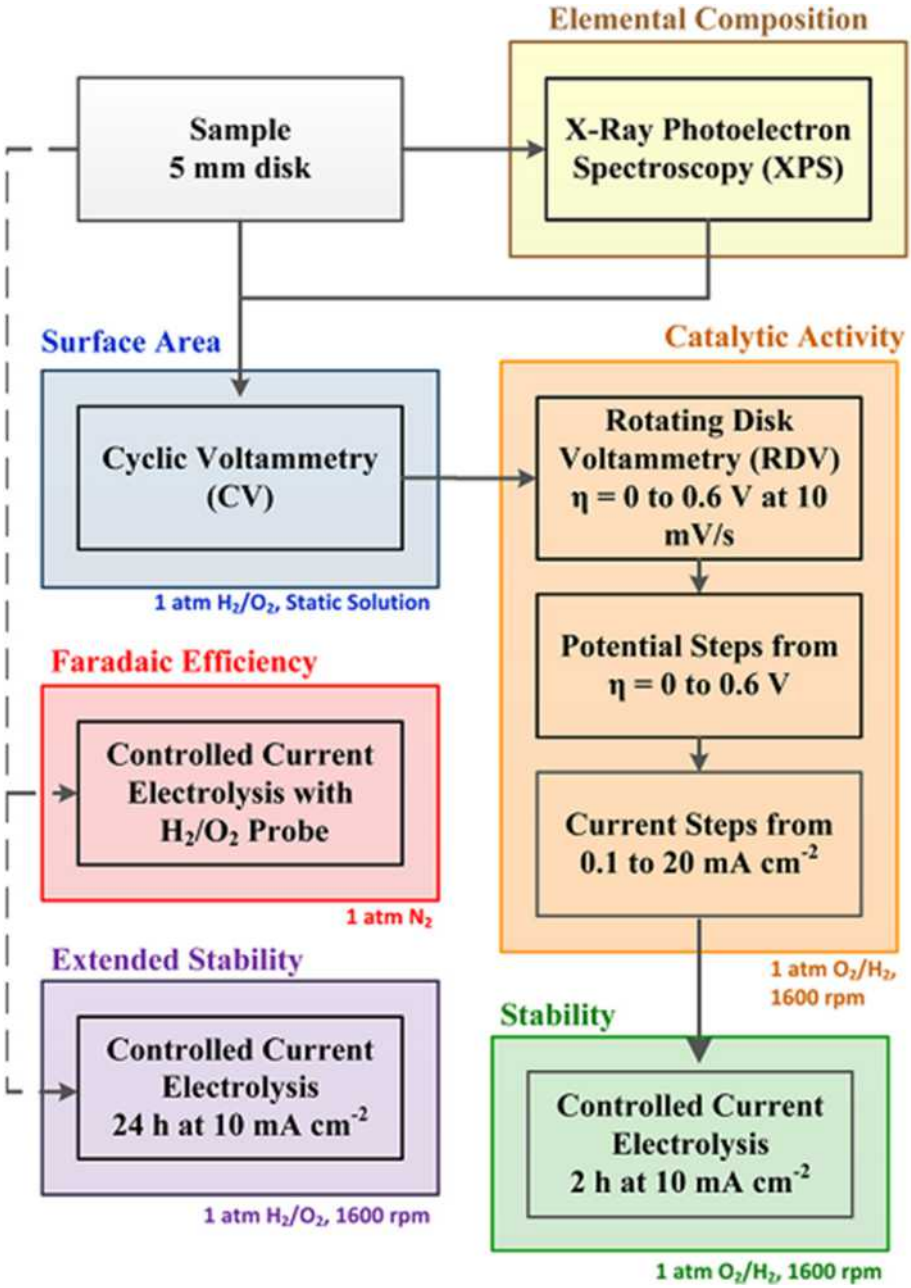

Fig. 2. Protocol for benchmarking the performance of heterogeneous electrocatalysts for HER.

(i) controlling the usage and exposing facet of Pt via forming alloy, core-shell and branch structure; (ii) loading nanostructure Pt on some building blocks with special structure or property. To this context, much work has been done to select and synthesize some promising substrates.

2.2.1. Construct alloy or core-shell structure

Achieving low-content Pt catalysts via alloying with other metals is an appealing and practical stratagem as which can not only copy the individual advanced properties of Pt and other metals, but also usually exhibit amazing catalytic performance because of their possible synergetic effect [30]. Therefore, many researchers have focused on fabricating Pt alloy catalysts with optimized structure to achieve high catalytic activity but with extreme low-content of Pt. Typically, the PtNiCu alloyed nanochains were synthesized, and exhibited excellent HER activity with a nearly negligible overpotential, a Tafel slope of 28 mV dec^{-1} and the 200 mA cm^{-2} at only overpotential of 75 mV, which was almost 5 times than the equivalent Pt mass of state-of-the-art Pt catalysts [31]. This high performance was mainly attributed to the nanochains structure to provide abundance of clean active facets on edge sites besides synergistic effect. To controllable synthesis alloy components, Xiong et al. synthesized the PtFeCo alloy nanostructures in a tristar shape (Fig. 3) [32]. Thanks to the optimization of electronic and surface structure, the tristar sample displayed remarkably higher activity than nanoparticles, and the 1325 mA cm^{-2} could be achieved just at potential of 400 mV. Meanwhile, it also exhibited excellent durability with negligible decay before and after 5000 CV cycles. Importantly, they provided a different perspective to improve the HER performance via tuning the d-band center and interatomic charge polarization.

Recently, alkaline electrolysis has received extensive attention because of its advantages, such as broad reactant availability and high product purity. However, the HER performance of Pt-based catalysts in alkaline solution is far away from that in acidic conditions. One strategy to improve the alkaline HER performance is integrating Pt nanostructures with the metal hydroxides as the edges of metal hydroxides contributes to the dissociation of water [33]. For example, ultrathin Pt nanowires on single-layered $Ni(OH)_2$ nanosheets were fabricated which exhibited 4–5 times higher HER activity than commercial Pt/C in alkaline solution [34]. The superior HER activity is ascribed to that the $Ni(OH)_2$ substrates can activate the HO—H bond and thus remedy the limited capability of Pt in water dissociation, and the ultrathin Pt nanowires may expose more active sites while retaining improved electrons transport. One issue in this method is that the lattice spacing of metal hydroxides is usually larger than that of Pt, which is unfavorable to form intimate interface between metal hydroxides and Pt, so the enhancement of HER activity is limit. Thus, the phase- and interface-engineered Pt–Ni nanowires catalysts were prepared [35]. Due to the presence of proper NiO_x/Pt_3Ni interfaces, this catalyst exhibited excellent activity with a low overpotential of 40 mV at 10 mA cm^{-2} in 1 M KOH and maintained its catalytic activity for 3 h with 10% activity loss. This study provides a surface and phase-engineering strategy to further optimize the catalysts. Besides, the hexapod-like ternary PtNiCo alloy nanostructures were synthesized. Similarly, the oxidation of Ni species facilitated the H–OH cleavage reaction and overall reaction kinetics, thus exhibiting 10 times greater specific activity than Pt/C [36].

Generally, one serious issue, that is the leaching of non-Pt metal in the electrolyte, particularly in the acid medium, plagues on Pt alloy catalysts, resulting in relatively low stability. In this context, the construction of core-shell structure is an attractive strategy to decrease the Pt usage but with high stability since the non-Pt core is protected by the thin-layer Pt. Note that only several outer layer Pt atom can be fully used in catalysis, further highlighting the superiority of core-shell structure in view of making most use of Pt atom. In the past decades, many active Pt core-shell catalysts have been successfully constructed [37–39]. Chen's group synthesized the Pt-WC core-shell catalyst by atomic layer deposition (ALD) [37], and after ten ALD cycles, the HER catalytic activity could be close to the Pt/C catalyst, wherein the amount of Pt were nearly ten

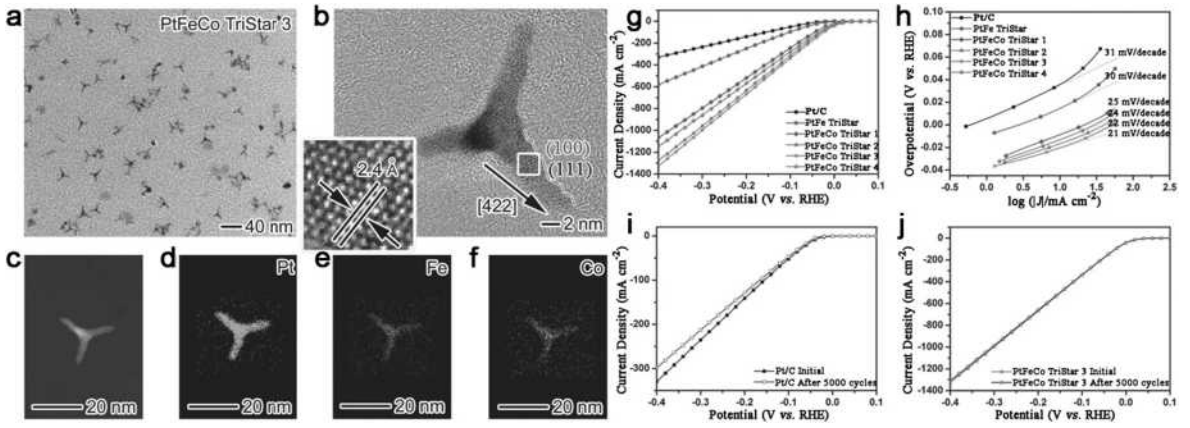

Fig. 3. (a) TEM and (b) HRTEM images of $Pt_{81}Fe_{28}Co_{10}$ nanostructures in a tristar shape. (c–f) STEM image and EDS mapping profiles of a single PtFeCo nanostructure showing the elemental Pt, Fe, and Co. (g) Polarization curves of samples. (h) Corresponding Tafel plots. Durability tests for (i) Pt/C and (j) PtFeCo tristar sample.

times less than bulk Pt catalyst to achieve the equivalent HER activity. Besides, the Cu-Pt core-shell nanowires were also fabricated and the obtained highest mass activities could reach up to eight times higher than Pt/C for HER at neutral electrolyte [38].

In addition to the above, the catalysts including multi-precious metals for core-shell structure are also prepared which can provide special interface or surface polarization. The unique Pt-Pd-graphene stack structures were fabricated and the surface polarization was enhanced with reduction of Pt thickness which caused the electron density of catalyst surface increased (Fig. 4), thus contributing to improve HER activity [40]. By optimizing the Pt thickness, the obtained catalyst exhibited the high activity with the 791 mA cm^{-2} at potential of 300 mV and a Tafel slope of 10 mV dec^{-1}, as well as the excellent stability with negligible decay before and after 5000 CV cycles. Thus, using ALD technique to offer monolayer Pt deposition may further enhanced HER activity with minimal usage of Pt. Moreover, isolated and layered growth of Pt on Pd were prepared (Fig. 5) [41], and finally, the isolated growth exhibited the superior HER activity than layered growth because of the high surface area and more exposed Pd/Pt interface. Besides, the well-defined Ru@Pt core-shell nanocatalysts were synthesized which showed ultralow charge-transfer resistance [42]. However, the ultrasmall Pt particles without core atoms were predicted to be the best Pt catalyst for HER by new density functional theory (DFT)-based global optimization theoretical methods [43].

2.2.2. Choose special supports

In addition to exerting the advantages of Pt alloy and core-shell catalysts, low loading these Pt-based catalysts on excellent supports with high corrosion resistance and abundant sites becomes another effective stratagem. The transition metal carbides (TMCs) are widely used to support Pt because of their Pt-like catalytic properties [44–47]. For the monolayer precious metals on TMC substrates, Chen's group has made the great contribution to this area, and an instructive finding about volcano relationship between HER activity and DFT-calculated HBE is obtained [48], which is similar to previous study [28,49,50]. These materials exhibited high catalytic activity near to bulk Pt. However, their long-term stability and unsuitable applying in the high current density electrolysis devices are still the challenge because of the low surface areas [51]. Based on this, recently, low-loadings of Pt supported on six TMCs powders were synthesized [45]. And eventually, the results show that different carbides do not obviously change the intrinsic activity of the Pt/TMC catalysts, but have a significantly effect on the dispersion of Pt, which causes the different electrochemical surface areas.

Besides, another special structure that the monolayer Pt deposited on carbon-covered faceted rhenium (C/Re) $(1\,1\,\bar{2}\,1)$ surface was constructed and showed higher HER activity than bulk Pt (1 1 1) surface which may be due to the substantially reduced HBE (Fig. 6) [52]. This is the first application of faceted metal surfaces as templates to synthesize the electrocatalyst with well-defined surface structure and size on nanometer scale. Recently, single Pt atom and clusters supported on N-doped

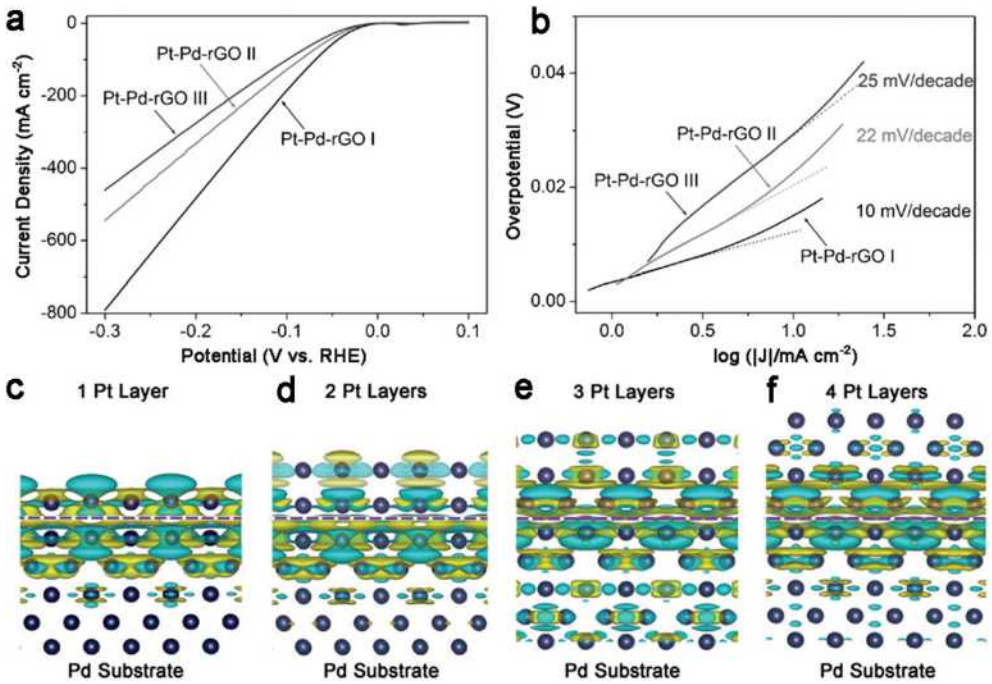

Fig. 4. (a) Polarization curves of samples with different Pt thickness. (b) Corresponding Tafel plots. Differential charge density by first-principles simulations illustrating the alterations of electron distributions with the Pt thickness: (c) 1 layer, (d) 2 layers, (e) 3 layers, and (f) 4 layers. The olive and cyan represent increase and decrease in electron density, respectively.

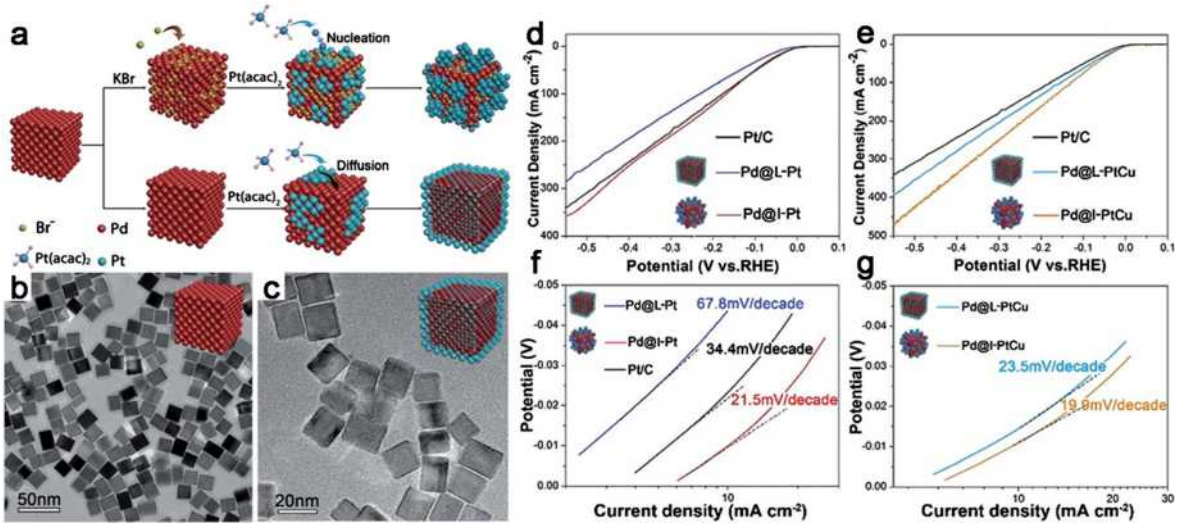

Fig. 5. (a) Schematic illustration of the major steps involved in the synthesis of Pd@Pt core-shell cubes with two different growth models. (b) TEM image of Pd cubes. (c) TEM image of Pd@L-Pt core-shell cubes with layered growth mode. (d, e) Polarization curves of the Pd@Pt and Pd@PtCu with layered growth mode compared with island growth mode. (f, g) Tafel plots obtained from the polarization curves.

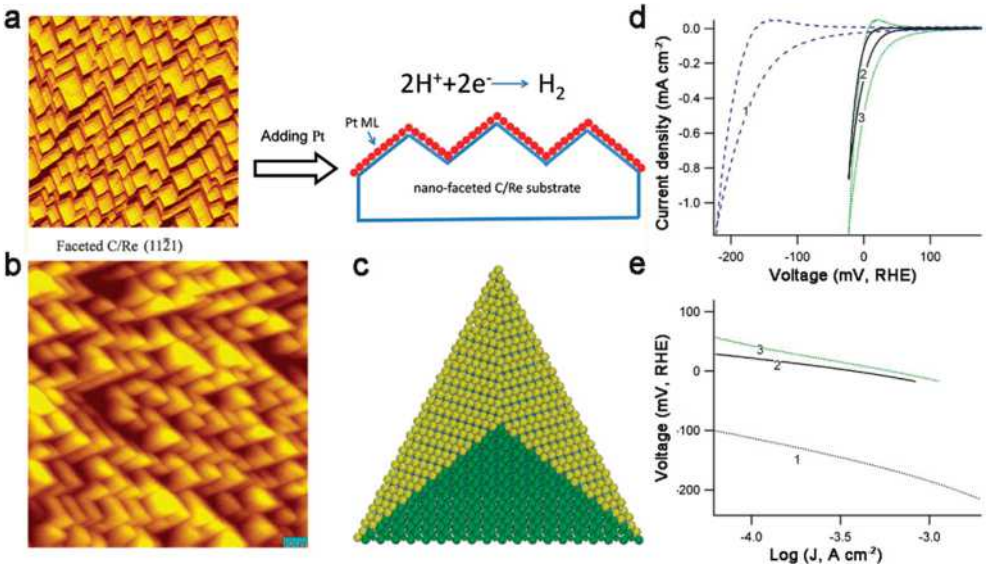

Fig. 6. (a) Schematic illustration of monolayer Pt on the nano-faced C/Re substrate. (b) STM image of a faceted C/Re (1 1 $\bar{2}$ 1) surface. (c) Hard sphere model of a single pyramid from the faceted C/Re (1 1 $\bar{2}$ 1) surface. (d) HER polarization curves of (1) Re (1 1 $\bar{2}$ 1), (2) Pt (1 1 1), and (3) Pt ML supported on faceted C/Re (1 1 $\bar{2}$ 1). (e) Corresponding Tafel plots.

graphene nanosheets were synthesized by ALD [53], and the mass activity of this catalyst exhibited 37.4 times greater than commercial Pt/C catalyst. Importantly, the X-ray absorption near-edge structure (XANES) spectrum was also used to study the local electronic structure of Pt catalysts and their interaction with the support material. Finally, the excellent performance was attributed to the partially unoccupied density of states of the Pt atoms' 5d orbitals on the nitrogen-doped graphene based on XANES and DFT. There is no doubt that the single atom catalysis can markedly decrease the Pt loading and increase the Pt utilization efficiency. In addition, the ultra-low mass loading of Pt nanoparticles on carbon nanofibers and the Pt nanocuboids supported on reduced graphene oxide (rGO) were also designed and showed good catalytic activity [54,55].

Although the Pt/C is the typical support enhanced HER catalyst, it suffers the carbon corrosion, migration and aggregation of Pt and low stability. Therefore, some researchers reported the non-carbon robust supports, such as the Pt nanowires on metal hydroxides nanosheets. Considering the high specific surface area of ultrathin transition metal dichalcogenides (TMDs) nanosheets, the single-layer TiS_2 and TaS_2 nanosheets were prepared as novel dispersible platforms to deposit Pt

and Au nanoparticles [56], and the Pt-TiS_2 composite exhibited the good catalytic performance. Apart from the non-precious metal templates, the monolayer Pt supported on Au was also synthesized as the photoelectrochemical catalyst for HER [57], meanwhile the other precious metal catalysts, such as Pd, Au, Ag, Rh or their alloys were also constructed [58–69], but which were beyond the scope of our discussion. Table 2 lists and compares some excellent precious metal catalysts for HER performance.

By means of these advanced routes, much progress has been made for Pt-based HER catalysts, which have possessed extremely low loading of Pt, proper exposed active sites, high BET surface, stable structure, and thus high catalytic activity and long-term durability. However, these issues including the aggregation and recombination of Pt, its low reserves and high cost cannot be completely eliminated. Therefore, replacing Pt with other non-precious metal or metal free catalysts for HER will be a promising way for the sustainable society.

To address the aforementioned problems of precious metal catalysts, intensive scientific researches have spotlighted on the non-precious metal catalysts which are cheap and earth abundant. In general, the element compositions and interaction with each part can control the intrinsic activity; meanwhile the specific surface and pore structure will determine the electron and mass transport properties, as well as the accessible parts of the active sites. Until now, the non-precious elements for synthesizing the HER catalysts are mostly molybdenum (Mo), tungsten (W), iron (Fe), cobalt (Co), nickel (Ni), copper (Cu) and tin (Sn), and a series of these catalysts with preferable morphology and structure have been established for HER. Therefore, for introducing conveniently, we divide the non-precious metal HER catalysts into catalysts based on Mo and W and catalysts based on Fe, Co and Ni.

2.3. Catalysts based on Mo and W

Among various established HER electrocatalysts, the catalysts based on Mo and W are widely considered to be promising substitutes for precious metals, and accounted for a large proportion of non-precious metal catalysts. Originally, the MoS_2 was reported that hold great potential to serve as a HER electrocatalyst because the edge sites of MoS_2 was similar to nitrogenase's, which can drive HER effectively and the theoretical free energy of hydrogen adsorption on such catalyst is near to that of Pt ($\Delta G_H^\circ \approx 0$) [70]. Subsequently, the active site which was clearly bound up with the catalytic activity was identified by Jaramillo and co-workers [71]. Henceforth, numerous materials based on Mo and W, such as the sulfides, selenides, carbides, nitrides and phosphides are extensively reported to boost the catalytic activity. Conventionally, these materials based on Mo and W in bulk form show poor catalytic activity toward HER either in acid or alkaline medium. To this context, three fascinated approaches are widely used to settle this fatal issue: (i) increasing the surface area to expose more active sites; (ii) doping suitable heteroatoms to optimize the surface electronic structure and (iii) coupling with conductive species to improve the electrical contact with active sites, or both. Normally, tailoring the structures of catalysts can achieve the above purposes. Therefore, tremendous research efforts are invested in the constructing special structures. Herein, we introduced the catalysts based on Mo and W by different structures, including zero/one-dimension (0/1D), two-dimension (2D) and three-dimension (3D) nanostructures.

2.3.1. Zero/one-dimension nanostructure

2.3.1.1. Particles, wires or rods. Compared to the bulk materials, engineering nanostructures in the form of particles, wires/rods can usually afford the catalysts with preferable facet or active sites, relatively large specific surface area, optimized electronic structure and some other special properties, thus remarkably boosting their HER performance. Therefore, the nanoparticle catalysts based on Mo and W are widely synthesized [72–77]. Hu et al. showed the MoS_2 particles as an efficient catalyst for the reduction of aqueous protons [78], and their group also first showed the molybdenum boride (MoB) and carbide (Mo_2C) were active HER catalysts in both acidic and basic solutions in detail [79]. Meanwhile, they proposed the catalytic activity can be improved by optimizing the particle size, but the mechanistic questions of these catalysts are not clarified. Considering from decreasing the particle size, the WS_2 nanodots were prepared by liquid-phase exfoliation method, and the high activity was due to a high concentration of 1T-WS_2 as well as the quantum confinement and edge effects [80].

Table 2
Summary of HER performance of some excellent precious metal catalysts.

Catalysts	Electrolyte	Loading (mg cm^{-2})	Overpotential (mV)	Tafel slope (mA cm^{-2})	Exchange current density (mA cm^{-2})	Stability	Ref.
PtNiCu nanochains	0.5 M H_2SO_4	0.06	η_{200} = 75	28	N/A	1000 CV cycles	[31]
TriStar PtFeCo shape	0.5 M H_2SO_4	0.05	η_{1325} = 400	21	N/A	5000 CV cycles	[32]
Pt NWs/$Ni(OH)_2$ NSs	0.1 M KOH	0.016	$\eta_{6.3}$ = 70	N/A	N/A	4000 s	[34]
Pt-Ni NWs	1 M KOH	0.015	η_{10} = 40	N/A	N/A	3 h	[35]
PtNiCo nanohexapod	0.1 M KOH	0.01	η_5 = 22	N/A	1.4	N/A	[36]
Pt–Pd–Gr	0.5 M H_2SO_4	0.01	η_{791} = 300	10	N/A	5000 CV cycles	[40]
Pd@I-PtCu	0.5 M H_2SO_4	0.16	η_{251} = 300	20	N/A	N/A	[41]
Single atom Pt/N-Gr	0.5 M H_2SO_4	N/A	η_{16} = 50	29	N/A	1000 CV cycles	[53]
Pt/carbon nanofibers	0.5 M H_2SO_4	N/A	η_{10} = 55	32	N/A	1000 CV cycles	[54]
Cuboid-like Pt-CNSs/rGO	0.5 M H_2SO_4	0.17	η_{10} = 75	29	0.18	2000 CV cycles	[55]

And ultra-small Cu_7S_4@MoS_2 hetero-nanoframes were also fabricated and exhibited high activity because of the nanoframe heterostructure and Cu_7S_4 template supporting which was crucial to maintain the full exposure of active edge sites [81]. Moreover, to expose more edge sites, a strategy to chemically unzip WS_2 nanotubes to form WS_2 nanoribbons was provided and displayed enhanced HER activity [82].

In addition, the amorphous MoS_x catalysts were also widely studied as they were not only facilely synthesized [83,84], but also inherited some advantages of crystalline MoS_2 [72,76,85–88]. Thereinto, the structural transformation of amorphous MoS_3 to amorphous MoS_2 and then crystalline MoS_2 during electrolytic process was confirmed [86]. However, the enhanced HER activity may still attribute to the amorphous MoS_2 as the crystalline domains are extremely limited. Moreover, the active sites of amorphous MoS_x were hardly quantified because of uncertain structure and atomic-scale heterogeneity [89–91]. Until recently, the polymeric structure and molecular nature of amorphous MoS_x were revealed, which consisted of discrete $[Mo_3S_{13}]^{2-}$ building blocks [92]. Thereinto, two of the terminal disulfide (S_2^{2-}) ligands were shared to form polymer chain, and another remained free and generated molybdenum hydride moieties, which was regarded as the active site

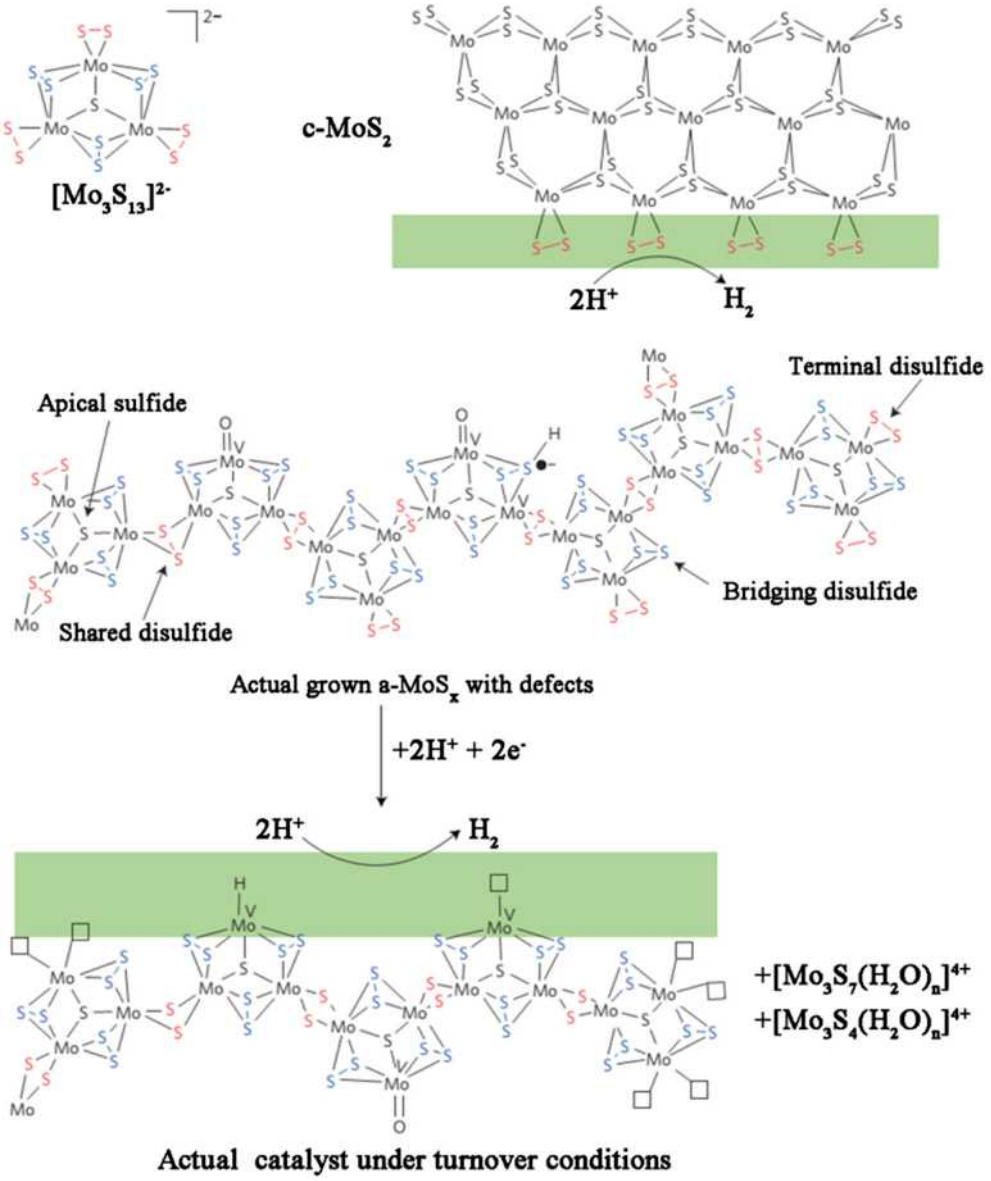

Fig. 7. Structures of molybdenum sulfide materials. Top left: $[Mo_3S_{13}]^{2-}$ cluster. Top right: crystalline MoS_2. Centre: actual amorphous MoS_x coordination polymer with $[Mo_3S_{13}]^{2-}$ building block units. Bottom: the same amorphous MoS_x catalyst under catalytic H_2 evolution turnover conditions. Within amorphous MoS_x, four different ligands are thus identified: apical sulfide μ-S^{2-}, bridging disulfides $(S–S)^{2-}_{br}$, shared $(S–S)^{2-}_{sh}$ and terminal disulfides $(S–S)^{2-}_{t}$.

for H_2 evolution (Fig. 7). Based on such clear structure understanding, the catalytic activity can be improved by further optimizing the structure.

With respect to molybdenum carbides, Leonard et al. fabricated the nanoparticles with four phases (α-MoC_{1-x}, η-MoC, γ-MoC and β-Mo_2C) for HER, and the γ-MoC showed great potential to be an effective catalyst as verified by theoretical and experimental analysis [93]. But the size and shape control of MoC was hard, which seriously affected its catalytic performance. Thus, synthesis the MoC with special structures is the key to improve HER activity. For instance, the nanoporous Mo_2C nanowires were synthesized by simply calcining a MoO_x/amine hybrid precursor [94], and the bimetallic carbide nanowire structure was also fabricated by a hydrothermal method and then facile carburization process, which consisted of nanosized Mo_2C particles integrated on the highly conductive WC backbone [95]. Undoubtedly, their enhanced activity was owing to the advantages derived from unique structure. Moreover, the core-shell MoO_3-MoS_2 nanowires [96] and heteronanowires of MoC-Mo_2C [97] were also applied for HER effectively. Thereinto, the HER activity of MoO_x/MoS_2 core-shell nanowires can be enhanced by hydrazine treatment which acts as an electron dopant to increase the overall conductivity [98]. Recently, Lou et al. synthesized the hierarchical β-Mo_2C nanotubes by carburizing Mo-polydopamine nanotubes [99]. Thanks to the well-defined structure, this catalyst also exhibited high activity in both acidic and alkaline conditions.

Recently, the molybdenum oxide is studied because of the low cost, nontoxic and high stability. Typically, the mesoporous molybdenum oxide with nanosized crystalline walls was prepared by using a soft template synthesis method, which exhibited high activity and excellent stability (longer than 12 h) under both acidic and alkaline conditions [100]. This high performance was mainly attributed to the mesoporosity and oxygen vacancies which could facilitate HER activity by generating unusual electronic state near the Fermi level.

Apart from the sulfide and carbide of molybdenum, molybdenum phosphide nanoparticles were also proposed as HER catalysts [101]. Moreover, the degree of phosphorization is largely correlated with catalytic activities and stabilities, and a higher degree of phosphorization resulted in better performance [102]. Recently, the P-rich WP_2 submicroparticles were synthesized and exhibited excellent HER performance with the overpotential of 161 mV to afford 10 mA cm^{-2} and a Tafel slope of 57 mV dec^{-1} [103]. In addition, the multicomponent catalysts were also prepared [104–107].

2.3.1.2. Doping. Introducing the extra non-metal element is an effective way to enhance the HER activity of host material via tuning their electronic and surface structures [108]. The $MoS_{2(1-x)}P_x$ solid solution was prepared and the 10 mA cm^{-2} was obtained at the overpotential of about 150 mV [109]. Considering the optimization of conductivity and active sites simultaneously, the S-decorated Mo_2C nanostructures were designed and showed superior HER activity though the decoration of S produced some adverse effect, such as reducing the electrochemically active surface areas and enlarging the impedance resistance [110]. Besides, N-rich iron-tungsten carbonitride (Fe-WCN) core-shell nanostructures were also constructed and demonstrated the good HER activity due to the existence of N-bound W species [111]. This strategy might be expanded to synthesize other functional metallic nitrides. Additionally, they also found that N-content in Fe-WCN had a good relationship with HER activity, and the low N-content could lead to the poor HER performance. But the possible role of Fe in this catalyst was not discussed.

Besides the non-metal doping, metal doping is also used to improve the catalytic activity which might improve the intrinsic catalytic properties and increase effective electrochemical surface area [112–116]. As indicated by Hu et al., the Fe, Co and Ni could promote the catalytic activity of amorphous MoS_3 films via leading to a high surface area or even increasing the intrinsic activity of the MoS_3 film [114]. After that, the Co/Ni-W-sulfide ($CoWS_x$ and $NiWS_x$) were synthesized as efficient electrocatalysts for the HER over a wide pH range [116]. What's more, they found that MWS_x (M is Co or Ni) catalysts possessed WS_2-like layered structure and M-S-W bimetallic sulfide centres, moreover the primary catalytic activity was located in the M-S centres. This contributed to understand how HER activity was promoted in metal-doped molybdenum and tungsten sulfide materials. Recently, Ni-MoS_2 hybrid nanoclusters were fabricated, and exhibited a 100 mV shift in the HER onset potential and an almost 3-fold increase in exchange current density compared with the undoped MoS_2 nanoclusters [112]. Besides, the molybdenum-based ternary or multinary catalysts were also synthesized and showed excellent activity [117–119].

The transition metals (Fe, Co and Ni) introduced into Mo_2C were also discussed. Fe doped β-Mo_2C catalysts were synthesized via an amine–metal oxide composite method, and the enhanced activity was attributed to broader valence bands of β-Mo_2C and more electrons around the Fermi level, the graphitic carbon supports, and highly active $Fe_2(MoO_4)_3$ species on the surface after Fe was doped [115]. Ni-doped β-Mo_2C was also synthesized by the same method, but gave lower HER activity than Fe-doped β-Mo_2C. Moreover, considering further-improved HER activity by optimizing structure, a series of Co-doped Mo_2C nanowires were developed [113], and the low overpotential (η_{10} = 140 and 118 mV), small Tafel slope (39 and 44 mV dec^{-1}) were obtained in 0.5 M H_2SO_4 and 1.0 M KOH, respectively. Certainly, the Ni-doped Mo_2C nanowires were also fabricated [120].

2.3.1.3. Combine with conductive substrates. Combining nanoparticles with conductive substrates is a well-known route to improve the electronic conductibility and also prevents the aggregation of the nanoparticles, thus greatly enhancing the catalytic activity. A large number of studies have been carried out to improve the HER activity by this method [121–131]. Jaramillo et al. deposited the MoS_2 nanoparticles on a clean Au (1 1 1) substrate [71], which determined the active sites for hydrogen evolution of MoS_2 nanoparticles, and they also proposed that tuning the electronic structure of edge was benefited for improving the activity. After that, the graphite was also used as substrate to support $[Mo_3S_4]^{4+}$ molecules, which exhib-

ited high per-molecule catalytic efficiency, but the observed electrocatalytic stability was not satisfactory because of the desorption of catalyst molecules from the surface [132]. Dai's group applied rGO as the support for MoS_2 nanoparticles [133], and the obtained MoS_2/rGO catalyst showed admirable HER activity with an onset potential of 100 mV and a low Tafel slope of 41 mV dec^{-1}. This was mainly attributed to the strong chemical and electronic coupling between the GO sheets and MoS_2. The chemical coupling made the MoS_2 selectively grow on GO free of aggregation, and the obtained small size and high dispersion of MoS_2 on GO afforded abundant and accessible edges which can serve as active catalytic sites for the HER. Meanwhile, the electronic coupling contributes to the electron transport from the less-conducting MoS_2 nanoparticles to the electrode. After that, MoS_2 nanoparticles on mesoporous graphene foams were also synthesized [134], and the resultant catalyst exhibited superior HER activity with 100 mA cm^{-2} achieved at 200 mV.

Recently, the P modified WN on rGO was prepared which exhibited high activity with a Tafel slope of 54 mV dec^{-1} and an overpotential of 85 mV at 10 mA cm^{-2} [135]. The interaction of P could cause the interfacial polarization which would increase the electron density on the catalyst surface, and then improved the reaction activity. In addition, a hybrid material based on MoO_2, P-doped nanoporous carbon and rGO was fabricated which exhibited high activity and stability (Fig. 8) [136]. What's more, the metallic WO_2-carbon mesoporous nanowires were obtained by the calcination of inorganic/organic WO_3-ethylenediamine hybrid precursors. Thanks to the high concentration of oxygen vacancies and the large amount of active sites, this catalyst exhibited outstanding catalytic activity with a Tafel slope of 46 mV dec^{-1} and a low overpotential of 58 mV at 10 mA cm^{-2} [137].

To further enhance the HER activity of molybdenum carbide, the Mo_2C nanoparticles combined with carbon materials have been widely adopted [138–141], as well as the molybdenum compounds [142,143] and multimetallic carbide [144]. The enhanced activity were mainly due to the low HBE, high conductivity and the compound support which contributed to alleviate aggregation of the Mo_2C, provide large electrolyte-accessible surface area and accelerate the electron transfer. Thereinto, to avoid the inevitable aggregation and/or excessive growth of Mo_2C nanoparticles as well as the easy oxidation of their surface which will reduce the catalytic activity, the ultrafine Mo_2C nanoparticles (less than 3 nm) uniformly embedded within a carbon matrix were designed [145]. Thanks to the cooperative effects of ultrafine Mo_2C nanoparticles, ultrathin graphene shells and N dopant, this catalyst exhibited excellent activity with a low onset potential of 6 mV, a Tafel slope of 41 mV dec^{-1} and the overpotential of 78 mV at 10 mA cm^{-2}, as well as good stability during 12 h continuous operation. Similarly, Mo_2C encapsulated by N, P-codoped carbon shells and N, P-codoped rGO were designed (Fig. 9) [146], and the HER activity approached the performance of commercial Pt/C that the 10 mA cm^{-2} could be achieved at the overpotential of only 34 mV. Besides, molybdenum or tungsten carbide nanoparticles rigidly embedded into the vertically aligned graphitic carbon nanosheets were synthesized [147]. Furthermore, the Ni-encapsulated N-doped carbon vesicle material modified

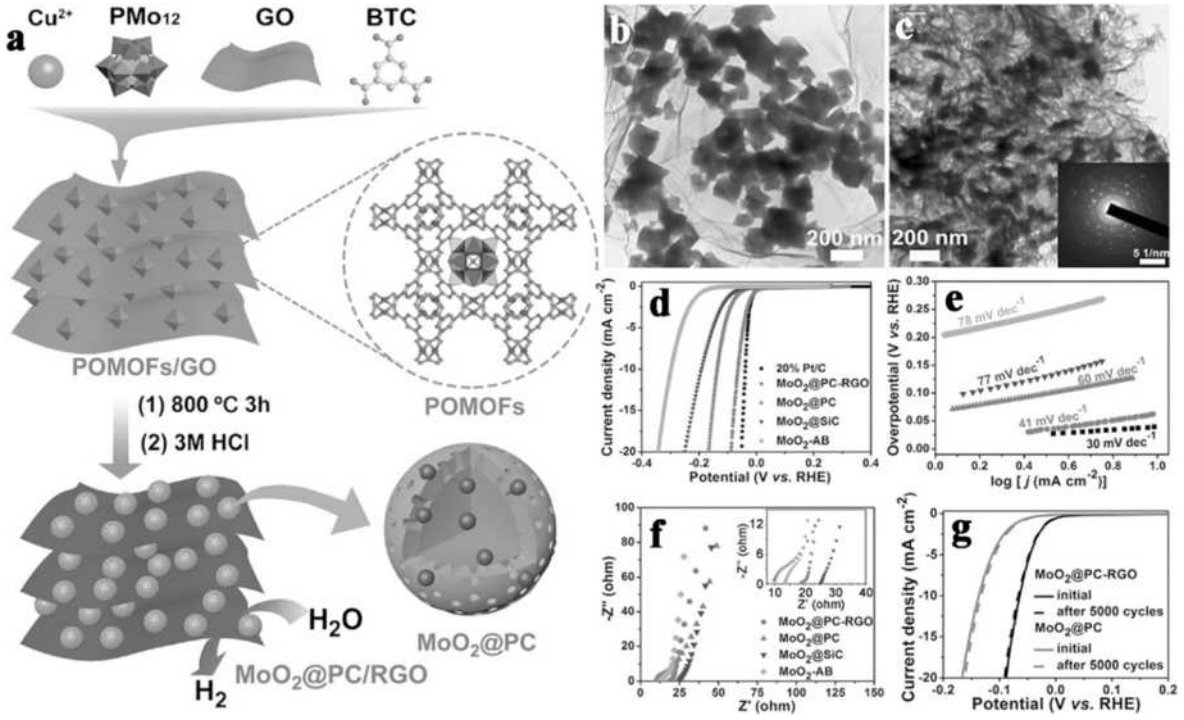

Fig. 8. (a) Preparation process of the MoO_2@PC-RGO nanocomposite. TEM images of (b) POMOFs/GO (8 wt%) and (c) MoO_2@PC-RGO. (d) Polarization curves for four electrocatalysts and 20% Pt/C. (e) Tafel plots of the corresponding polarization curves. (f) Electrochemical impedance spectra of four electrocatalysts. (g) Durability measurements with MoO_2@PC-RGO and MoO_2@PC.

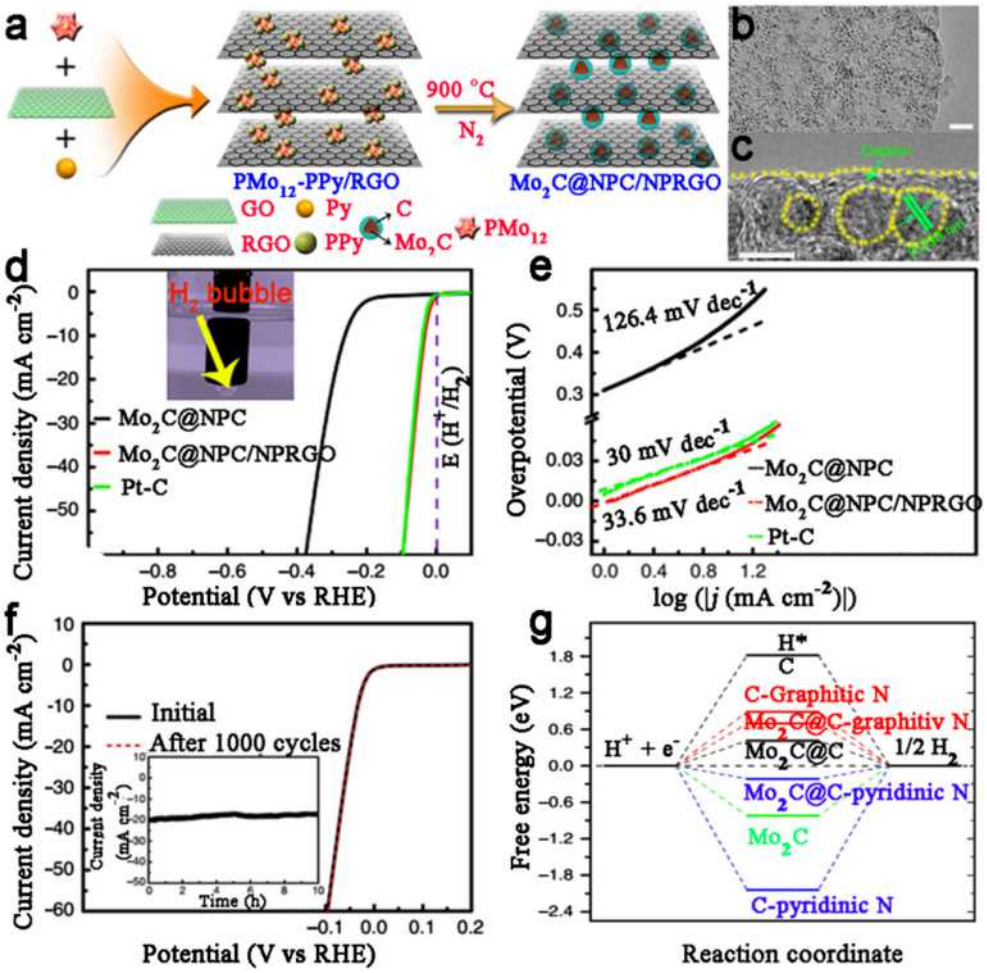

Fig. 9. (a) Schematic illustration of the synthetic process of Mo_2C@NPC/NPRGO. (b) TEM and (c) HRTEM of Mo_2C@NPC/NPRGO. (d, e) Polarization curves and Tafe plots of different samples. (f) Polarization curves of Mo_2C@NPC/NPRGO initially and after 1000 CV cycles. Inset: Time-dependent current density curve of Mo_2C@NPC/NPRGO under a static overpotential of 48 mV for 10 h. (g) Calculated free energy diagram for HER on various studied system.

by Mo_xC were also synthesized [148], and the existence of Ni ion made the Mo_xC nanoparticles effectively decorate on the substrate Ni@NCV. Thus, this catalyst exhibited high HER activity and durability with a low overpotential of 68 mV at 10 mA cm^{-2}.

Very recently, well-defined pomegranate-like N,P-doped Mo_2C@C nanospheres were fabricated and showed an extremely low overpotential of 47 mV at 10 mA cm^{-2}, which was attributed to uniform N,P-doped in the conductive carbon shell/matrix and nanoporous structure [149]. In addition, Lou et al. also developed a MOFs-assisted strategy to synthesize porous molybdenum carbide octahedral nanoparticles which relied on the in situ and confined carburization reaction. The prepared catalyst showed remarkable HER activity in both acidic and basic solutions because of the desirable nanostructure with unusual η-MoC phase embedded in an amorphous carbon matrix and a uniform mesoporous structure [150]. Similarly, the porous MoP nano-octahedrons, as well as the Mo_2C and MoN, were also prepared by analogous method and showed high activity [151]. Some excellent HER performance of zero/one-dimension materials based on Mo and W is listed in Table 3.

Over the past decades, many inspired zero/one dimension electrocatalysts have been achieved for HER via abundant and rational strategies to optimize structures, such as synthesizing from nanoparticle and nanodots to nanowires, doping and choosing conductive substrate. Typically, these catalysts, characterizing with high special surface area, sufficient active sites, good electron and mass transport properties, show high HER performance. However, the aforementioned problems are not completely avoided, calling for more attention to the mechanism of forming catalysts and the according electrocatalytic mechanisms.

Table 3
Summary of HER performance of some zero/one-dimension materials based on Mo and W.

Catalysts	Electrolyte	Loading (mg cm^{-2})	Overpotential (mV)	Tafel slope (mA cm^{-2})	Exchange current density (mA cm^{-2})	Stability	Ref.
γ-Mo_2N NPs	0.5 M H_2SO_4	0.102	η_{10} = 381	100	N/A	1000 CV cycles	[74]
	1 M KOH		η_{10} = 353	108	N/A		
WS_2 nanodots	0.5 M H_2SO_4	0.016	N/A	51	0.11	1000 CV cycles	[80]
Cu_7S_4@MoS_2 nanoframes	0.5 M H_2SO_4	0.28	η_{200} = 206	48	0.019	5000 CV cycles	[81]
WS_2 nanoribbons	0.5 M H_2SO_4	N/A	η_{10} = 225	68	N/A	1000 CV cycles	[82]
MoC-Mo_2C heteronanowires	0.5 M H_2SO_4	0.14	η_{10} = 126	43	0.011	3000 CV cycles	[97]
	1.0 M KOH		η_{10} = 120	42	N/A		
β-Mo_2C NTs	0.5 M H_2SO_4	0.75	η_{10} = 172	62	0.017	8 h	[99]
	0.1 M KOH		η_{10} = 112	55	0.087		
Mesoporous MoO_{3-x}	0.1 M KOH	0.2	η_{10} = 140	56	N/A	12 h	[100]
MoP NPs	0.5 M H_2SO_4	0.86	η_{30} = 180	54	0.034	40 h	[101]
	1 M KOH		N/A	48	0.046	Corrosion	
WP_2 submicroparticles	0.5 M H_2SO_4	0.5	η_{10} = 161	57	0.017	5000 CV cycles	[103]
Molybdenum carbonitride	0.5 M H_2SO_4	0.4	η_{10} = 140	46	N/A	1000 CV cycles	[105]
$MoS_{2x}Se_{2(1-x)}$ NTs	0.5 M H_2SO_4	0.32	η_{10} = 219	55	N/A	1000 CV cycles	[107]
$MoS_{2(1-x)}P_x$ solid solution	0.5 M H_2SO_4	0.285	η_{10} = 120	57	N/A	20,000 CV cycles	[109]
MoS_x@Mo_2C	0.5 M H_2SO_4	0.213	η_{178} = 400	44	0.128	1000 CV cycles	[110]
Co-Mo_2C NWs	0.5 M H_2SO_4	0.14	η_{10} = 140	39	0.0051	3000 CV cycles	[113]
	1.0 M KOH		η_{10} = 118	44	N/A		
Ni–Mo–N	0.5 M H_2SO_4	1	η_{20} = 53	39	0.91	24 h	[118]
	1.0 M KOH		η_{20} = 43	40	0.67		
Ni-Mo_2C NWs/Ni foam	6.0 M NaOH	N/A	η_{100} = 150	36.8	0.51	10,000 CV cycles	[120]
WC/CNTs	0.5 M H_2SO_4	N/A	η_{10} = 145	72	N/A	1000 CV cycles	[121]
	0.1 M KOH		η_{10} = 137	106			
MoS_2 quantum dots/RGO	0.5 M H_2SO_4	0.285	η_{10} = 64	63	0.669	1000 CV cycles	[125]
Porous MoC@graphite shell	0.5 M H_2SO_4	0.76	η_{10} = 124	43	0.015	3000 CV cycles	[127]
	1.0 M KOH		η_{10} = 77	50	0.212	N/A	
P-WN/rGO	0.5 M H_2SO_4	0.337	η_{10} = 85	54	0.35	20 h	[135]
MoO_2@PC-RGO	0.5 M H_2SO_4	0.14	η_{10} = 64	41	0.48	5000 CV cycles	[136]
WO_2-C NWs	0.5 M H_2SO_4	0.35	η_{10} = 58	46	0.64	2000 CV cycles	[137]
Mo_2C/NCF	0.5 M H_2SO_4	0.28	η_{10} = 144	55	N/A	10,000 CV cycles	[139]
	1.0 M KOH		η_{10} = 100	65		Corrosion	
Mo_2C@NPC/NPRGO	0.5 M H_2SO_4	0.14	η_{10} = 34	33.6	1.09	1000 CV cycles	[146]
Mo_xC-Ni@NCV	0.5 M H_2SO_4	1.1	η_{10} = 68	45	0.95	3000 CV cycles	[148]
Mo_2C@C nanospheres	0.5 M H_2SO_4	0.9	η_{10} = 141	56	0.029	2000 CV cycles	[149]
	1.0 M KOH		η_{10} = 47	71	2.042	1000 CV cycles	
MoC_x nano-octahedrons	0.5 M H_2SO_4	0.8	η_{10} = 142	53	0.023	3000 CV cycles	[150]
	1.0 M KOH		η_{10} = 151	59	0.029	Corrosion	
MoP@PC	0.5 M H_2SO_4	0.41	η_{10} = 153	66	0.21	2000 CV cycles	[151]

2.3.2. Two-dimension nanostructure

The 2D materials have been widely applied in many fields (such as electronics, energy storage/conversion and electrocatalysis) in view of their unique structural and electronic properties, such as ultrahigh specific surface area, strong quantum confinement of electrons in plane and surface structural disorder/defects [152–154]. Moreover, the 2D materials catalysts based on Mo and W have been extensively researched.

2.3.2.1. Nanosheets. The chalcogenides nanosheets are widely synthesized. Thereinto, MoS_2 which has a layered crystal structure exhibits a quite strong tendency to form sheet-like morphology. The MoS_2 nanosheets with more active edge sites were designed [155], and the optimization of lamellar structure was achieved via changing the annealing temperature which had an important influence on the amount of exposed active sites and stack height. Further improving the catalytic activity by doping Co on edge sites and then coating on supports with large surface area and high conductivity was also proposed. Recently, the pure and stable metallic-phase MoS_2 nanosheets were synthesized which showed superior HER activity with the 10 mA cm^{-2} at overpotential of 175 mV and a Tafel slope of 41 mV dec^{-1} [156].

In addition to the synthesis of pure nanosheets, engineering the nanosheets with highly oriented structure and rich defects can further improve the HER activity [157–160]. Few-layer MoS_2 with an expanded (0 0 2) plane and highly oriented structure were synthesized, and exhibited good performance because of the high ion and mass transport, and abundant active sites [157]. The defects engineered monolayer MoS_2 was synthesized by oxygen plasma exposure and hydrogen treatment [159]. The introduced defects led to a high density of exposed edges which were benefited for the enhanced catalytic activity. Similarly, Xie et al. synthesized the defect-rich MoS_2 ultrathin nanosheets [158]. The additional active edge sites could be exposed because of the abundant defects that caused partial cracking of the catalytically inert basal planes. So the obtained catalyst exhibited superior HER activity than the pure MoS_2 with an onset potential of 120 mV and a Tafel slope of 50 mV dec^{-1}, as well as a good stability with negligible difference before and after 3000 CV cycles. This novel method

could be also used to construct other effective catalysts with the controllable defect. Moreover, this group also firstly synthesized atomically-thin MoN nanosheets with active surface sites by liquid exfoliation of the MoN bulk material [161], and theoretical calculations demonstrated the metallic behavior of this atomically-thin nanosheets, which could effectively facilitate electron transport during the catalytic process. Meanwhile, structural analyses showed the special surface of these nanosheets were only composed of apical Mo atoms. As a result, it was confirmed the apical Mo atoms on the surface were catalytically active for HER. Besides, the cobalt molybdenum nitride with a four-layered mixed closed packed structure was constructed as a highly active and stable electrocatalyst for HER [162]. The layered nature of this structure has unique features, but much work should be done to achieve optimal activity, such as exploiting synthetic routes to control over particle size and/or access different Mo oxidation states, and the extra mechanism of this structure type should be discussed.

What's more, the MoS_2 nanosheets with controllable layers were successfully fabricated [163], and the HER activity could be enhanced by reducing the layer number, thus the optimized single-layer MoS_2-CNTs exhibited long-term durability and high HER activity. Furthermore, monolayer WS_2 nanosheets was also reported as an efficient catalyst for HER [164], and the enhanced electrocatalytic activity of WS_2 stemmed from the high concentration of strained metallic 1T (octahedral) phase in the as-exfoliated nanosheets. Similarly, this group also obtained the MoS_2 nanosheets containing rich metallic 1T phase [165]. They also found that electrochemical oxidation of the edges had a significance effect on catalytic activity of 2H phase nanosheets, but no effect for 1T phase, and the catalytic performance of 2H phase can be promoted by the CNTs, suggesting the critical role of both edges of nanosheets and charger transfer properties in improving the HER performance. And recently, targeted synthesis of 2H and 1T phase MoS_2 monolayers were achieved [166]. Besides, the catalytic performance of MoS_2 monolayers can be improved dramatically by catalyst size reduction and surface S depletion [167].

The basal plane of MoS_2, which has been long considered to be inert for HER, is successfully activated and optimized with excellent intrinsic HER activity by creating and further straining S vacancies [168]. Moreover, the local electronic structure of the S-vacancies was directly probed using scanning tunneling microscopy/spectroscopy (STM/STS). Combined with theoretical results, the presence of S-vacancies introduced additional electronic states in the gap, and the ΔG_{H*} could be further optimized by proper combinations of S-vacancy and strain, which led to the highest intrinsic HER activity (Fig. 10). Then the strained S vacancy has an electron-transfer rate 4 times higher than that of the unstrained S vacancy based on the combinational approach of scanning electrochemical microscopy measurements and multiphysics modeling [169]. Moreover, the electron transport of MoS_2 can be facilitated through electric field [170]. Very recently, the contributions to HER of all catalytic active sites of MoS_2, including phase, sulfur vacancies, edges and grain boundaries, have been revealed [171,172]. The phase serves as the key role in determining the HER performance, and both edges and S-vacancies also contribute significantly to the catalytic activity, while the grain boundaries may only provide minor benefit. Thus, engineering MoS_2 with enriched 1T phase, sulfur defects and edge sites is the effective way to enhance the HER activity.

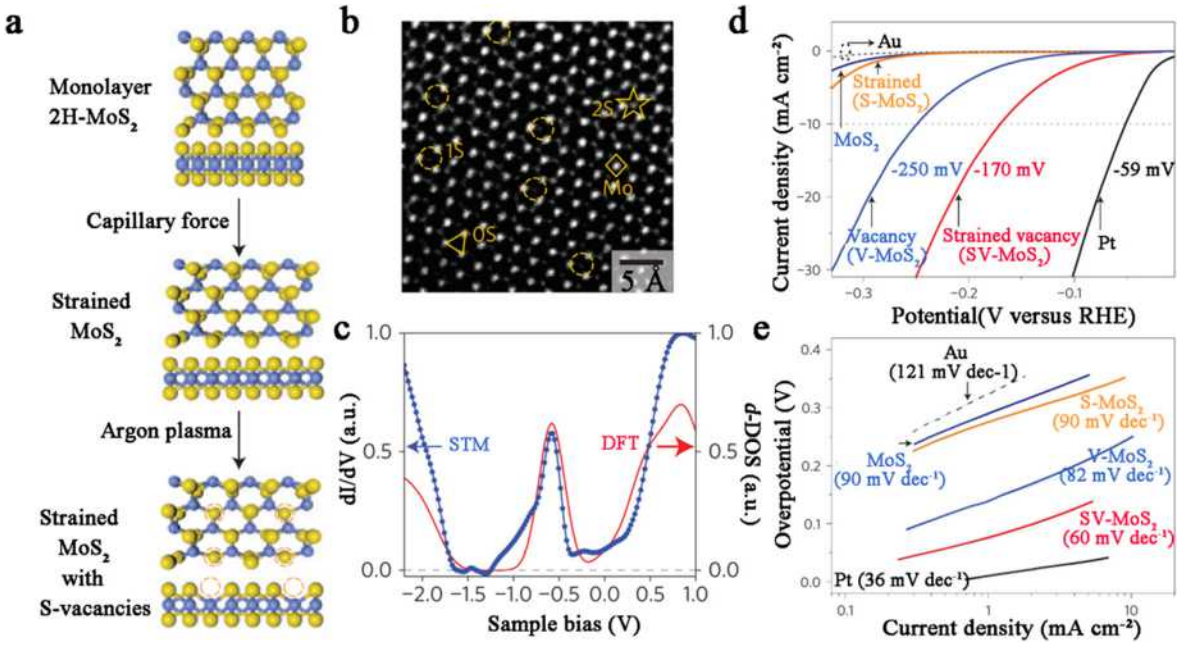

Fig. 10. (a) Schematic of the top (top panel) and side (lower panel) views of pristine monolayer 2H-MoS. (b) ACTEM image of a 4×4 nm^2 MoS_2 monolayer with about 43S-vacancies (11.3% S-vacancy). (c) STM/STS measured dI/dV (left y-axis) and DFT calculated projected d-orbital density of states on the Mo atom of the S-vacancy (right y-axis) versus sample bias for the S-vacancy sites (under 12.5% S-vacancy). (d, e) Polarization curves and Tafe plots of different samples.

Additionally, decorating or incorporating elements is also considered to induce special active sites. Generally, disorder engineering could contribute to generate more active unsaturated sulfur atoms, and elemental incorporation was widely used to adjust the electronic structure to tune the conductivity of materials. To balance the benefits between rich active sites and good conductivity, Xie group firstly proposed a new method that elemental incorporation with controllable disorder engineering to synthesize the oxygen incorporated MoS_2 ultrathin nanosheets with a moderate degree of disorder [173]. As expected, this catalyst showed superior HER performance and long-term stability, which broadened our vision to improve the catalytic activity by synergistically structural and electronic modulations. Similarly, other non-metal elements [174–177] or metal elements [178–180] introduced into nanosheets were also synthesized and showed excellent HER activities. Thereinto, the MoS_2 doped with numbers of transition metals was screened by virtue of DFT calculations, resulting in a volcano plot (Fig. 11), which was further confirmed by testing the HER measurements of Co- and Ni-doped MoS_2 [178]. Besides, few-layered sheets of MoS_2 interspersed with MoS_2 quantum dots was constructed [181], harvested the high catalytic activity due to the large concentration of active edge.

In addition to construct ultrathin structure and importing with extra elements, coating the nanosheets on conductive supports is another way to improve the HER activity because of enhanced electrical conductivity and high number of exposed sites. The low crystalline MoS_2 nanosheets coated CNTs were synthesized [182], and exhibited high activity with an onset potential of 90 mV and a Tafel slope of 45 mV dec^{-1}. Zheng et al. synthesized MoS_2 nanosheets/rGO composite as a HER catalyst [183], and the influence of oxidation degree of graphene for HER activity was also discussed. Eventually, the medium oxidation of MoS_2/rGO_2 composite which possessed the abundance of exposed active edge sites and excellent internal electrical conductivity showed superior HER activity with an onset potential of 140 mV and a small Tafel slope of 41 mV dec^{-1}. This further indicates that there is a balance between the numbers of exposed active sites and internal conductive channels. Similar work has been studied [184–193], especially the MoS_2, $MoSe_2$ and WS_2 combined with carbon materials, but the property of these catalysts has not been greatly promoted.

What's more, decorating or selecting doped substrate, such as N or S doped carbon, is also fabricated because of the advantages of synergistic effect besides enhanced conductivity and exposed more sites [194–196]. The ultrathin MoS_2/N-rGO were synthesized to show the enlarged interlayer spacing can significantly improve the HER activity (Fig. 12) [197]. The amorphous MoS_x layer directly bound at vertical NCNT forest surface were prepared [198], and thanks to special structure as well as the synergistic effect from the dense catalytic sites and fluent charge transport, the obtained MoS_x/NCNT catalyst showed excellent HER activity with an onset overpotential of ~75 mV and a small overpotential of 110 mV for 10 mA cm^{-2}. To design the MoS_2 with few layers, a small size and rich in S atom, S-rich single-layered MoS_2 nanoplates embedded in N-doped carbon nanofibers were fabricated [199], and showed extraordinary HER activity with a Tafel slope of 38 mV dec^{-1}.

Inspired by the volcano plot [71], the catalysts included more elements are prepared for HER. Chen et al. synthesized NiMo nitride nanosheets on a carbon support ($NiMoN_x$/C) [200], which showed excellent activity with a small overpotential of 78 mV and a Tafel slope of 35 mV dec^{-1}. They attributed this to highly exposed reactive sites and synergetic effects among its components. Moreover, other complicated structures, such as the MoO_2@N-doped MoS_2 nanosheets [201], the layered MoS_2 or $MoSe_2$ on SnO_2 nanotubes [202,203], Se doped layered Cu_2MoS_4 [204] and the MoS_2/rGO decorated with nano-sized WC [205] were also synthesized. The catalysts including multi-elements prepared by doping or other methods may achieve good results, but they have some disadvantages, such as the complicated synthetic processes, the low yields and the difficulty to characterize which one played a major role in catalyst.

2.3.2.2. 2D binder-free planar electrode. Conventionally, either the nanosheets or composites based catalysts are usually prepared by drop/dip-casting on conductive electrodes (such as glass carbon, ITO) using the polymer binder (Nafion, PTEE), but at the price of cost and buried active sites, blocked mass/electron transport, reduced electrocatalytic activity and question-

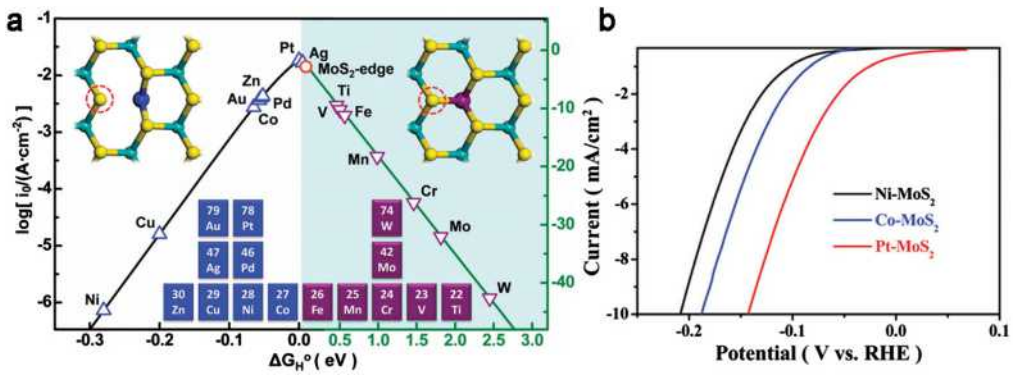

Fig. 11. (a) The relation between currents ($log(i_0)$) and $\Delta G_H°$ presents a volcano curve. (b) HER polarization curves for Ni–MoS_2, Co–MoS_2 and Pt–MoS_2, respectively.

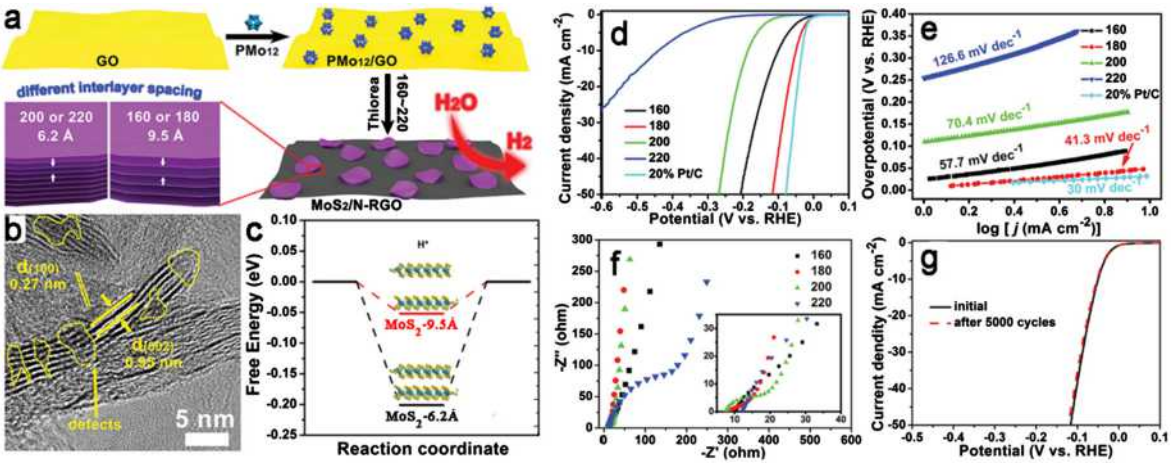

Fig. 12. (a) Schematic preparation process of MoS_2/N-RGO-T nanocomposite. (b) HRTEM of MoS_2/N-RGO-180. (c) Calculated free energy diagram for HER on MoS_2-6.2 Å and MoS_2-9.5 Å. (d) Polarization curves and (e) corresponding Tafel plots of MoS_2/N-RGO-T and commercial 20% Pt/C. (f) Nyquist plots of different samples. (g) Cycling stability of MoS_2/N-RGO-180 before and after 5000 CV cycles.

able durability. To bypass these issues, the catalysts directly grown on the current collectors to form 2D planar electrode have been widely adopted. Monolayer MoS_2 on commercially available Au foils were first scalable synthesized [206], which exhibited good activity. This result exhibited great potential to design effective HER electrodes except the precious metal substrate. Then, the amorphous MoS_2 porous thin films on Mo substrate were fabricated [207], which exhibited long stability and excellent HER performance with a small overpotential of 120 mV and a low Tafel slope of 41 mV dec^{-1}. They ascribed this to the amorphous feature, porous structure, optimized thickness and tight binding between the film and substrate. Besides, the atomic MoS_2 thin films were synthesized to prove the strong interconnection of catalytic activity of MoS_2 films and electrons hopping [208]. As a result, the hopping efficiency of electrons in vertical direction played a key role in catalysis. And the MoS_x clusters-N doped graphene hybrid hydrogel film was also prepared to provide the dual-active-site centers for HER [209].

To expose more edges sites, the plasma-engineered or edge-oriented MoS_2 films have been discussed [210,211]. The properly tailored edge-oriented MoS_2 films on Mo foil were designed which showed excellent HER activity and long-term stability [210]. However, the thermodynamics favors the presence of inert basal planes, thus limiting the number of active sites at the surface. So engineering the surface structure of MoS_2 is often used to preferentially expose edge sites. Furthermore, the double-gyroid MoS_2 films with a tunable thickness were synthesized by electrodeposition of Mo into a silica template, followed by sulphidization. After etching the silica template, the obtained catalyst showed high HER activity [212]. This work provides a strategy that various templates can be used to construct special structures of electrocatalysts to improve the catalytic activity.

Similarly, to maximally expose the edges, Cui et al. synthesized the MoS_2 and $MoSe_2$ thin films on substrate with vertically aligned layers (Fig. 13a) [213]. They also confirmed that the number of edge sites rather than crystalline quality was critical for HER activity, and this unique structure could make the edges of layered materials to be used more effectively. Afterwards, their group synthesized the $MoSe_2$ and WSe_2 nanofilms with vertical layer orientation on curved and rough surfaces (Fig. 13b) [214]. This structure might contribute to enhance the catalytic activities because of the increasing of surface area and the perpendicular orientation of layers. Eventually, the catalysts on curved and rough surfaces showed superior HER activity compared to the flat substrates because of the unique layer orientation, and these catalysts exhibited high stability due to the strong bonding between the layers and substrate. They also claimed that increasing the thickness of nanofilms or doping with Ni atoms could further improve the catalytic activities. In addition, they used the electrochemical Li^+ ions intercalation method to tune the layer of vertically aligned MoS_2 nanofilms continuously, and thus optimized the HER activity [215].

Macroporous $MoSe_2$ films were also demonstrated for HER, but the initial $MoSe_3/MoO_3$ films showed poor catalytic activity [216]. However, this films were reductively converted to macroporous $MoSe_2$ under the HER process and exhibited enhanced HER activity and long-term stability. Considering the numerous advantages of PPy, such as excellent conductivity, large electrochemical surface area, as well as good stability, the extremely active PPy–MoS_x films were fabricated via the electrochemical copolymerization method, which showed outstanding HER activity with a positive onset potential of 0 V and a small Tafel slope of 29 mV dec^{-1} because of the higher S to Mo ratio and more bridging S_2^{2-} active sites, but the stability was unsatisfactory without protection of Nafion as the composition of the films readily changed in this electrolyte, as well as the mechanism for the formation of the PPy-MoS_x films was unclear [217].

In addition, nanostructured MoS_2 films on Ti foils were synthesized [218], and a strategy was provided to enhance the activity that constructing gas evolution catalytic material into a "superaerophobic" surface to removal of formed gas bubbles

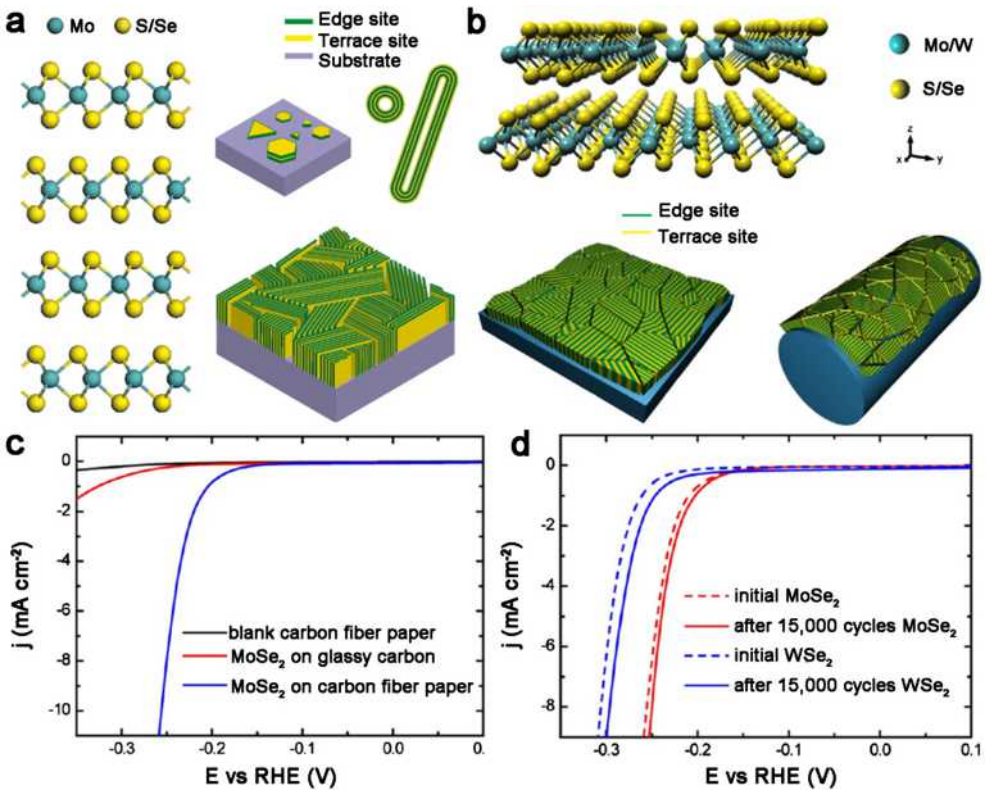

Fig. 13. (a) Nanostructures of layered MoS_2 and $MoSe_2$. Idealized structure of edge-terminated molybdenum chalcogenide films with the layers aligned perpendicular to the substrate. (b) Molybdenum (or tungsten) chalcogenide nanofilm with molecular layers vertically standing on a flat substrate and a curved surface. (c) Polarization curves of $MoSe_2$. (d) Electrochemical stability test of $MoSe_2$ and WSe_2.

easily. The P doped MoO_2 nanoparticles on Mo foil was fabricated [219], and displayed good activity with a Tafel slope of 62 mV dec^{-1} and the 10 mA cm^{-2} obtained at an overpotential of 135 mV. To explore the benefits of surface phosphosulfide for HER, the molybdenum phosphosulfide (MoP/S) supported on Ti foils was prepared [220]. As a result, such catalyst captured excellent stability and HER performance with a low overpotential of 86 mV to deliver the 10 mA cm^{-2}. This work indicates that introducing a surface phosphosulfide onto other metals may contribute to improve the activity and stability. However, the reason of this high catalytic activity is ambiguous. Finally, some excellent HER performance based on two-dimension materials of Mo and W are listed in Table 4.

Though vast endeavors are devoted to optimize the 2D materials or electrodes via exposing abundant special active sites, tuning the electronic and porous structure, increasing the electrochemical active surface area, etc., huge progress has been achieved at Mo and W based electrocatalysts toward HER. And these novel strategies promote deep insights in the electrocatalysis HER. Furthermore, for future practical application, more attentions should be paid for exploring the catalytic mechanism and thus designed the preferable integrated electrodes attached with robust electrocatalysts.

2.3.3. Three-dimension nanostructure

As the HER always occurs at the surface of electrode, the electron and mass transport properties of catalyst is of great significance for enhancing the performance. Therefore, the strategies to design 3D materials with porous structure and increased electroactive surface area to expose more active sites have been widely explored.

2.3.3.1. 3D structure materials. The catalysts with 3D structure can highly expose more edge sites. The amorphous MoS_2 nanoflowers were synthesized and the enhanced activity was obtained by synergistically structural and electronic modulations [221], and then a flower-like MoS_2-SiC hybrid structure was fabricated which showed superior HER activity with a low overpotential of 40 mV (Fig. 14a) [222]. Similarly, the ultrathin WS_2 nanoflakes were prepared (Fig. 14b) [223]. As the abundant accessible edges of this ultrathin nanoflakes, the catalyst showed high HER performance with an overpotential of 100 mV and a Tafel slope of 48 mV dec^{-1}. Besides, the hierarchical MoS_2 microboxes were synthesized to be used as a HER electrocatalyst, and it could also serve as an anode material for lithium-ion batteries (Fig. 14c) [224].

Table 4
Summary of HER performance of some two-dimension materials based on Mo and W.

Catalysts	Electrolyte	Loading (mg cm^{-2})	Overpotential (mV)	Tafel slope (mA cm^{-2})	Exchange current density (mA cm^{-2})	Stability	Ref.
MoS_2 NSs	0.5 M H_2SO_4	0.285	$\eta_{4.5}$ = 150	68	0.0389	1000 CV cycles	[155]
M-MoS_2 NSs	0.5 M H_2SO_4	0.043	η_{10} = 175	41	N/A	1000 CV cycles	[156]
Defect-rich MoS_2 NSs	0.5 M H_2SO_4	0.285	η_{13} = 200	50	0.00891	3000 CV cycles	[158]
MoN NSs	0.5 M H_2SO_4	0.285	η_{38} = 300	90	0.084	3000 CV cycles	[161]
$Co_{0.6}Mo_{1.4}N_2$ NSs	0.1 M $HClO_4$	0.24	η_{10} = 200	N/A	0.23	3000 CV cycles	[162]
Exfoliated WS_2 NSs.	0.5 M H_2SO_4	0.0065	N/A	60	0.02	120 h	[164]
O-MoS_2 NSs	0.5 M H_2SO_4	0.285	η_{126} = 300	55	0.0126	3000 CV cycles	[173]
N-MoS_2 NSs	0.5 M H_2SO_4	0.32	η_{100} = 121	41	0.52	5000 CV cycles	[174]
Se-MoS_2 NSs	0.5 M H_2SO_4	0.285	η_{43} = 400	55	N/A	9000 s	[175]
N-WS_2 NSs	0.5 M H_2SO_4	0.32	η_{100} = 197	69.69	0.174	5000 CV cycles	[176]
S-$MoSe_2$ NSs	0.5 M H_2SO_4	0.28	η_{30} = 156	60	N/A	10000 CV cycles	[177]
V-MoS_2 NSs	1 M H_2SO_4	0.285	N/A	69	N/A	1000 CV cycles	[178]
MoS_2 NSs/CNT	0.5 M H_2SO_4	0.136	N/A	44.6	N/A	2000 CV cycles	[182]
MoS_2/RGO NSs	0.5 M H_2SO_4	0.2	η_{23} = 200	41	N/A	500 CV cycles	[184]
MoS_2 NSs/GO	0.5 M H_2SO_4	0.204	η_{10} = 172	43	N/A	3000 CV cycles	[185]
$MoSe_2$ NSs/RGO	0.5 M H_2SO_4	0.285	η_{10} = 195	67	N/A	1000 CV cycles	[187]
MoS_2/$MoSe_2$ NSs/GO	0.5 M H_2SO_4	0.47	N/A	61	N/A	1000 CV cycles	[188]
MoS_2/C NSs	0.5 M H_2SO_4	0.57	η_{88} = 200	60	N/A	1000 CV cycles	[189]
C-MoS_2 NSs	0.5 M H_2SO_4	N/A	η_{10} = 159	56.1	N/A	1000 CV cycles	[190]
CNT@$MoSe_2$ NSs	0.5 M H_2SO_4	0.283	η_{10} = 178	58	N/A	3000 CV cycles	[191]
WS_2/rGO NSs	0.5 M H_2SO_4	0.562	η_{10} = 170	52	N/A	3000 CV cycles	[193]
MoS_2@S-C NSs	0.5 M H_2SO_4	N/A	η_{10} = 160	60	0.316	1000 CV cycles	[194]
MoS_2@N-C NSs	0.5 M H_2SO_4	0.217	η_{10} = 135	48	0.0242	1000 CV cycles	[195]
Mo_2C/N-C NSs	0.5 M H_2SO_4	0.566	η_{10} = 19	28.9	1.9	1000 CV cycles	[196]
MoS_2 NSs/N-RGO	0.5 M H_2SO_4	0.14	η_{10} = 56	41.3	0.72	5000 CV cycles	[197]
MoS_x/N-CNT NSs	0.5 M H_2SO_4	N/A	η_{10} = 110	40	0.0331	1000 CV cycles	[198]
S-rich MoS_2/N-C NSs	0.5 M H_2SO_4	N/A	η_{10} = 120	38	N/A	1000 CV cycles	[199]
MoO_2@N-MoS_2 NSs	0.5 M H_2SO_4	0.285	N/A	47.5	N/A	2000 CV cycles	[201]

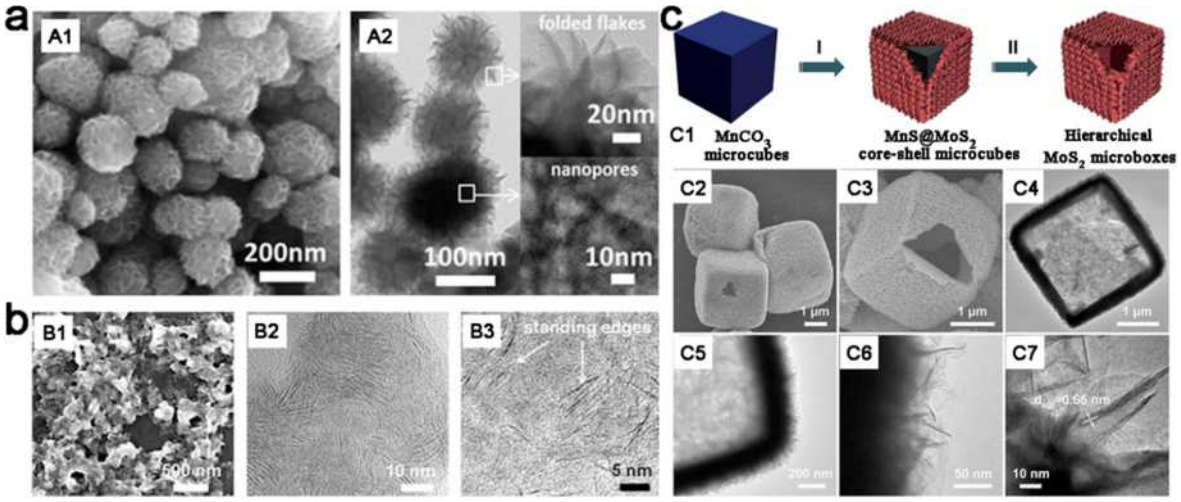

Fig. 14. (a) (A1) SEM and (A2) TEM images of MoS_2–SiC hybrid. (b) (B1) SEM and (B2, B3) high-resolution TEM images of WS_2 nanoflakes. (c) (C1) Schematic illustration of the template-assisted formation of hierarchical MoS_2 microboxes. (C2, C3) FESEM and (C4–C7) TEM images of hierarchical MoS_2 microboxes.

2.3.3.2. 3D integrated electrode. To avoid burying the active sites and low electron contact surface area caused by the insulated polymer binder, as well as alleviating the gas accumulations for stabilizing the electrode during electrolysis process, the 3D integrated HER electrodes are actively pursued. The MoS_2 nanosheets grown on the carbon cloth (CC) or carbon paper (CP) were studied and exhibited good activity [225–231]. Besides, the 3D integrated electrodes based on $MoSe_2$, Mo_2C, WS_2, WN and MoP were also fabricated and showed high activity because of the superior structures [232–238]. Recently, the porous Mo–W–P hybrid nanosheets grown on CC were synthesized through in situ phosphidation of Mo–W–O hybrid nanowires [239]. Thanks to the structural advantage and synergistic effect, the Mo–W–P/CC exhibited high HER activity with a low overpotential of 138 mV to achieve 100 mA cm^{-2} and a Tafel slope of 52 mV dec^{-1}. Besides, it showed excellent durability with no significant decay before and after 3000 CV cycles. Moreover, the 3D hierarchical porous NiMoN on CC was also

structured [240]. Chen et al. designed monolayer MoS_2 films on the curved surface of 3D nanoporous gold [241]. The HER activity was enhanced by lattice strain engineering. Furthermore, other cheap nanoporous metals to substitute the gold substrate are also considered. The MoS_2 nanoflowers coated on rGO paper were also synthesized [242], but the HER activity still needed to be improved. Moreover, the nanoflower-like MoO_2 on Ni foam were harvested, and exhibited high activity with a Tafel slope of 66 mV dec^{-1} and the 10 mA cm^{-2} obtained at 55 mV [243]. Some other catalysts with nanoflakes were also successfully fabricated [244,245].

In addition, component controllable $WS_{2(1-x)}Se_{2x}$ nanotubes on carbon fibers were constructed [246]. As a result, the catalyst which had more active sites and high conductivity exhibited excellent HER performance, and the composition $MoS_{1.0}Se_{1.0}$ displayed the highest HER activity among the $MoS_{2(1-x)}Se_{2x}$ [247]. Qiao et al. obtained the 3D WS_2 nanolayers through artificial assembly of 2D WS_2 nanolayers and P, N and O-doped graphene sheets by a vacuum filtration process [248]. The high activity (a Tafel slope of 52.7 mV dec^{-1} and 10 mA cm^{-2} obtained an overpotential of 125 mV) was gained owing to the 3D hierarchical porous structure, highly active 1T-WS_2 and heteroatoms-doping onto the graphene sheets. Table 5 lists some excellent HER performance based on three-dimension materials of Mo and W.

All the inspired ways detailed above afford new perspectives on the HER electrocatalysts based on Mo and W. In view of the intrinsic character and the well-designed structure, the Mo and W based catalysts have been comparable or even superior to the precious metal catalysts. Inspired by the process of identifying edge sites as the real active sites for HER, the HER mechanisms of other materials should be promoted. Furthermore, porous structure will not only lead to the high surface area to provide more active sites, but also facilitate sufficient transport of reactants and products. Without porous structure, the electrolyte is only able to contact the surface of catalysts, leading to the possible accumulation of electrons/ions/molecules and further decrease the reaction efficiency. Thereinto, nanowire catalysts with abundant porosity can enable rapid diffusion of ions and electrons favoring a better activity. And the porous nanosheets structure will provide the maximum number of edge sites, which are considered as active sites for many electrochemical reactions. While for the 3D porous structure, more pathways for ion and mass transport with a minimal diffusion resistance giving facile electrocatalytic kinetics are provided. On this basis, it is still of great challenges to explore more facile and scalable methods to form robust electrocatalysts for practical applications.

2.4. Catalysts based on Fe, Co and Ni

Over the past decades, the transition-metal (Fe, Co, Ni) based materials have been explored as potential alternatives toward HER because of their earth abundant and environmentally friendly nature, and considerable catalytic performances. Here, we introduce the catalysts based on single element and the compounds of Fe, Co and Ni.

2.4.1. Catalysts based on Fe

Over the past decades, various HER catalysts based on the most abundant and cheapest Fe, have been attracted more attentions by virtue of their highly catalytic activities. Among them, the iron phosphides are the successful examples. For instance, FeP nanoparticles were prepared and showed good activity [249,250], and the HER performance could be enhanced after stability test due to reduce surface-charge-transfer resistance in the HER process [249]. Then, the nanoparticles combined with carbon materials were synthesized to fast electron transport and avoid agglomeration [251–256]. Thereinto, the Fe nanoparticles encapsulated in carbon were also fabricated [257,258], Especially, to protect the active metal nanoparticles from oxidation and the desired access of the reactants to the vicinity of the metal, the Fe encapsulated in a single-layer carbon cage were reported, which showed a low Tafel slope of 40 mV dec^{-1} and overpotential of 77 mV to achieve 10 mA cm^{-2} [257]. In addition, the FeP nanosheets were discussed [259], but the activity should be improved.

For nanowires, it possesses many structure advantages, such as the high aspect ratios, few lattice boundaries and smooth crystal planes. Thus, the FeP nanowire arrays were widely synthesized to construct the 3D integrated electrode, and exhib-

Table 5
Summary of HER performance of some three-dimension materials based on Mo and W.

Catalysts	Electrolyte	Loading (mg cm^{-2})	Overpotential (mV)	Tafel slope (mA cm^{-2})	Exchange current density (mA cm^{-2})	Stability	Ref.
MoS_2 nanoflowers	0.5 M H_2SO_4	0.071	$\eta_{13.8}$ = 300	52	0.014	1000 CV cycles	[221]
WS_2 nanoflakes	0.5 M H_2SO_4	0.35	N/A	48	N/A	10000 CV cycles	[223]
MoS_{2+x}/N-CNT/CP	0.5 M H_2SO_4	N/A	η_{10} = 160	36	N/A	1 h	[225]
CF-NG@MoS_2	0.5 M H_2SO_4	0.32	η_{10} = 170	53	N/A	1000 CV cycles	[228]
MoS_2 NSs/CC	0.5 M H_2SO_4	N/A	η_{10} = 224	58	N/A	1000 CV cycles	[229]
MoP sponge	0.5 M H_2SO_4	N/A	η_{10} = 105	126	3.052	60000 s	[233]
WS_2/GO/Ni foam	0.5 M H_2SO_4	6	η_{10} = 119	43	N/A	2000 CV cycles	[234]
MoP_2 NSs/CC	0.5 M H_2SO_4	7.8	η_{10} = 58	63.6	0.83	2000 CV cycles	[235]
$MoSe_2$ NSs/CC	0.5 M H_2SO_4	N/A	η_{10} = 220	76	0.0153	1000 CV cycles	[237]
Mo-W-P/CC	0.5 M H_2SO_4	N/A	η_{100} = 138	52	0.288	4000 CV cycles	[239]
MoO_2/Ni foam	1 M KOH	4.5	η_{10} = 55	66	1.8	15,000 CV cycles	[243]
WS_2@P, N, O-graphene	0.5 M H_2SO_4	0.113	η_{10} = 125	52.7	0.131	20 h	[248]

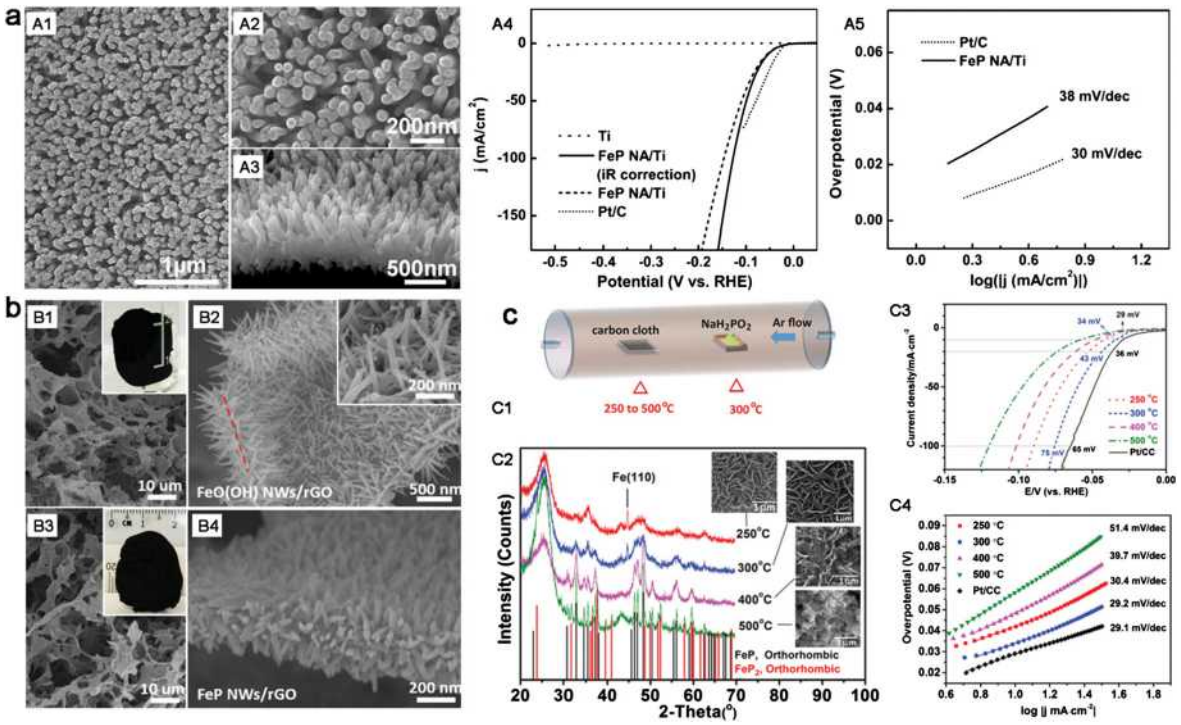

Fig. 15. (a) (A1) Low- and (A2) high-magnification SEM images of FeP NA/Ti. (A3) Cross-section SEM image of FeP NA/Ti. (A4) Polarization curves and (A5) Tafel plots of different samples. (b) (B1, B2) and (B3, B4) SEM images of the FeO(OH) NWs/rGO precursor and FeP NWs/rGO. (c) (C1) Schematic illustration for the phosphidation process. (C2) XRD and SEM images for the FeOOH/carbon cloth samples after phosphidation at various temperatures. (C3) Polarization curves for the catalysts prepared at different phosphidation temperatures. (C4) Tafel slopes extracted from the polarization curves.

ited better HER activity than others [260–263]. Notably, the FeP nanowire arrays on Ti plate were developed from its β-FeOOH nanowire arrays/Ti precursor through the low temperature phosphidation reaction [262], which was used directly as the self-supported 3D HER electrode and showed extremely high catalytic activity and good stability in acidic medium with a low Tafel slope of 38 mV dec^{-1} and 10 mA cm^{-2} obtained at the low overpotential of 55 mV (Fig. 15a). Then, the porous FeP nanowire arrays on graphene sheets were gained and showed good activity (Fig. 15b) [261]. Similarly, the rugae-like FeP nanocrystal assembly on CC were fabricated which exhibited exceptional activity with Tafel slope of about 29.2 mV dec^{-1}, and impressively, the required overpotential to reach 10 mA cm^{-2} is only 34 mV (Fig. 15c) [264]. Their high activity can be attributed to the elaborate structure which favors fast electron transport along the nanowires, releases formed gas bubble immediately, and allows easy diffusion of electrolyte into all the active sites and consequently more efficient use of the entire electrode. Besides, the FeS_2 nanostructures were also explored as efficient catalysts for the HER [265–267]. Overall, the facile and low cost of Fe, admirable HER activity and optimizable fabrication process all confirmed its greatly promising feasibility in electrochemical water splitting.

2.4.2. Catalysts based on Co

As for Co based HER catalysts, more efficient candidates mainly concentrate upon chalcogenides and phosphides. And optimizing catalysts morphology or tuning electronic structure is the focus to improve their activity.

2.4.2.1. Chalcogenides. Cobalt sulfides, especially those with fine nanostructures, are emerging as an attractive HER catalysts. The Co-S film was prepared by electrochemical deposition and showed an active HER catalyst in neutral condition, but the catalytic performance in acidic media is inferior to that in basic [268]. Specific morphology of CoS_2 including film, microwire and nanowire was prepared by controlling synthesis (Fig. 16) [269], wherein the CoS_2 nanowire showed superior catalytic activity than others owing to the increased effective electrode surface area and easily detaching of hydrogen gas bubbles from the electrode surface. This clearly demonstrated the relationship of structure and property. Recently, the amorphous cobalt sulfide was also identified as the HER catalyst, and the high density of accessible S atoms was considered to account for highly active performance based on the combination of Raman and X-ray absorption spectroscopy (XAS) experiments [270].

Substituting non-metal elements to tune the electronic structure to change ΔG_{H*} can also further improve the activity. For instance, nanostructured ternary pyrite-type CoPS electrode was synthesized which could achieve 10 mA cm^{-2} at an overpotential of 48 mV [271]. And then the CoS|P nanoparticles grown on CNTs were designed and showed excellent activity

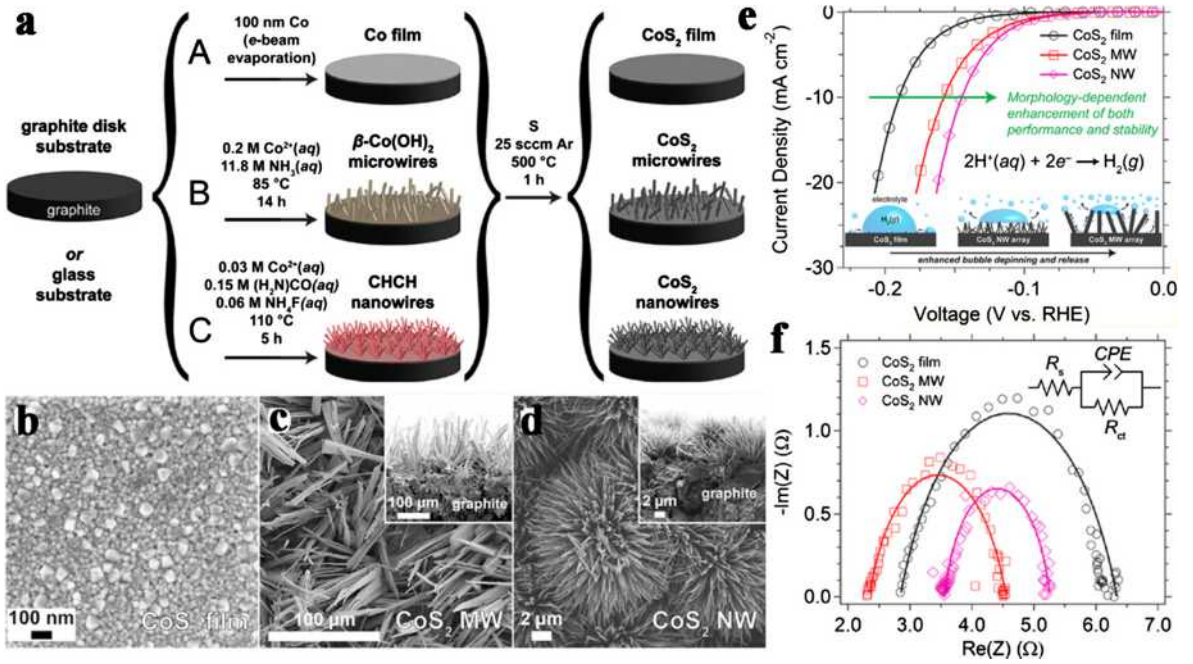

Fig. 16. (a) Schematic depictions of the preparation of a cobalt pyrite film, microwire array, or nanowire array on a graphite disk substrate. (b) A polycrystalline CoS_2 film. (c) CoS_2 MWs. (d) CoS_2 NWs on graphite. (e) Electrochemical characterization of CoS_2 film, microwire array, and nanowire array electrodes for HER. (f) Electrochemical impedance spectroscopy Nyquist plots of the different CoS_2 electrodes.

[272]. Furthermore, the effect of phosphorus substitution to the chemical stability and catalytic durability was revealed by the DFT calculations and XAS data. Besides, the CoS_2 combined with rGO and CNT were also synthesized [273]. Thanks to the special structural and electrical features of rGO, highly conductive and porous properties, the synergistic effect of them endowed CoS_2/rGO-CNT with high HER activity.

The widely accepted integrated electrodes are also fabricated. The metallic Co_9S_8 nanosheets on CC were synthesized [274]. Though the activity should be further improved, the stability could retain 100 h under neutral conditions. And the P doped CoS_2 nanosheets arrays on CP were also discussed. Thereinto, the enhancing HER performance was attributed to P doping which played significant roles in promoting charge transfer, facilitating proton adsorption as well as the integrated structure [275].

As another important chalcogenides, $CoSe_2$ has also been widely used as the electrocatalysts for HER. Cubic pyrite-type $CoSe_2$ was prepared [276], and the $CoSe_2$ nanoparticles on graphite disks showed high HER activity with a Tafel slope of 40 mV dec^{-1}. Then the polymorphic $CoSe_2$ with mixed orthorhombic and cubic phases were synthesized [277], and the low onset overpotential of 70 mV and small Tafel slope of 30 mV dec^{-1} were harvested by this catalyst. Recently, a systematic and in-depth understanding of the clear relationship between $CoSe_2$ crystal structure and intrinsic electrocatalytic activity was revealed by the X-ray absorption fine structure (XAFS) analysis and DFT calculations [278]. The cubic phases exhibited greatly enhanced HER activity over orthorhombic under alkaline conditions because of the higher electrical conductivity, ideal water adsorption energy, and faster transformation efficiency of H_{ads} into hydrogen.

Besides, Cui et al. synthesized the 3D electrode of $CoSe_2$ nanoparticles on CP (Fig. 17a) [279], which showed high HER activity and stability with a Tafel slope about 40 mV dec^{-1} and a low overpotential of 180 mV at 100 mA cm^{-2}. Then, the $CoSe_2$ nanowires array on CC were also prepared (Fig. 17b) [280], and the resulted $CoSe_2$ nanowires/CC exhibited excellent catalytic activity with the overpotential of only 164 mV to achieve 100 mA cm^{-2}, and high durability with 48 h continuous operation in acidic media. In spite of other complex and high energy input synthesis processes, this work provided a cost-effective method to design the arrayed transition-metal chalcogenide electrode for large-scale applications. The other integrated electrodes, such as $CoSe_2$ nanoneedles/Ti foils and ternary $CoS_{2x}Se_{2(1-x)}$ nanowires/CP were also synthesized for the HER and exhibited high activity [281–283].

2.4.2.2. Phosphides. Another large class of Co based catalysts, Co_xP, can be facilely and large-scale synthesized by facile low-temperature phosphidation reaction [284]. Three different morphologies of nanostructured CoP, including nanowires, nanosheets and nanoparticles, were prepared [285]. Similarly, CoP nanowires possessed the highest catalytic activity and stability. Then, the CNTs decorated with Co_xP nanocrystals were prepared to improve the conductivity and exhibited high activity [286,287]. Recently, Guo et al. developed CoP on various carbon materials, including imporous rGO, macroporous carbon (MPC), mesoporous carbon vesicles (MCVs) and ordered mesoporous carbon (OMC) [288]. Thereinto, the CoP-OMC

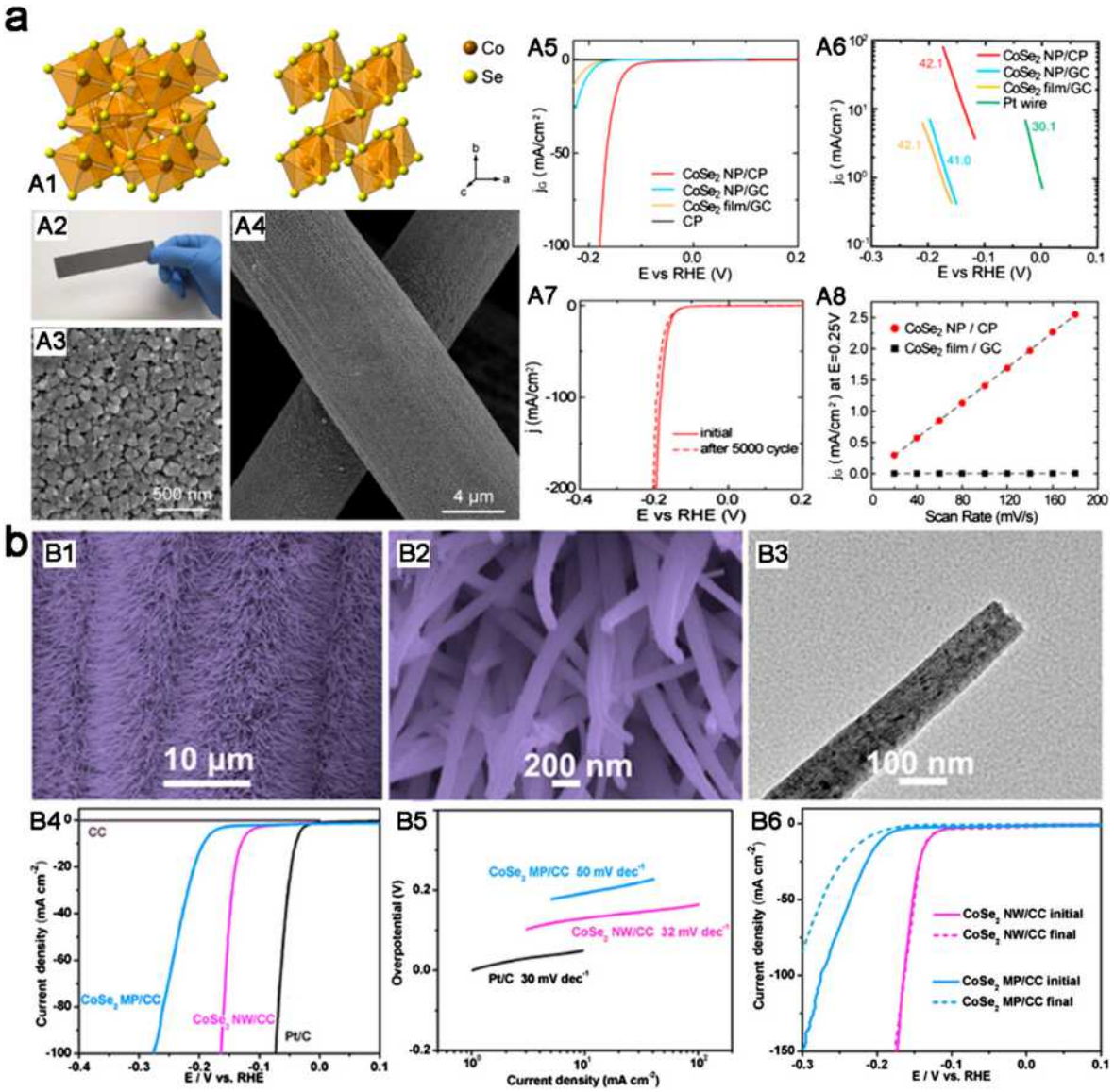

Fig. 17. (a) (A1) Crystal structure of $CoSe_2$ in cubic pyrite-type phase (left) and orthorhombic macarsite-type phase (right). (A2) Photograph, (A3) SEM image and (A4) High-resolution SEM image of $CoSe_2$/CP. (A5) Polarization curves of different samples. (A6) Corresponding Tafel plots. (A7) Stability tests of $CoSe_2$ NPs/CP catalyst. (A8) Capacitive currents as a function of scan rate. (b) (B1, B2) SEM and (B3) TEM images of $CoSe_2$ NW/CC. (B4) Polarization curves, (B5) Tafel plots and (B6) Stability tests.

displayed the highest activity with an onset potential of 78 mV, a Tafel slope of 57 mV dec^{-1} and outstanding long-term stability, as well as the 10 mA cm^{-2} could be achieved at overpotential of 112 mV. These indicated that the HER performance was deeply relied on highly active catalytic sites, abundant mesoporous nanostructures and excellent electron transfer kinetics.

The integrated electrodes based on CoP are widely considered because of the simple synthesis process and high activity [289–291]. For instance, the CoP/Ti electrodes was constructed [289], which exhibited high activity with the 20 mA cm^{-2} at only an overpotential of 85 mV. Afterwards, the CC was chose as a 3D scaffold, then nanoporous CoP nanowire arrays on CC were developed via low-temperature phosphidation of the Co(OH)F/CC precursor [291]. This catalyst showed excellent catalytic activity with an onset potential of 38 mV, a Tafel slope of 51 mV dec^{-1}, and retained its activity for at least 80000 s in acidic media. Not only that, the catalyst could be used in both neutral and basic conditions (Fig. 18). Besides, CoP films on a Cu substrate were also designed, and showed an 85 mV overvoltage at 10 mA cm^{-2} [292]. These high activities have a close correlation with the integrated structure.

Furthermore, the N-doped carbon-coated Co nanorod arrays supported on a Ti mesh were synthesized [293], and Zou et al. synthesized cobalt-embedded nitrogen-rich CNTs as a highly active electrocatalyst for HER [294]. The Co-NRCNTs

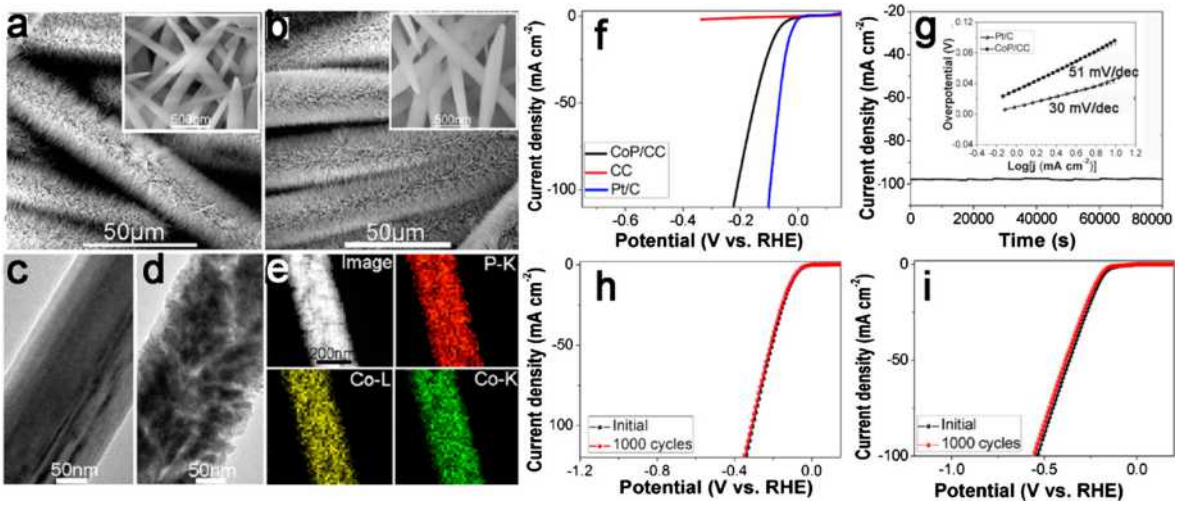

Fig. 18. SEM images of (a) Co(OH)F/CC and (b) CoP/CC. TEM images of (c) Co(OH)F and (d) CoP nanowire. (e) STEM image and EDX elemental mapping of P and Co for the CoP nanowire. (f) Polarization curves of different samples. (g) Time-dependent current density curve for CoP/CC under static overpotential of 200 mV for 80000 s and (inset) Tafel plots. Polarization curves of CoP/CC in (h) 1.0 M PBS (pH 7) and (i) 1.0 M KOH (pH 14).

exhibited good activity with a small Tafel slope of 69 mV dec^{-1} and the 10 mA cm^{-2} obtained at 260 mV. The result indicated that N dopants, concomitant structural defects and metal nanoparticles might attribute to its catalytic activity. Recently, the Co-C-N complex was synthesized for HER, and exhibited high activity that the 100 mA cm^{-2} could be achieved at about 200 mV [295–297]. In addition, the cobalt boride was also prepared for HER, and exhibited good performance [298,299].

2.4.3. Catalysts based on Ni

As the second highest abundance and lowest price after Fe among non-precious metals, Ni is also used to design catalysts, and it is proved that Ni has the highest HER activity among the non-precious metals because of the appropriate ΔG_{H*} [50]. Typically, three different shapes of nickel structures, including dendrites, particles and films, were formed on the glassy carbon by electrodeposition [300]. Therein, Ni dendrites were proved to have superior active and stable HER performance than others in alkaline electrolyte because of a structural advantage to decrease the overpotential of HER and large electrochemical surface area. The wool-ball-like Ni-CNTs composite were synthesized and showed favorable activity as the large surface area and interaction between Ni matrix and CNTs [301]. Another nickel–carbon-based catalyst was also synthesized by carbonization of MOFs (Fig. 19), and electrochemical potential was applied to activate this Ni–carbon catalyst to obtain atomically isolated Ni species anchored on graphitized carbon which exhibited excellent activity with 10 mA cm^{-2} at a low

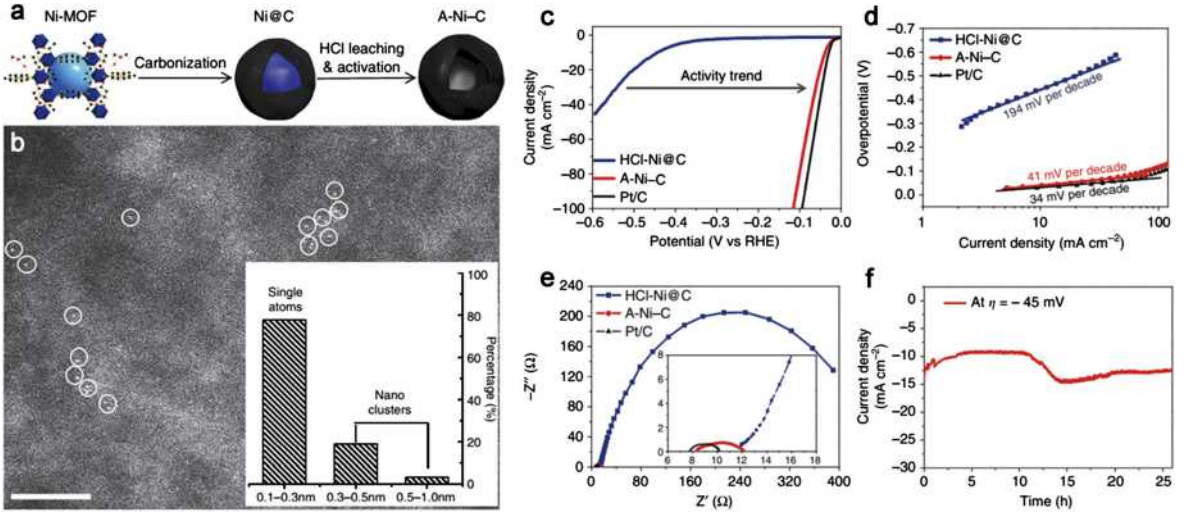

Fig. 19. (a) Schematic diagram of synthesis and activation process of the Ni–C catalysts. (b) HAADF STEM image of A-Ni–C and size distribution. (c) LSV curves of different samples. (d) Tafel plots obtained from LSV curves. (e) EIS spectra of samples. (f) Chronoamperometric curve of A-Ni–C.

overpotential of 34 mV, a Tafel slope of 41 mV dec^{-1}, a large exchange current density of 1.2 mA cm^{-2} and the long durability of 25 h [302]. This opens a new area of tuning structure and functionality of metal-carbon-based catalyst at atomic scale, and indicating the large potential of single atom catalysis.

The hollow and multifaceted Ni_2P nanoparticles were synthesized, and then deposited it on Ti foils [303], but the stability needed to be improved, especially in basic solutions. And then, Feng et al. prepared polydispersed Ni_2P nanoparticles deposited on glass carbon [304]. It clearly showed the stability was improved both in acidic and basic solutions. Recently, monocrystalline $Ni_{12}P_5$ hollow spheres were prepared because of the considering of ultrahigh specific surface areas [305], and the NiS and Ni_3S_2 nanoparticles were also synthesized to investigate the structure effects for HER, and then the importance of an appropriate atomic configuration was illustrated [306].

As we all know, the integrated electrodes can avoid the adverse effect of binder use. Thus, P-rich NiP_2 nanosheet arrays supported on CC (NiP_2 NS/CC) were constructed [307], which showed higher catalytic activity than NiP_2 microparticles/CC using Nafion. This was mainly attributed to the following factors: (i) the direct intimate contributed to electrons transfer from CC to NiP_2 during proton reduction process; (ii) the high electrical conductivity of transition metal phosphides favored fast electron transport along NiP_2 NS; (iii) the 3D structure of NiP_2 NS/CC and high special surface area of NiP_2 NS ensure the efficient electrolyte diffusion and maximum utilization of more active sites; (iv) the binder-free feature not only effectively avoided blocking of active sites and inhibited diffusion, but resulted in improved conductivity. Moreover, the NiP_2 NS/CC exhibited excellent stability with at least 57 h continuous electrolysis, which was superior than Ni_2P/Ti and Ni_2P/glass carbon, and it also well performed in alkaline conditions. Ni_2P films grown on Ti plate was also synthesized [308], and showed remarkable catalytic activity in acidic media with a Tafel slope of 60 mV dec^{-1} and the 100 mA cm^{-2} at 188 mV overpotential, meanwhile it maintained its catalytic activity for 15 h. Besides, $Ni_{12}P_5$ nanoparticles loaded on the surface of silicon nanowires were synthesized, and proved to be an robust catalyst for HER [309]. In addition, the nickel arsenide was constructed for integrated HER electrode and showed high catalytic activity [310–312].

2.4.4. Compounds of Fe, Co and Ni

In addition to the monometallic catalysts, considering from the other metal introducing might cause the surface area and electronic structure changed, fine structures with bimetallic or multicomponent are constructed as efficient electrocatalysts toward HER. The DFT was used to investigate HER mechanism of [NiFe] hydrogenase [313], and revealed the importance of ΔG_{H*}. In general, doping metal atoms is often used to modify the electronic structure to optimize ΔG_{H*} and therefore improve HER catalytic activity. Keep this in mind, the Co-doped iron pyrite (FeS_2) on CNT ($Fe_{1-x}Co_xS_2$/CNT) hybrid catalysts were fabricated [314]. Through tuning Co doping ratio, the resulted $Fe_{0.9}Co_{0.1}S_2$/CNT hybrid catalyst exhibited high activity with about 120 mV overpotential at 20 mA cm^{-2}, a Tafel slope of 46 mV dec^{-1}, and long-term durability over 40 h in acid electrolyte. Recently, hollow Co-based bimetallic sulfide ($M_xCo_{3-x}S_4$, M = Zn, Ni, and Cu) polyhedras were prepared by a simple self-template strategy [315]. Finally, the combination of hollow structure and homoincorporation of a second metal significantly enhanced the activity of Co_3S_4 as the homogeneous doping optimized the ΔG_{H*} and improved the electrical conductivity (Fig. 20). Besides, the Fe-Ni sulfide ultrathin nanosheets were synthesized and proved to be excellent HER catalyst because of the high specific surface area, facile ion transport and charge transfer, abundant electrochemical active sites

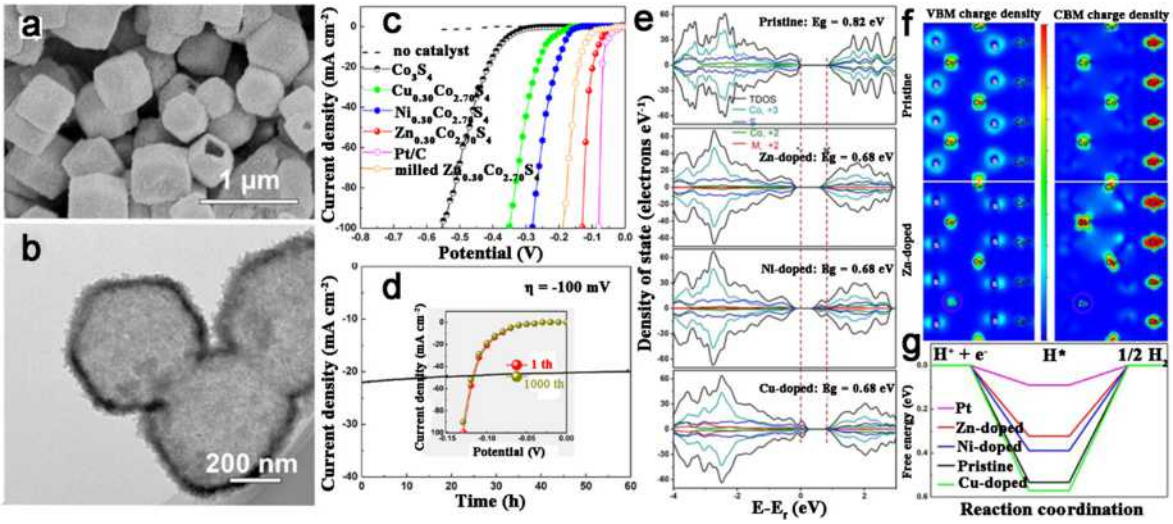

Fig. 20. (a) SEM and (b) TEM images of $Zn_{0.30}Co_{2.70}S_4$. (c) Polarization data of different samples. (d) Time-dependent current density curve of HER over $Zn_{0.30}Co_{2.70}S_4$. (e) Projected density of states of pristine and Zn-, Ni-, and Cu-doped Co_3S_4. (f) Difference charge density of valence band (left) and conduction band (right) in pristine and Zn-doped Co_3S_4. Red and blue colors represent electron accumulation and electron depletion. (g) Calculated free-energy diagram of HER at equilibrium potential on pristine and Zn-, Ni-, and Cu-doped Co_3S_4.

as well as the suitable ΔG_{H*} [316]. Inspired by the idea that Ni species functionalized $CoSe_2$ nanobelts to be an efficient catalyst for HER, the Ni/NiO/$CoSe_2$ nanocomposite was synthesized [317]. However, the high temperature annealing for generating over-oxidized NiO shells would increase the internal resistance and block the active sites. So the excellent activity was obtained with an onset potential of about 30 mV, a small Tafel slope of 39 mV dec^{-1} and the exchange current density of 1.4×10^{-2} mA cm^{-2} in acid solutions. They attributed the enhanced property to the compact configuration of the Ni/NiO core/shell nanoparticles anchored onto the spacious $CoSe_2$ nanobelts and provided a referenced strategy to couple with mul-

Table 6
Summary of HER performance of some excellent catalysts based on Fe, Co and Ni.

Catalysts	Electrolyte	Loading (mg cm^{-2})	Overpotential (mV)	Tafel slope (mA cm^{-2})	Exchange current density (mA cm^{-2})	Stability	Ref.
FeP NPs	0.5 M H_2SO_4	N/A	η_{10} = 154	65	N/A	6000 s	[249]
FeP–GS	0.5 M H_2SO_4	0.28	η_{10} = 123	50	0.12	1000 CV cycles	[252]
FeP_2/C	0.5 M H_2SO_4	0.425	N/A	66	0.00175	2000 CV cycles	[253]
HM-FeP@C	0.5 M H_2SO_4	N/A	η_{10} = 115	56	0.191	3000 CV cycles	[255]
FeP–CS	0.5 M H_2SO_4	0.28	η_{10} = 122	56	0.12	1000 CV cycles	[256]
C-Fe NPs	0.5 M H_2SO_4	0.18	η_{10} = 77	40	0.19	1000 CV cycles	[257]
FeP arrays/CC	0.5 M H_2SO_4	1.5	η_{10} = 58	45	0.5	5000 CV cycles	[260]
P-FeP NWs/rGO	0.5 M H_2SO_4	0.204	η_{10} = 107	58.5	N/A	1000 CV cycles	[259]
FeP NWs/Ti	0.5 M H_2SO_4	3.2	η_{10} = 55	38	0.42	15 h	[261]
FeP NSs/CC	0.5 M H_2SO_4	4.9	η_{10} = 34	29.2	0.68	24 h	[262]
CoS_2 NWs	0.5 M H_2SO_4	1.7	η_{10} = 145	51.6	N/A	Corrosion	[269]
CoPS nanoplates	0.5 M H_2SO_4	N/A	η_{10} = 48	56	0.984	36 h	[271]
CoS|P/CNTs	0.5 M H_2SO_4	1.6	η_{10} = 48	55	1.14	2000 CV cycles	[272]
CoS_2/RGO-CNT	0.5 M H_2SO_4	1.15	η_{10} = 142	51	0.0626	500 CV cycles	[273]
Co_9S_8 NSs/CC	0.5 M H_2SO_4	0.33	η_{10} = 152	N/A	N/A	11 h	[274]
	pH = 7		η_{10} = 175			100 h	
	1 M KOH		η_{10} = 270			30 h	
P-CoS_2 NSs/CP	0.5 M H_2SO_4	N/A	η_{10} = 67	50	0.47	3000 CV cycles	[275]
Cubic-$CoSe_2$/CC	1 M KOH	N/A	η_{10} = 190	85	N/A	12 h	[278]
$CoSe_2$ NPs/CP	0.5 M H_2SO_4	2.5	η_{100} = 180	42	0.0049	5000 CV cycles	[279]
$CoSe_2$ nanoneedle/Ti	0.5 M H_2SO_4	N/A	η_{20} = 125	45	0.043	3000 CV cycles	[281]
$Co(S_xSe_{1-x})_2$ NWs/CP	0.5 M H_2SO_4	N/A	η_{10} = 104	44	N/A	5000 CV cycles	[282]
Co_xP	0.5 M H_2SO_4	0.56	η_{10} = 144	58	N/A	4 h	[284]
CoP NWs	0.5 M H_2SO_4	0.35	η_{10} = 110	54	N/A	50 h	[285]
CoP/CNT	0.5 M H_2SO_4	0.285	η_{10} = 122	54	0.13	18 h	[286]
CoP–OMC	0.5 M H_2SO_4	0.285	η_{10} = 112	57	0.161	2000 CV cycles	[288]
CoP NPs/Ti	0.5 M H_2SO_4	2	η_{20} = 85	50	N/A	24 h	[289]
CoP NWs/CC	0.5 M H_2SO_4	0.92	η_{10} = 67	51	0.288	5000 CV cycles	[291]
Co@N-C/Ti	0.5 M H_2SO_4	11.2	η_{10} = 106	78.2	N/A	1000 CV cycles	[293]
Co-N-CNTs	0.5 M H_2SO_4	0.28	η_{10} = 260	80	0.01	8.5 h	[294]
	pH = 7		η_{10} = 540	N/A	N/A	10 h	
	1.0 M KOH		η_{10} = 370				
Co-C-N/CF	0.5 M H_2SO_4	N/A	η_{10} = 138	55	N/A	2000 CV cycles	[296]
	pH = 7		η_{10} = 273	107			
	1.0 M KOH		η_{10} = 178	102			
CoN_x/C	0.5 M H_2SO_4	2	η_{10} = 133	57	0.07	5000 CV cycles	[297]
CoB	pH = 7	N/A	η_{10} = 251	75	0.25	1000 CV cycles	[299]
Ni@C	0.5 M H_2SO_4	0.283	η_{10} = 34	41	1.2	25 h	[302]
Ni_2P NPs	0.5 M H_2SO_4	1	η_{100} = 180	46	0.033	500 CV cycles	[303]
$Ni_{12}P_5$ hollow spheres	0.5 M H_2SO_4	0.71	η_{10} = 144	46	N/A	3000 CV cycles	[305]
NiP_2 NSs/CC	0.5 M H_2SO_4	4.3	η_{10} = 75	51	0.26	57 h	[307]
Ni_2P NPs/Ti	1 M H_2SO_4	2	η_{100} = 188	60	N/A	1000 CV cycles	[308]
NiSe NWs/Ni foam	1 M H_2SO_4	2.8	η_{10} = 96	120	N/A	1000 CV cycles	[310]
Porous $NiSe_2$/Ni foam	0.5 M H_2SO_4	N/A	η_{10} = 143	49	0.0157	2000 CV cycles	[311]
$Fe_{1-x}Co_xS_2$/CNT	0.5 M H_2SO_4	7	η_{20} = 120	46	N/A	1000 CV cycles	[314]
Hollow $Zn_{0.30}Co_{2.70}S_4$	0.5 M H_2SO_4	0.285	η_{10} = 80	47.5	0.15	1000 CV cycles	[315]
	pH = 7		η_{10} = 90	N/A	N/A	N/A	
	1.0 M KOH		η_{10} = 85				
Fe-Ni-S NSs	0.5 M H_2SO_4	N/A	η_{10} = 105	40	0.02	40 h	[316]
Ni/NiO/$CoSe_2$ nanocomposite	0.5 M H_2SO_4	0.28	N/A	39	0.014	N/A	[317]
Ni–Co–P nanocubes	1.0 M KOH	N/A	η_{10} = 150	60.6	N/A	1000 CV cycles	[318]
CoMn-S@NiO/CC	1.0 M KOH	6.9	η_{100} = 253	147.3	N/A	12 h	[319]
Mn-CoP NSs/Ti	0.5 M H_2SO_4	5.61	η_{10} = 49	55	N/A	1000 CV cycles	[320]
	pH = 7		η_{10} = 86	52			
	1.0 M KOH		η_{10} = 76	82			
Co_9S_8-Ni_xS_y/Ni foam	1.0 M KOH	9	η_{10} = 163	88	N/A	12 h	[321]
$NiCo_2S_4$ NFs/Ni foam	1.0 M KOH	N/A	η_{10} = 65	84.5	N/A	10000 s	[323]

tifunctional nanostructures together to design effective catalysts. Besides, nickel cobalt phosphides quasi-hollow nanocubes were also fabricated [318].

The integrated electrode based on multicomponent catalysts are also designed [319–323]. A novel Co_9S_8–Ni_xS_y/Ni foam composite was prepared through the thermal decomposition of a cobalt–thiourea molecular precursor [321], and self-assembled ultrathin $NiCo_2S_4$ nanoflakes grown on Ni foam were synthesized by the complete sulfidation of networked ultrathin NiCo-layered double hydroxide nanoflakes [323]. The advantages of this unique architecture, such as the ultrathin and porous $NiCo_2S_4$ nanoflakes which can provide a huge number of exposed active sites, the highly-conductive Ni foam which can promote the transfer of electrons, and the 3D networked structure which can facilitate the diffusion and penetration of electrolyte, all contributed to the enhanced HER activity. Table 6 lists some excellent HER performance of catalysts based on Fe, Co and Ni.

Albeit with relatively low stability, Fe, Co and Ni based catalysts are highly desirable in view of their obvious advantages including high abundance, low-cost, environmentally friendly and high catalytic activity. It is worth noting that the Fe, Co and Ni based catalysts are usually active for oxygen evolution reaction (OER) [324–333], the anode reaction of water splitting, such as CoO_x@CN [332], CP/CTs/Co-S electrode [325], FeP on CC [331], endowing them as the promising bifunctional catalysts for HER and OER operating in the same electrolyte for overall water splitting, which are very valuable for the practical application. Besides, the catalysts based on Cu, Sn, Ti and V are also synthesized to be used as electrocatalysts for HER, but its catalytic activity still need to be improved [334–339].

2.5. Metal free catalysts based on carbon

In view of terrestrial scarcity and high cost of precious metal catalysts, and environment issues caused by metal releasing of the non-precious metal catalysts, metal-free catalysts based on carbon for HER have aroused intensive research interests. The ordered carbon nitride grown on various substrates (FTO, TiO_2) were explored as HER electrodes in neutral and alkaline environments [340]. Then, the graphitic-carbon nitride coupled with nitrogen-doped graphene (C_3N_4@NG) was fabricated and exhibited the overpotential of 240 mV to achieve 10 mA cm^{-2} and a Tafel slope of 51.5 mV dec^{-1} [341]. The thermodynamic calculations revealed that the unusual electrocatalytic performance was attributed to a synergistic effect of this hybrid nanostructure, where g-C_3N_4 provided highly active hydrogen adsorption sites, while N-graphene facilitated electron-transfer process for the proton reduction.

In addition, the single-wall CNTs and some graphitic carbons also show catalytic activity after treatment [342]. And the pristine CNTs can be activated as a highly active metal free electrocatalyst by acidic oxidation and then further cathodic pretreatment [343]. Afterwards, an onset potential of 100 mV, and the Tafel slope of 71 mV dec^{-1} were determined for this treated CNTs. Moreover, the negligible current loss indicated its good corrosion stability even after long-term test. Meanwhile, SWCNTs were also verified to acquire the similar result. Because of the satisfactory properties of stability, conductivity and surface modifying, CNTs may have better HER activity compared to $C_{60}(OH)_8$ [344] and C_3N_4.

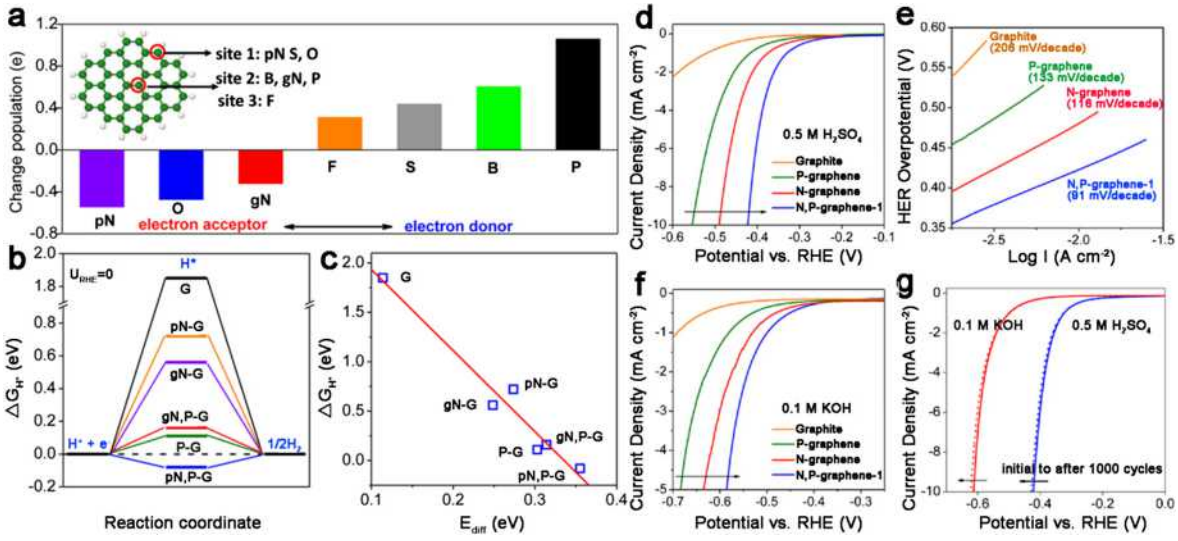

Fig. 21. (a) NBO population analysis of six different nonmetallic heteroatoms in graphene matrix. pN and gN represent pyridinic and graphitic type of N, respectively. Inset shows the proposed doping sites for different elements, sites 1 and 2 are the edge and center in-plane sites, respectively, and site 3 is an out-of-plane center site in graphene. (b) The calculated free energy (ΔG_{H^*}) diagram for HER at the equilibrium potential (U_{RHE} = 0 V) for N- and/or P-doped graphene models. (c) Relationship between ΔG_{H^*} and E_{diff} for various models. Polarization curves and the corresponding Tafel plots of N- and/or P-doped graphene electrocatalysts in (d, e) 0.5 M H_2SO_4 and (f) 0.1 M KOH. (g) Stability tests.

Nowadays, heteroatom doping has become an effective way to tailor the electronic structure of carbon-based materials and thus enhance the catalytic activity [345,346]. The metal-free, B-substituted graphene (B-SuG) was demonstrated as an effective electrocatalyst for HER with a Tafel slope of 99 mV dec^{-1} and fine stabilization [347]. Recently, the borocarbonitride sheets were fabricated as excellent catalysts for HER by experiment and theoretical studies [348]. And the activity can be further improved by compositional and morphological modifications.

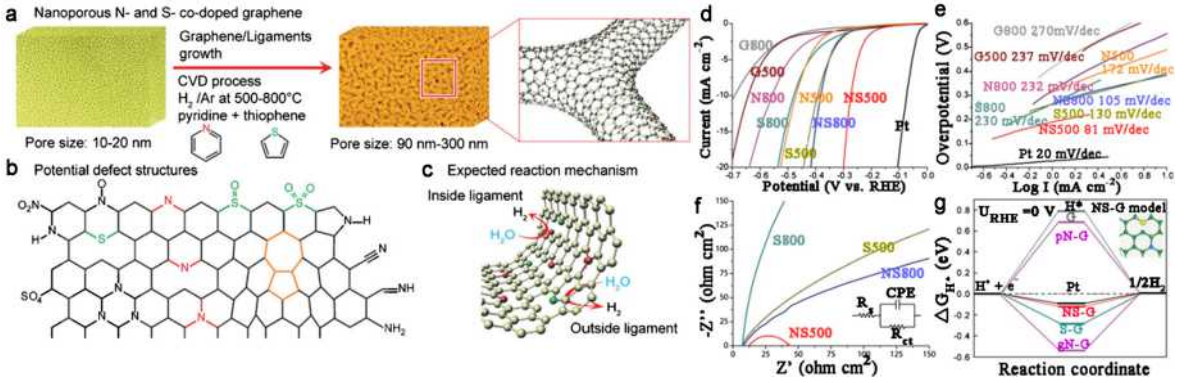

Fig. 22. (a) Preparation of nanoporous NS-doped graphene by CVD. (b) Potential defect structures in NS-doped nanoporous graphene. (c) Expected reaction mechanism on nanoporous graphene. (d) CV curves of different samples. (e) Tafel plots for the different graphene samples. (f) Electrochemical impedance spectroscopy of the graphene samples. (g) DFT-calculated HER activities of chemically doped nanoporous graphenes with a geometric lattice defect.

Table 7
Summary of HER performance of some excellent metal free catalysts.

Catalysts	Electrolyte	Loading (mg cm^{-2})	Overpotential (mV)	Tafel slope (mA cm^{-2})	Exchange current density (mA cm^{-2})	Stability	Ref.
C_3N_4@NG	0.5 M H_2SO_4	0.1	η_{10} = 240	51.5	0.00035	1000 CV cycles	[341]
Activated CNTs	0.5 M H_2SO_4	N/A	η_{10} = 220	71.3	0.016	4000 CV cycles	[343]
B-GR	0.5 M H_2SO_4	N/A	N/A	99	0.0014	18 h	[347]
$B_xC_yN_z$	0.5 M H_2SO_4	N/A	η_{10} = 70	100	0.051	24 h	[348]
N,P-GR	0.5 M H_2SO_4	0.2	η_{10} = 422	91	N/A	1000 CV cycles	[352]
P-C_3N_4@N-GR	0.5 M H_2SO_4	0.57	η_{10} = 80	49.1	0.43	5000 CV cycles	[353]
N,P-Carbon networks	0.5 M H_2SO_4	0.3	η_{30} = 210	89	0.16	4 h	[354]
N,P-Carbon nanofiber	0.5 M H_2SO_4	N/A	η_{10} = 151	69	N/A	2000 CV cycles	[355]
N,S-nanoporous GR	0.5 M H_2SO_4	N/A	η_{10} = 280	80.5	0.0084	1000 CV cycles	[356]
N,S-porous carbon	0.5 M H_2SO_4	0.285	η_{10} = 100	57.4	N/A	1000 CV cycles	[357]

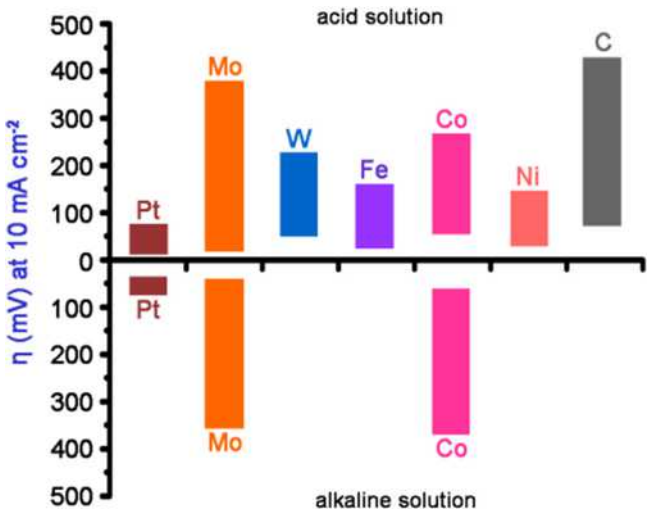

Fig. 23. Comparison of HER activities of different materials reviewed in this article.

Additionally, other heteroatoms (N, P and S) doped graphene have been widely prepared for electrocatalysis HER. And Qiao's group has made great contribution to this area [349–351]. The DFT investigation showed co-doping of N and P could result in excellent HER activity. Thus, a typical chemical doping procedure was performed to incorporate N and P heteroatoms into the graphene simultaneously. Obviously, the N,P-graphene catalyst possessed much lower onset potential, smaller Tafel slope and higher exchange current density than single-doped ones (Fig. 21). Meanwhile, it can be used in a wide pH range of conditions with robust stability [352]. Their group also synthesized porous C_3N_4 nanolayers with N-doped graphene sheets by a simple vacuum filtration method, which showed high HER activity [353]. Moreover, the activity origin and catalyst design principles for electrocatalytic HER on heteroatom-doped graphene were also discussed [351]. Besides, the N, P doped porous graphitic carbon networks were synthesized by self-assembling melamine–phytic acid supermolecular aggregate in the presence of GO, followed by pyrolysis [354]. And the binder free N, P co-doped porous carbon nanofiber network could also be prepared by in situ electropolymerization and the subsequent pyrolysis [355].

The N and S co-doped nanoporous graphene was synthesized by nanoporous Ni-based chemical vapor deposition (CVD) (Fig. 22) [356]. The carbon defects alone in the graphene lattice showed inferior activity for HER, but the coupling of S and N dopants with geometric defects in the graphene lattice produced an synergistic effect in tuning the H^* absorption and then leading to the outstanding HER catalysis. Besides, the N and S co-doped porous carbons were prepared by simple pyrolysis of human hair which exhibited high activity with a Tafel slope of 57.4 mV dec^{-1} and the 10 mA cm^{-2} obtained at 100 mV [357]. The synergistic interactions between N dopants and C–S–C moieties in the graphitic skeleton might play an essential role in improving the HER performance. The listed metal free HER catalysts are summarized in Table 7.

Compared to the precious and non-precious metal based catalysts, the current metal free catalysts possess inferior catalytic activity. However, the metal-free materials hold great promise in catalysis HER due to its excellent features with long-term durability and low-cost. Besides, they can also service the suitable support for the metallic catalysts. Therefore, it is highly desirable to select metal free catalysts with comparable catalytic activity but better stability compared to precious metal catalysts for the further hydrogen supply. Besides, comparison of HER activities of different materials reviewed in this article is shown in Fig. 23.

3. Heterogeneous catalytic decomposition of HCOOH

H_2, considered as one of the most promising alternative energy carriers, can enable a clean energy future, but because of its insecurity and difficulty to store, a safe, efficient hydrogen storage and delivery system is needed to develop urgently [358]. Solid-state storage is thus being investigated as an alternative. Carbon-based structures are particularly attractive for hydrogen storage because carbon is a light element, and graphene has potentially the most favorable gravimetric density among the carbon-based materials. However, pristine carbon nanostructures are chemically too inert to act as possible hydrogen storage medium [359]. Studies have shown that, at room temperature and under ambient pressure, the hydrogen storage capacity and the adsorption energy E_{ad} value of H_2 with pristine graphene and CNTs are both too small, which may not exceed 1 wt% and −0.030 eV, respectively [360,361]. Attempts have thus been made to improve the binding of H_2 with functionalized carbon nanostructures. One possible approach to increase their chemical activity is to modify the nanostructures by decoration, doping or substitution of alkali metals [362,363], transition metals [364,365], rare earth metals [366], Al element [367–369] etc, which improves their hydrogen storage capacity. For example, Li decorated CNTs and graphene can increase E_{ad} of H_2 remarkably to −0.15 eV [361], and the E_{ad} can be further tuned through external electric field [362]. Graphene modified by Al can increase the corresponding E_{ad} significantly because the Al atoms can act bridges to link H_2 molecules and graphene, thus increasing the hydrogen storage capacity significantly up to 13 wt% [360,367–369].

Another storage type is atomic hydrogen storage through hydrogenation. The use of chemisorption as a storage mechanism requires overcoming the high H_2 chemi(de)sorption barriers (1.5 eV/atom) to achieve loading/release kinetics at room temperature. Possible catalytic strategies for hydrogen adsorption/desorption involve the functionalization of graphene with metals such as palladium [370], known to catalyze the dissociation of hydrogen molecules into ions onto the graphene surface. Recently, it is reported that an applied electric field could facilitate hydrogenation in N-doped graphene [371] and silicone [372], with the dissociatively adsorbed H atoms diffusing on the surface with a low energy barrier in the presence of the electric field; furthermore, the removal of the electric field led to the efficient release of hydrogen from the fully hydrogenated N-doped graphene [373]. These new findings provide a new mechanism for hydrogenation/dehydrogenation of graphene and thus provide a pathway for the development of high-performance graphene-based atomic hydrogen storage materials.

Besides, liquid-phase chemical hydrogen storage materials, especially HCOOH, are regarded as attractive carriers for the production and storage of H_2 due to the easy transportation, handling and storage [374]. Hydrogen stored in HCOOH can be released through a catalytic dehydrogenation reaction ($HCOOH \rightarrow CO_2 + H_2$, $\Delta G_{298\ K} = -48.8$ kJ mol^{-1}), while the undesirable dehydration pathway ($HCOOH \rightarrow CO + H_2O$, $\Delta G_{298\ K} = -28.5$ kJ mol^{-1}) should be strictly controlled [375]. Moreover, CO_2, the co-product of decomposition, can be electrocatalytic reduction back to HCOOH, which gives a way of realizing a CO_2-neutral hydrogen storage cycle (Scheme 1). Recently, heterogeneous catalytic decomposition of HCOOH has been intensely investigated for hydrogen generation. And we briefly discussed here.

Although the heterogeneous catalyst for decomposition of HCOOH can be traced to early age [376,377], much attention was aroused until that well-dispersed Au species on Al_2O_3 could dehydrogenate HCOOH with much higher metal-time yields

than Pt clusters [378]. Then, Xu group developed Au nanoparticles encapsulated within amine-functionalized Si nanospheres for HCOOH decomposition, which exhibited outstanding catalytic activity and 100% H_2 selectivity for the full decomposition of HCOOH at 363 K, and the presence of amines can make the Au nanoparticles highly active due to the strong metal-molecular support interaction [379]. Cao et al. also deposited ultradispersed Au nanoparticles on zirconia as catalysts for selective dehydrogenation of HCOOH-amine mixture [380]. The reaction proceeded efficiently and selectively under ambient conditions, with no CO byproduct generation and giving a TOF of 1590 h^{-1} at 323 K. Recently, the incorporation of potassium ions in Au/Al_2O_3 to enhance the catalytic activity toward the dehydrogenation of HCOOH was also reported [381].

Pd-based catalysts have been reported to be the most active for HCOOH decomposition [382,383]. And suitable support materials can play important roles in controlling the dispersion and growth of metal nanoparticles, thus boosting the catalytic performance [384]. Hence, fabricating well-dispersed ultrafine metal nanoparticles has attracted tremendous attention. For example, nonoporous carbon supported Pd nanocatalyst showed notably catalytic activity with the TOF as high as 2623 h^{-1} at 323 K and 100% H_2 selectivity [385]. Moreover, selecting modified substrate can further improve the activity due to the synergistic effect. Pd nanoparticles dispersed uniformly on mesoporous g-C_3N_4 substrate showed eminent catalytic activity for boosting HCOOH decomposition at room temperature with a TOF of 144 h^{-1} [386]. Xu et al. modified GO with 1,4-phenylenediamine (PDA), and synthesized ultrafine Pd nanoparticles on PDA-rGO, which exhibited the TOF of 3810 h^{-1} at 323 K for HCOOH dehydrogenation under ambient conditions [387]. Very recently, Cao et al. has used a pyridinic-N-doped carbon composite as support material to improve the efficiency of Pd nanoparticles for hydrogen generation, which showed superior activity for HCOOH dehydrogenation with almost full conversion (97.5%), achieving a TOF of 5530 h^{-1} and turnover number of 50040 at 298 K [388]. This is the highest values ever reported under room temperature compared with other heterogeneous catalysts.

To overcome the deactivation of Pd catalyst caused by the CO byproduct, bi/tri-metallic Pd-based composites, alloys or core-shell nanostructures were constructed to enhance the catalytic activities and H_2 selectivity by modifying the catalytic surface of Pd nanoparticles [389–397]. Xing et al. demonstrated that Pd-Ag and Pd-Au alloy supported on carbon catalysts could overcome the poisoning by CO by-product and obtain H_2 evolved steadily from the decomposition of HCOOH at low temperature [398]. Moreover, the catalytic performance can be improved by the promotion effect of rare earth elements (such as Ce and Eu) [399].

Besides, MOFs have emerged as very promising hybrid materials for the immobilization of functional nanoparticles because of their high surface area and porosity [400]. Thus, the catalysts using the MOFs as the support were also prepared [401–404]. Xu et al. firstly represented AuPd/MIL-101 and AuPd/ED-MIL-101 as highly active MOF-immobilized metal catalysts for the full conversion of HCOOH to H_2 at convenient temperature [404]. Recently, Yan et al. developed a AuPd-MnO_x nanoparticles immobilized on ZIF-8-rGO [401]. Thereinto, MOF structure can effectively limit the growth and aggregation of nanoparticles due to the "confinement effect", and the existence of graphene can modify the electron structure of the supported nanoparticles. As a result, the resultant AuPd-MnO_x/ZIF-8-rGO hybrid displayed eminent activity for the dehydrogenation of HCOOH without any additive, and with a TOF of 382.1 h^{-1} at 298 K.

Table 8
Summary of performance of some catalysts for the decomposition of HCOOH.

Catalyst	Additive	Temp. (K)	TOF (h^{-1})	CO evolution	Ref.
Au/ZrO_2	NEt_3	323	1590	N/A	[380]
Pd-B/C	SF	303	1184	N/A	[382]
Pd/C	SF	298	64	N/A	[383]
Pd/MSC-30	SF	323	2623	N/A	[385]
	SF	298	750	N/A	
Pd/mpg-C_3N_4	None	298	144	N/A	[386]
Pd/PDA-rGO	SF	323	3810	N/A	[387]
$Pd/CN_{0.25}$	None	298	5530	N/A	[388]
AuPd-CeOx/N-rGO	None	298	52.9	N/A	[389]
Au@Pd/N-rGO	None	298	89	N/A	[390]
$Ag_{0.1}Pd_{0.9}$/rGO	None	298	105.2	N/A	[391]
Pd/basic resin	SF	348	820	<5 ppm	[392]
AgPd/C	None	212	382	N/A	[393]
$RtRuBiO_x$/C	None	353	312	N/A	[394]
AgAuPd/rGO	None	298	73.6	N/A	[396]
$CrAuPd/N\text{-}SiO_2$	None	298	730	N/A	[397]
PdAu-CeOx/C	SF	365	227	<140 ppm	[398]
PdAuEu/C	SF	365	387	<100 ppm	[399]
AuPd-MnOx/ZIF-8-rGO	None	298	382.1	N/A	[401]
$Ag_{20}Pd_{80}$@MIL-101	None	353	848	N/A	[402]
Pd/NH_2-MIL-125	None	305	214	<5 ppm	[403]
AuPd/ED-MIL-101	SF	363	106	Yes	[404]
$(Co_6)Ag_{0.1}Pd_{0.9}$/RGO	SF	323	2736	N/A	[407]
CoAuPd/DNA-rGO	None	298	85	N/A	[408]
$Co_{0.3}Au_{0.35}Pd_{0.35}$/C	None	298	80	N/A	[409]

Up to now, most of the reported heterogeneous catalysts are comprised only of precious metals, such as Pd, Au, Ag, and Pt, hindering the large-scale practical applications due to their shortage and high cost [378,405]. The incorporation of first-row transition metal into the noble metal structure could improve the acidic resistance of first-row transition metal, reduce the dosage of noble metals, and enhance the catalytic activity. Thus, the catalysts with first-row transition metals were synthesized [406–409]. Yan et al. firstly synthesized a trimetallic $Co_{0.30}Au_{0.35}Pd_{0.35}$/C nanocatalyst with a TOF of 80 h^{-1} and conversion of 91% at 298 K, which exhibited a much better activity for HCOOH dehydrogenation than the mono- and bi-metallic counterparts [409]. Xu et al. firstly reported a non-noble metal sacrificial method to synthesize highly dispersed AgPd nanoparticles on rGO, which can efficiently prevent the primary AgPd particles from aggregation. The as-synthesized $(Co_6)Ag_{0.1}Pd_{0.9}$ hybrid showed excellent catalytic activity with a TOF of 2739 h^{-1} for the hydrogen generation at 323 K [407]. Finally, the performances of some catalysts for HCOOH decomposition are summarized (Table 8).

4. Electrochemical CO_2 reduction to HCOOH

With the increasing trepidations about CO_2-induced problems, another important energy conversion reaction, the electroreduction of CO_2 to value-added chemicals and fuels using renewable energy, has become the focus of attention [410,411]. HCOOH, regarded as the promising chemical hydrogen storage material, can be produced by CO_2 reduction. Therefore, one attractive hydrogen storage system: CO_2–HCOOH could be obtained (Scheme 1). So the electrocatalysts for CO_2 reduction to HCOOH in aqueous solutions at ambient conditions are discussed here.

Although the reaction mechanism of electrochemical reduction of CO_2 to HCOOH (or formate) remains uncertain, the commonly accepted possible reaction pathways are described as follows: the first step is to form the intermediate CO_2^{-*} by one-electron transfer to adsorbed CO_2^*. Subsequently, the $HCOO^{-*}$ is formed by electron transfer and proton migration to cleave C—O bonds. The HCOOH (or formate) is ultimately formed in aqueous media by desorbing from the electrocatalyst surface and diffusing into electrolyte [412]. Based on the previous works, the Tafel slope is very useful for investigating the reaction mechanism. A Tafel slope of 118 mV dec^{-1} means the rate determining step is the initial one-electron transfer to form the CO_2^- key intermediate, whereas the Tafel slope of 59 mV dec^{-1} implies a one-electron pre-equilibrium step before a later rate-limiting chemical step [410].

Due to the extremely stable of linear CO_2 molecule, some problems of electrocatalysts for CO_2 reduction should be overcome, such as the large overpotential, low selectivity and inferior stability [413]. Therefore, to realize the wide application of CO_2 reduction, electrocatalysts should possess both high activity and selectivity toward the particular product of interest. To date, some metals, such as Sn, Co, Pb, are known to be selective for CO_2 to HCOOH (or formate) in aqueous media.

4.1. Catalysts based on Sn

Back in 1983, Kapusta et al. found that CO_2 could be reduced to HCOOH (or formate) on Sn electrode in aqueous solutions [414], but the energetic efficiency is low because of the high overpotential. From then on, more and more studies about CO_2 electroreduction to HCOOH (or formate) on Sn electrode were reported [415–418]. And the factors for activities were also discussed. For example, the FE to HCOOH on Sn electrode could be influenced by the applied potential, the concentration and pH of electrolyte, and the decrease of FE to HCOOH in the long electrolysis might be related to its own oxidation on the anode, since the diffusion of HCOOH through the Nafion membrane could not be prevented completely [419]. Besides, the reason of FE for CO_2 reduction decreased at very negative potential may be attributed to the decrease in effective active surface area by deposition of alkali metal intermetallic [420]. The influence of electrolyte on the activity and selectivity of formate formation on Sn catalysts was further studied. It turned out that the presence of Na^+ and SO_4^{2-} could enhance FE and energy efficiency, while HCO_3^- and K^+ accelerated the generation of formate. Furthermore, the FE to formate showed a tendency of increasing with the decrease in electrolyte concentration [421].

Besides, to overcome mass transport limitations and achieve high current densities, the gas diffusion electrodes were introduced for CO_2 electroreduction [422,423]. And the gas diffusion electrode with Sn can allow for the production of formate at current densities up to 200 mA cm^{-2} with a FE of around 90% [423]. Recently, ultrathin metal layers have exhibited highly active for CO_2 electroreduction, but they tend to oxidation, which would lead to the decline of electronic conductivity and stability. Based on this consideration, ultrathin metallic Sn quantum sheets confined in graphene were synthesized (Fig. 24a) [424]. The low-coordinated surface metal atoms were confirmed by XAFS, which meant many dangling bonds were present (Fig. 24b and c). This contributed to stabilize the key CO_2^- intermediate (Fig. 24d), hence lowering the overall activation energy barrier. Thanks to the sandwich-like structure, the protection of graphene could avoid the oxidation of Sn quantum sheets. And the notably increased electrochemical active area ensured 9 times larger CO_2 adsorption capacity relative to bulk Sn (Fig. 24e), and the highly-conductive graphene favors rate-determining electron transfer from CO_2 to CO_2^-. Besides, this catalyst also displayed the small Tafel slope (83 mV dec^{-1}) and superior stability for formate. This work may provide a promising guidance for designing effective and robust catalysts for CO_2 electroreduction.

Recently, the presence of appropriate oxidation state on metal surfaces has received more attentions as it can stabilize the key CO_2^- intermediate and facilitate the transfer of electron immediately [425]. As a result, the metals with their oxides on surface exhibited higher CO_2 electroreduction activity. The significance of SnO_x was evaluated by comparing the activity of Sn electrodes with different pre-treatments [425,426]. As a result, the Sn electrode with a native SnO_x layer showed high CO_2

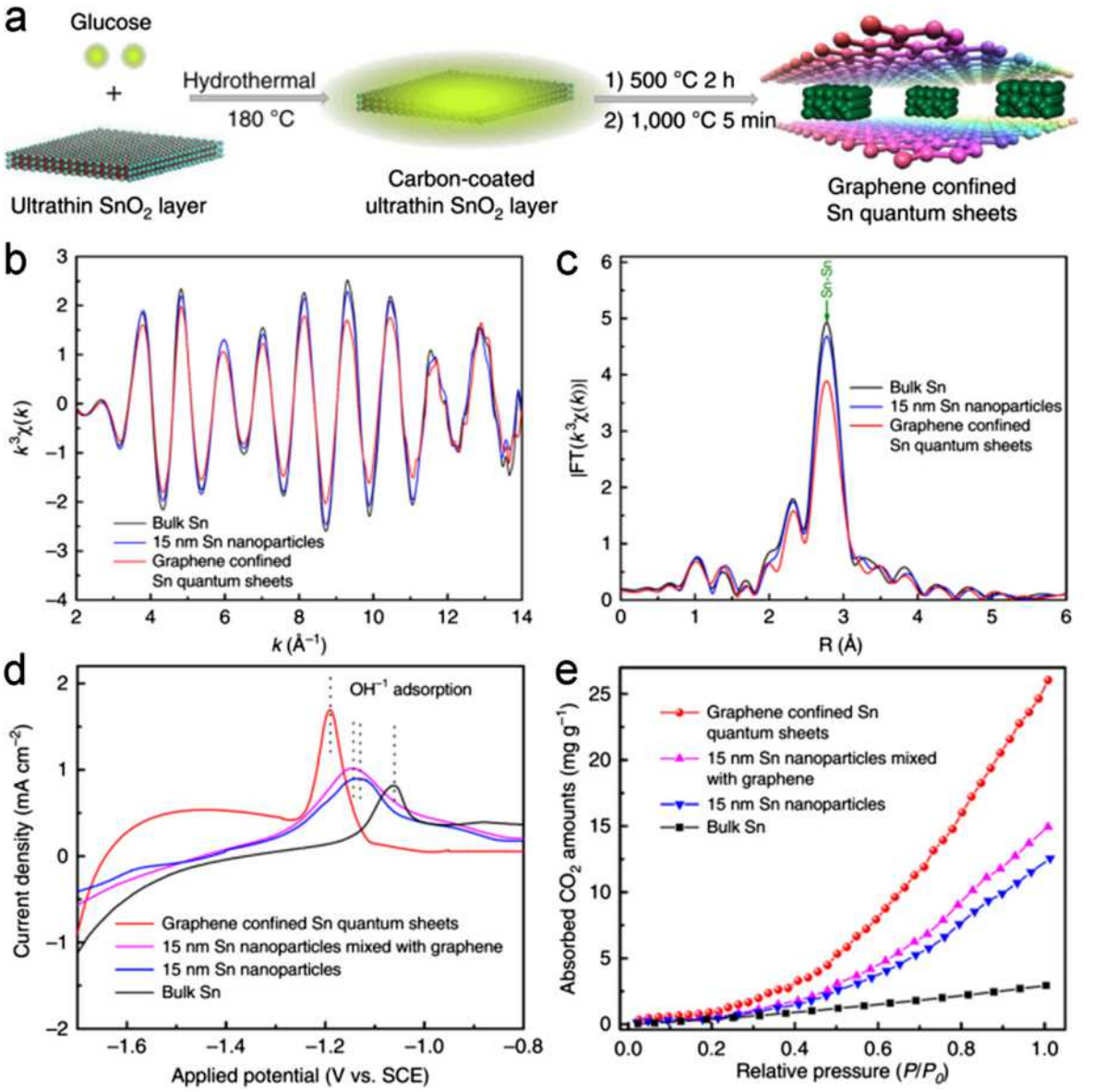

Fig. 24. (a) Scheme illustration for the formation of Sn quantum sheets confined in grapheme. (b) Sn K-edge extended XAFS oscillation function $k^3\chi(k)$, (c) the corresponding Fourier transforms FT($k^3\chi(k)$) for the graphene confined Sn quantum sheets, 15 nm Sn nanoparticles and bulk Sn, respectively. (d) single oxidative LSV scans in N_2-saturated 0.1 M NaOH for the different samples. (e) CO_2 adsorption isotherms.

reduction activity, while the electrode etched to expose fresh Sn^0 surface exhibited almost exclusive H_2 evolution [425]. Moreover, the role of oxide layer thickness was also discussed by using the Sn-based gas diffusion electrode [427]. The catalysts with a 3.5 nm thick layer exhibited the highest FE for $HCOO^-$, and the 7.0 nm thick layer exhibited the highest FE for CO, while the FE for H_2 increased with increasing the oxide thickness. This may imply that the change of surface structure during the CO_2 electrolysis may influence not only the activity but also selectivity to products. Moreover, in situ attenuated total reflectance infrared spectroscopy was applied to study the mechanism of CO_2 reduction on Sn films [428]. A metastable oxide layer was present on Sn cathode even under reducing potentials, and a mechanism governing the reduction of CO_2 on Sn electrodes was proposed. Besides, the oxidation state change of SnO_2 was also monitored in the process of CO_2 electroredution [429]. They found that SnO_2 showed a higher FE to formate at moderate potentials, while the FE to formate significantly dropped at more negative potentials since SnO_2 was reduced to metallic Sn. Recently, Luc et al. constructed a core-shell catalyst with Ag_3Sn core and ultrathin SnO_x shell, and a volcano-like correlation between the bulk composition and electrocatalytic performance was observed [430]. The optimal thickness of partially oxidized SnO_x shell was ~1.7 nm. DFT calculations showed that oxygen vacancies on the SnO (1 0 1) surface are stable at highly negative potentials and crucial

for CO_2 activation. And such volcano-like relationship arises from the competing effects of favorable stabilization of OCHO* by lattice expansion and the electron conductivity loss due to the increased thickness of SnO_x layer. Lately, Sn/SnS_2 electrode derived from SnS_2 nanosheets was also applied for CO_2 reduction to formate with the maximum FE of 84.5% [431].

Pure SnO_2 materials can also be used for CO_2 electroreduction with a pretreatment of electrochemical reduction. For instance, the effect of particle size at the reduced nano-SnO_2 surfaces was discussed, and the FE to formate could reach the maximum on 5 nm particles, which might be due to an optimized affinity to surface binding of intermediates [432]. The FE to formate at reduced nano-SnO_2/graphene increased to 93.6% with about 10.2 mA cm^{-2}. In addition, the reduced nano-SnO_2 catalysts were quite stable during electrolysis, and it may improve the current density by 1–2 orders of magnitude by using flow cell or gas diffusion electrodes. Furthermore, a 3D integrated electrode composed of mesoporous SnO_2 nanosheets on CC was also constructed, and exhibited a partial current density of 45 mA cm^{-2} at a moderate overpotential (0.88 V vs. Ag/AgCl) with a high FE of 87% [433]. Besides, SnO_2 porous nanowires with a high density of grain boundaries exhibited a higher energy conversion efficiency of CO_2-into-HCOOH (ca. 56%) than analogous catalysts [434].

4.2. Catalysts based on Co

In the past year, Xie et al. has made great contributions to Co-based electrocatalysts of CO_2 reduction to formate [435–437]. In order to explore the role of metal and metal oxide sites, the 4-atom-thick Co sheets with and without surface Co oxide were constructed [437]. Compared to the bulk metals, the surface Co atoms of the atomically thin sheets exhibited higher activity and selectivity for formate at lower overpotential, and the partially oxidized Co 4-atom-thick layers showed an outstanding activity with 90% FE for formate at an overpotential of only 0.24 V vs. SCE, and the value of FE could remain over 40 h test with negligible decay in current density (>10 mA cm^{-2}). The high activity was attributed to the high ECSA and CO_2 adsorption content, and the oxidation of Co atom layer contributed to stabilize the key CO_2^- intermediate and facilitate the rate-determining chemical reaction of H^+ transfer. The work provided a novel direction that controlling the correct

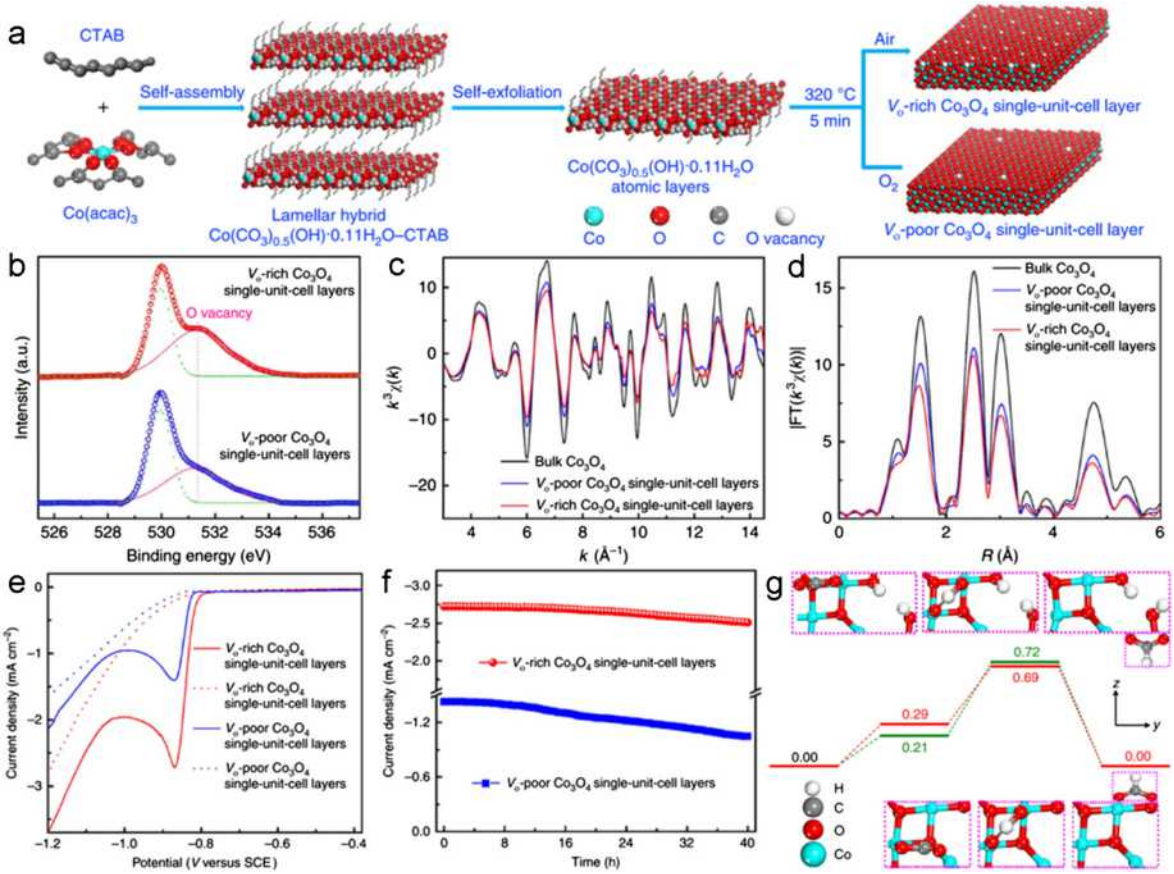

Fig. 25. (a) Scheme for the formation of V_o-rich and V_o-poor Co_3O_4 single-unit-cell layer, respectively. (b)O 1s XPS spectra of V_o-rich and V_o-poor Co_3O_4 single-unit-cell layers. (c) Co K-edge extended XAFS oscillation function $k^3\chi(k)$. (d) The corresponding Fourier transforms FT($k^3\chi(k)$). (e) Linear sweep voltammetric curves in a CO_2-saturated (solid line) and N_2-saturated (dashed line) 0.1 M $KHCO_3$ aqueous solution. (f) Chronoamperometry results at the potential of −0.87 V versus SCE. (g) Calculated free energy diagrams.

morphology and oxidation state could improve the activity of CO_2 reduction unexpectedly, even transformed a nearly non-catalytic material into an active catalyst.

To verify the influence of exposed active sites and electrical conductivity, the ultrathin Co_3O_4 layers with 1.7 nm or 3.51 nm thick were prepared [435]. The DFT calculations demonstrated that the charge density near Fermi level increased and become more dispersed with decreasing the thickness, enabling enhanced electronic conductivity. And the atomic thickness means the majority of lowered-coordination-number Co atoms are exposed on the surface, which served as the active sites to adsorb higher amounts of CO_2 and stabilize the rate-determining CO_2^- intermediate. Thus, the 1.72 nm thick Co_3O_4 layers exhibited the maximum FE to formate (>60%) at −0.88 V vs. SCE in long term electrolysis for 20 h.

Lately, to explore the effect of oxygen vacancies in CO_2 electroreduction, their group designed a model of oxygen-deficient cobalt oxide single-unit-cell layers [436]. As illustrated in Fig. 25a, V_o-rich and V_o-poor Co_3O_4 single-unit-cell layers were synthesized through a lamellar inorganic–organic hybrid intermediate strategy. The presence of oxygen vacancy was confirmed by the O 1 s XPS spectra and EXAFS results (Fig. 25b–d). Energy calculations demonstrated that the presence of oxygen vacancies lower the rate-limiting activation barrier via stabilizing the $HCOO^{-*}$ intermediate, which also facilitated CO_2 adsorption (Fig. 25g). Finally, the V_o-rich Co_3O_4 single-unit-cell layers exhibited current densities of 2.7 mA cm^{-2} with 85% formate selectivity during the tested period of 40 h at −0.87 V vs. SCE. This work made a clear atomic-level correlation between oxygen vacancies and CO_2 electroreduction (Fig. 25e and f).

4.3. Catalysts based on other metals

The metal Pd, typically considered the CO as the major CO_2 reduction product, can also produce formate [438]. And Kanan et al. exhibited Pd nanoparticles dispersed on a carbon support reached high mass activities and current density [439]. Electrokinetic measurements showed the rate-determining step was the addition of electrochemically generated surface adsorbed hydrogen to CO_2. The electrodes deactivate was attributed to the CO byproduct, and the activity can be recovered by removing CO with brief air exposure. Recently, the surface morphology of Pd nanoparticle to the activity of CO_2 electroreduction to formate was explored [440]. It was confirmed that Pd nanoparticles with high-index facets could suppress CO formation while promote the production of formate. Such a work contributes to the improvement of catalysts for the selective production of fuels from CO_2 electroredution.

Another metal considered the CO as the major CO_2 reduction product is Zn. However, rational design the Zn structure can also obtain the HCOOH. For instance, a novel Zn electrode was prepared and exhibited the current density of 12.8 mA cm^{-2} with 87.1% FE to formate [441]. Electrochemical studies showed that this Zn catalyst with a layer of nanoparticle had rough surface and granular nanostructure. They suggested that the improvement in catalytic performance was attributed to the active facets and special surface structure of Zn formed during reduction process of ZnO. Besides, Cu electrode also exhibited the formate selectivity, but the FE is unsatisfactory [442–444].

Apart from the aforementioned metals, some other metals, such as mercury (Hg), lead (Pb) and indium (In), are also reported for CO_2 electroreduction to produce HCOOH (or formate). However, applications of them are limited, which is attributed to their acute toxicity, expensiveness or both [410,445,446]. Recently, the Si-doped Ga_2O_3 electrode was reported that could selectively produce HCOOH with a FE of over 88% in aqueous solutions [447].

Table 9
The performance of recently reported catalysts for CO_2 electroreduction to HCOOH.

Catalyst	Electrolyte	Potential	FE	Stability	Ref.
Electrodeposited Sn	0.1 M $KHCO_3$	−1.4 V vs. SCE	91%	Unstable	[415]
Sn GDE-20 wt% Nafion	0.5 M $KHCO_3$	−1.6 V vs. SCE	80%	N/A	[417]
Sn	0.5 M $KHCO_3$	−1.8 V vs. Ag/AgCl	91%	N/A	[419]
Pure Sn	2 M KCl	−1.8 V vs. SCE	60%	6 h	[420]
Sn/GDE	0.1 M $KHCO_3$	−1.57 V vs. SHE	90%	5 h	[423]
Sn quantum sheets-graphene	0.1 M $NaHCO_3$	−1.8 V vs. SCE	85%	50 h	[424]
SnO_2 NPs@rGO	0.5 M NaOH	−1.1 V vs. Ag/AgCl	80%	N/A	[429]
Ag-Sn/SnO_2	0.5 M $NaHCO_3$	−0.8 V vs. RHE	80%	24 h	[430]
SnS/rGO	0.5 M $NaHCO_3$	−1.4 V vs. Ag/AgCl	84.5%	14 h	[431]
Nano-SnO_2/graphene	0.1 M $NaHCO_3$	−1.8 V vs. SCE	93%	18 h	[432]
SnO_2/CC	0.5 M NaHCO3	−1.6 V vs. Ag/AgCl	87 ± 2%	24 h	[433]
1.72 nm thick Co_3O_4 layers	0.1 M $NaHCO_3$	−0.88 V vs. SCE	64.3%	20 h	[435]
V_o-rich Co_3O_4 atomic layer	0.1 M $KHCO_3$	−0.88 V vs. SCE	87.6%	40 h	[436]
Partially oxidized Co atomic layer	0.1 M Na_2SO_4	−0.85 V vs. SCE	90.1%	60 h	[437]
Pd/C	0.5 M $KHCO_3$	−0.25 V vs. RHE	95%	N/A	[439]
Pd NPs	0.5 M $KHCO_3$	−0.2 V vs. RHE	97%	N/A	[440]
Si-doped Ga_2O_3	3 M KCl + 5 M NaOH	−1.8 V vs. Ag/AgCl	88.85%	N/A	[447]
PEI-NCNT	0.1 M $KHCO_3$	−1.8 V vs. SCE	87%	24 h	[450]
N-graphene	0.5 M $KHCO_3$	−0.84 V vs. RHE	73%	12 h	[451]

4.4. Catalysts based on carbon-based materials

Apart from above metals and metal oxides, renewable carbon-based catalysts have also attracted attention for CO_2 electroreduction [448,449]. However, the selectivity of formate should be improved. A N-CNT functioned with polyethylenimine as a co-catalyst was constructed and the maximum FE to formate was reached to 87% with the 9.5 mA cm^{-2} [450]. They found that polyethylenimine could stabilize the intermediate $CO_2^{\cdot-}$ and gather CO_2 in the overlayer. This study might open a new avenue for effective CO_2 electroreduction on carbon-based materials and inspire the application of co-catalysis strategies. Besides, N-graphene was applied for CO_2 electroreduction to formate with 73% FE [451]. At last the performances of these catalysts are illustrated in Table 9.

5. Electrochemical N_2 reduction to NH_3

NH_3 is regarded as another promising chemical hydrogen storage material due to the safety concerns, energy density considerations and abundant N_2 feedstock [452]. However, due to the special and inert structure of N_2, which has extremely high bond energy (940.95 kJ mol^{-1}) [453], and the absence of permanent dipole of the triple bond, the synthesis conditions of NH_3 using N_2 is extremely harsh, such as high temperature and pressure. And various endeavours have been applied to realize N_2 reduction under mild conditions. Thereinto, electrochemical N_2 reduction reaction can be favored because it can be powered by a renewable electricity source, and proceed at moderate temperature and atmospheric pressure. Here, we summary recent electrocatalysts on NH_3 synthesis by N_2 reduction in aqueous electrolyte.

In 1989, Furuya et al. reported the first electrochemical N_2 reduction at ambient temperature and pressure in aqueous solutions on the metal phthalocyanine catalyst [454]. However, the activity and durability were not satisfactory. After that, dinitrogen complexes were used for NH_3 synthesis [455,456], whereas most of them are susceptible to air and/or water. Then metal was also used to NH_3 synthesis. Zhang et al. used Ru/C electrode to realize N_2 reduction with useful activity and stability [457]. And the difference in current between N_2 and He showed that N_2 may be reduced, but the actual yield of NH_3 was not provided. Recently, Yan et al. successfully realized N_2 reduction under ambient conditions by use of tetrahexahedral Au nanorods [458]. The FE of N_2 reduction was around 4%, and the highest yield of NH_3 (1.648 μg h^{-1} cm^{-2}) was obtained at −0.2 V vs. RHE. Besides, hydrazine hydrate was also detected. Though N_2 can be reduced on Au nanorods, the activity was not satisfactory. As we know, the size of nano-materials and crystallinity will affect the catalytic activity. Therefore, sub-nanoclusters Au were synthesized for N_2 reduction [459,460]. By using tannic acid as reducing agent and stabilizer, Au/TiO_2 was successfully obtained. The ultra-small Au nanoparticles can form Au—O—Ti bonding, and this will deduce the charge of Au partially shifts. Thus Au active sites will prefer adsorb nitrogen rather than H^+. Finally, the highest yield of NH_3 was reached up to 21.4 μg h^{-1} mg_{cat}^{-1}, and the corresponding FE was 8.11%. As the amorphous material possessed high concentration of unsaturated sites, this might improve the chemical activity with respect to the interaction of small molecules [461]. The synthesized *a*-Au/CeO_x-rGO exhibited an NH_3 synthesis rate of 8.3 μg h^{-1} mg_{cat}^{-1} with FE of 10.1%. Recently, Centi et al. obtained an NH_3 production rate of 2.2×10^{-3} g_{NH3} h^{-1} m^{-2} on Fe supported on CNTs in a flow of N_2 under ambient conditions [462]. And the authors proposed that the interface between Fe nanoparticles and CNTs can activate N_2 and then hydrogenate it. In addition, their group also investigated the effects of Fe content, cell design, electrolyte and applied voltage for N_2 reduction [463]. As a result, the present data demonstrated that 30 wt% Fe_2O_3-CNT was found to be optimal, and the cell design

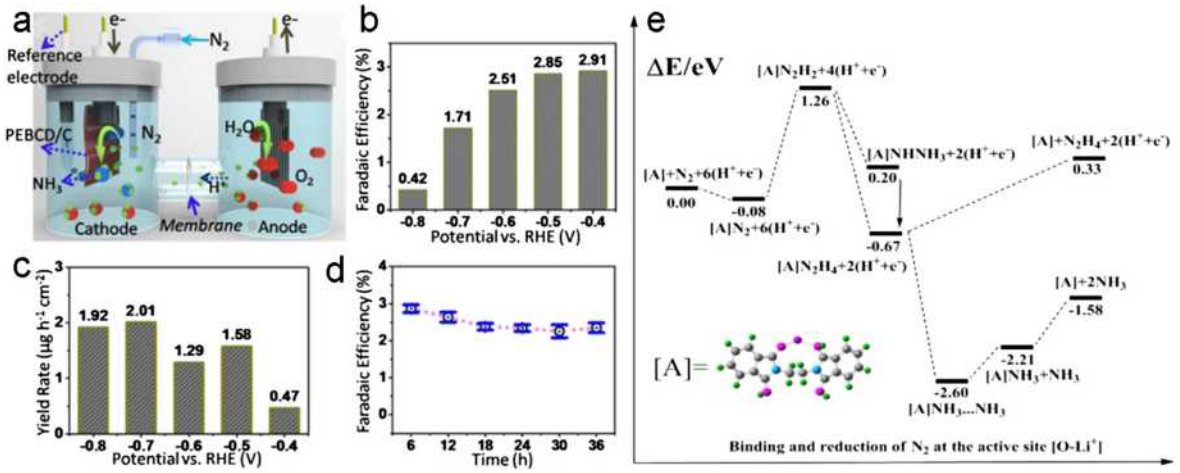

Fig. 26. (a) Schematic reaction cell for NRR. (b) Faradaic efficiency and (c) NH_3 yield rate at various potentials under 25 °C. (d) Cycling stability results. (e) Predicted relative energies for the electrochemical reduction of N_2 to NH_3 at the [O-Li^+] active site, where the chemical potential of [$H^+ + e^-$] is defined by the binding energy of a single hydrogen atom in H_2.

may affect NH_3 crossover through the membrane, and the electrolyte can affect the selectivity of NH_3. Recently, Wang et al. provided a Li^+ incorporation strategy to retard HER process and afford active sites for N_2 reduction [464]. Based on electrochemical evaluation and DFT calculations (Fig. 26), Li^+ association with the O atoms in the poly(N-ethyl-benzene-1,2,4,5-tetracar boxylic diimide) can retard the HER process and promote the adsorption of N_2 to afford a high potential scope for N_2 reduction process to proceed in the "$[O\text{-}Li^+]\cdot N_2\text{-}H_x$" alternating hydrogenation mode. This work provides an effective way to inhibit HER to enhance the N_2 reduction selectivity. Besides, other catalysts applied in different electrolyte systems, such as solid or molten salt electrolyte, are also discussed [465–467], but we don't discussed here. Recently, Zhang et al. designed the Li-N_2 battery and realized reversible N_2 fixation, exhibiting high FE and decreasing energy consumption, which might provide another perspective for N_2 reduction [468].

6. Summary and outlook

Herein, recent progress of catalysts for H_2 generation and storage, including the H_2 evolution, HCOOH decomposition, CO_2 and N_2 electroreduction to HCOOH and NH_3 respectively, are summarized.

For HER, the Pt-based catalysts show the best catalytic performance, however, which are limited by high price and few reserves. Recently, the single atom catalysis of precious metals can maximize their efficiency and meanwhile minimize the usage, which provide a strategy for precious metals usage, but the stability should be improved to meet the requirements of application. For non-precious metal compounds, the catalysts based on Mo have been widely discussed and many elegant strategies are developed to enhance the catalytic activity, such as designing different nanostructures, doping other various elements and connecting with conductive supports or both. Therefore, many Mo-related catalysts exhibited high HER performance, and a large number of theoretical studies based on MoS_2 on the active sites are also carried out. Besides, these strategies can also be used for other electrocatalysts. As the same group element with Mo, W is also used to synthesize different catalysts for HER, and WC, which showed Pt-like catalytic properties, can be used as promising supports. In addition, the VIII group elements (Fe, Co and Ni) based materials which have higher abundance than Mo and W are also explored for electrocatalysis HER, and some materials, such as phosphides, show extremely high catalytic activity, but many ambiguous understanding is still present, such as surface reconstruction. Recently, the metal-free catalysts, especially based on carbon materials, have been proposed as next generation HER catalysts which exhibit considerable catalytic activity and robust stability. However, compared with metallic catalysts, the HER activity of metal free catalysts need to be greatly improved. Although the structure optimization to achieve the excellent performance has been made for HER catalysts, but many challenges still puzzle this thriving field. And here some of them are listed. (i) Identifying the mechanism of catalysts, particularly the composites which showed excellent HER activity, should be at the forefront of the researches into HER, which can guide us to further optimize the properties of electrocatalysts. Conventionally, we often attribute the improved performance to the synergistic effects, wherein the real reason may be not so simple. Encouragingly, the investigation process of HER mechanism for MoS_2 greatly promotes the quick development of MoS_2-based HER catalysts, highlighting the importance of mechanism studies. To this end, *in-situ* characterization means and/or combining with the theoretical investigations should be extensively explored. (ii) In view of the harsh working environment, the stability of electrodes is another important and considerable problem. The catalyst which exhibits excellent HER activity, but has bad stability, is still not appropriate to participate in the actual application. Currently, most of the electrodes are only applicable in the single working environment, and much work only focuses on morphology architecture to improve the activity, but the discussion about stability is scant. Therefore, exploring an effective way to improve the stability is of great importance and challenge in the future works. (iii) Some HER catalysts can be used for oxygen evolution, so constructing the bifunctional and integrated electrode enabling the operation in the same electrolyte with satisfying catalytic activity toward OER and HER is also a good choice in view of the convenience and cost reduction in the overall water splitting. (iv) Most of the catalysts are used in strong acid condition, and only few can operate in all pH values. Considering the abundance of seawater, it is of great importance and need to design catalysts that can achieve high activity in the seawater. (v) Though the HER activity of Pt is superior to others, the performance under high current density is unsatisfactory. So searching the stable and efficiently catalysts under high current density should be considered.

Despite the remarkable advances achieved in HCOOH decomposition, there are still some issues to be addressed. Foremost, scalable production of stable non-precious catalysts to substitute noble-metal is imperative for practical applications. Then, a deep understanding about catalytic mechanisms, the effect of particles shape on activity, and the interaction between nanoparticles and supports are urgently needed, which may contribute to rational design the catalysts with desired properties.

For CO_2 electroreduction to HCOOH, though some catalysts have exhibited high selectivity and FE, the low energy efficiency and insufficient stability are still the challenges for commercial application. Therefore it is vital to enhance the performance of catalysts for CO_2 electroredution to formate from several aspects: (i) mechanistic and fundamental insights during CO_2 reduction process. Much attention should be paid to this field due to the presence of many vague understandings. (ii) Optimizing structure and composition of catalysts. The catalysts, which possess the different structure like ultrathin sheets, core-shell and sandwich-like, exhibit unexpected selectivity. And the presence of oxides can further enhance the activity. (iii) External test conditions. Besides improving the design of catalysts, several external conditions should be also considered, such as electrolytes. The ion species and pH values both have influence on the performance. Besides, the reactors should be optimized.

While for NH_3 synthesis by N_2 reduction, until now, experimental results displayed extremely poor performance, and only few catalysts could catalyze N_2 reduction. The most challenging problem is the adsorption and activation of N_2 on the surface of catalysts. Thus, much attention should be paid for mechanistic details and atomic-scale processes at the electrode-electrolyte interface. There is still much room for improvement of this promising but largely underexplored reaction. Overall, Many difficulties should be overcome for these reactions, but with the rapid progress in technology and materials engineering, we believe practical applications of sustainable energy systems based on hydrogen are expected.

Acknowledgements

This work was financially supported by Natural Science Foundation of China (Grant Nos. 51522101, 51631004, 51471075, and 51401084), and Program for JLU Science and Technology Innovative Research Team (2017TD-09).

References

[1] Hunter BM, Gray HB, Muller AM. Earth-abundant heterogeneous water oxidation catalysts. Chem Rev 2016;116:14120–36.
[2] Mai N, Tran PD, Pramana SS, Lee RL, Batabyal SK, Mathews N, et al. In situ photo-assisted deposition of MoS_2 electrocatalyst onto zinc cadmium sulphide nanoparticle surfaces to construct an efficient photocatalyst for hydrogen generation. Nanoscale 2013;5:1479–82.
[3] Gray HB. Powering the planet with solar fuel. Nat Chem 2009;1. 7-7.
[4] Tiwari JN, Tiwari RN, Kim KS. Zero-dimensional, one-dimensional, two-dimensional and three-dimensional nanostructured materials for advanced electrochemical energy devices. Progr Mater Sci 2012;57:724–803.
[5] Yu X, Tang Z, Sun D, Ouyang L, Zhu M. Recent advances and remaining challenges of nanostructured materials for hydrogen storage applications. Progr Mater Sci 2017;88:1–48.
[6] Zhang B, Kang F, Tarascon J-M, Kim J-K. Recent advances in electrospun carbon nanofibers and their application in electrochemical energy storage. Progr Mater Sci 2016;76:319–80.
[7] Morales-Guio CG, Stern LA, Hu XL. Nanostructured hydrotreating catalysts for electrochemical hydrogen evolution. Chem Soc Rev 2014;43:6555–69.
[8] Amoo LM, Fagbenle RL. An integrated impact assessment of hydrogen as a future energy carrier in Nigeria's transportation, energy and power sectors. Int J Hydrogen Energy 2014;39:12409–33.
[9] Muradov NZ, Veziroglu TN. "Green" path from fossil-based to hydrogen economy: an overview of carbon-neutral technologies. Int J Hydrogen Energy 2008;33:6804–39.
[10] Armor JN. Catalysis and the hydrogen economy. Catal Lett 2005;101:131–5.
[11] Rostrup-Nielsen JR, Nielsen R. Fuels and energy for the future: the role of catalysis. Catal Rev Sci Eng 2004;46:247–70.
[12] Fukuzumi S, Yamada Y, Suenobu T, Ohkubo K, Kotani H. Catalytic mechanisms of hydrogen evolution with homogeneous and heterogeneous catalysts. Energy Environ Sci 2011;4:2754–66.
[13] Abbasi T, Abbasi SA. 'Renewable' hydrogen: prospects and challenges. Renew Sust Energy Rev 2011;15:3034–40.
[14] Turner JA. Sustainable hydrogen production. Science 2004;305:972–4.
[15] Yin SF, Xu BQ, Zhou XP, Au CT. A mini-review on ammonia decomposition catalysts for on-site generation of hydrogen for fuel cell applications. Appl Catal A-Gen 2004;277:1–9.
[16] McKone JR, Marinescu SC, Brunschwig BS, Winkler JR, Gray HB. Earth-abundant hydrogen evolution electrocatalysts. Chem Sci 2014;5:865–78.
[17] Yan Y, Xia BY, Xu ZC, Wang X. Recent development of molybdenum sulfides as advanced electrocatalysts for hydrogen evolution reaction. ACS Catal 2014;4:1693–705.
[18] Tang ML, Grauer DC, Lassalle-Kaiser B, Yachandra VK, Amirav L, Long JR, et al. Structural and electronic study of an amorphous MoS_3 hydrogen-generation catalyst on a quantum-controlled photosensitizer. Angew Chem Int Ed 2011;50:10203–7.
[19] Anantharaj S, Ede SR, Sakthikumar K, Karthick K, Mishra S, Kundu S. Recent trends and perspectives in electrochemical water splitting with an emphasis on sulfide, selenide, and phosphide catalysts of Fe Co, and Ni: a review. ACS Catal 2016;6:8069–97.
[20] Wang J, Cui W, Liu Q, Xing Z, Asiri AM, Sun X. Recent progress in cobalt-based heterogeneous catalysts for electrochemical water splitting. Adv Mater 2016;28:215–30.
[21] Xiao P, Chen W, Wang X. A review of phosphide-based materials for electrocatalytic hydrogen evolution. Adv Energy Mater 2015;5:1500985.
[22] Voiry D, Yang J, Chhowalla M. Recent strategies for improving the catalytic activity of 2D TMD nanosheets toward the hydrogen evolution reaction. Adv Mater 2016;28:6197–206.
[23] Shi Y, Zhang B. Recent advances in transition metal phosphide nanomaterials: synthesis and applications in hydrogen evolution reaction. Chem Soc Rev 2016;45:1529–41.
[24] Thoi VS, Sun Y, Long JR, Chang CJ. Complexes of earth-abundant metals for catalytic electrochemical hydrogen generation under aqueous conditions. Chem Soc Rev 2013;42:2388–400.
[25] Wang M, Chen L, Sun L. Recent progress in electrochemical hydrogen production with earth-abundant metal complexes as catalysts. Energy Environ Sci 2012;5:6763–78.
[26] Pintado S, Goberna-Ferron S, Escudero-Adan EC, Galan-Mascaros JR. Fast and persistent electrocatalytic water oxidation by Co-Fe Prussian blue coordination polymers. J Am Chem Soc 2013;135:13270–3.
[27] Wang J, Li K, Zhong HX, Xu D, Wang ZL, Jiang Z, et al. Synergistic effect between metal-nitrogen-carbon sheets and NiO nanoparticles for enhanced electrochemical water-oxidation performance. Angew Chem Int Ed 2015;54:10530–4.
[28] Norskov JK, Bligaard T, Logadottir A, Kitchin JR, Chen JG, Pandelov S, et al. Trends in the exchange current for hydrogen evolution. J Electrochem Soc 2005;152:J23–6.
[29] McCrory CCL, Jung S, Ferrer IM, Chatman SM, Peters JC, Jaramillo TF. Benchmarking hydrogen evolving reaction and oxygen evolving reaction electrocatalysts for solar water splitting devices. J Am Chem Soc 2015;137:4347–57.
[30] Stamenkovic VR, Mun BS, Arenz M, Mayrhofer KJJ, Lucas CA, Wang G, et al. Trends in electrocatalysis on extended and nanoscale Pt-bimetallic alloy surfaces. Nat Mater 2007;6:241–7.
[31] Cao X, Han Y, Gao C, Xu Y, Huang X, Willander M, et al. Highly catalytic active PtNiCu nanochains for hydrogen evolution reaction. Nano Energy 2014;9:301–8.
[32] Du N, Wang C, Wang X, Lin Y, Jiang J, Xiong Y. Trimetallic triStar nanostructures: tuning electronic and surface structures for enhanced electrocatalytic hydrogen evolution. Adv Mater 2016;28:2077–84.
[33] Subbaraman R, Tripkovic D, Strmcnik D, Chang K-C, Uchimura M, Paulikas AP, et al. Enhancing hydrogen evolution activity in water splitting by tailoring Li^+-$Ni(OH)_2$-Pt interfaces. Science 2011;334:1256–60.
[34] Yin H, Zhao S, Zhao K, Muqsit A, Tang H, Chang L, et al. Ultrathin platinum nanowires grown on single-layered nickel hydroxide with high hydrogen evolution activity. Nat Commun 2015;6:6430.
[35] Wang P, Jiang K, Wang G, Yao J, Huang X. Phase and interface engineering of platinum-nickel nanowires for efficient electrochemical hydrogen evolution. Angew Chem Int Ed 2016;55:12859–63.

[36] Oh A, Sa YJ, Hwang H, Baik H, Kim J, Kim B, et al. Rational design of Pt-Ni-Co ternary alloy nanoframe crystals as highly efficient catalysts toward the alkaline hydrogen evolution reaction. Nanoscale 2016;8:16379–86.
[37] Hsu IJ, Kimmel YC, Jiang XG, Willis BG, Chen JG. Atomic layer deposition synthesis of platinum-tungsten carbide core-shell catalysts for the hydrogen evolution reaction. Chem Commun 2012;48:1063–5.
[38] Chen Z, Ye S, Wilson AR, Ha Y-C, Wiley BJ. Optically transparent hydrogen evolution catalysts made from networks of copper-platinum core-shell nanowires. Energy Environ Sci 2014;7:1461–7.
[39] Kelly TG, Lee KX, Chen JG. Pt-modified molybdenum carbide for the hydrogen evolution reaction: from model surfaces to powder electrocatalysts. J Power Sources 2014;271:76–81.
[40] Bai S, Wang C, Deng M, Gong M, Bai Y, Jiang J, et al. Surface polarization matters: enhancing the hydrogen-evolution reaction by shrinking Pt shells in Pt-Pd-graphene stack structures. Angew Chem Int Ed 2014;53:12120–4.
[41] Ren F, Lu H, Liu H, Wang Z, Wu Y, Li Y. Surface ligand-mediated isolated growth of Pt on Pd nanocubes for enhanced hydrogen evolution activity. J Mater Chem A 2015;3:23660–3.
[42] Wang JX, Zhang Y, Capuano CB, Ayers KE. Ultralow charge-transfer resistance with ultralow Pt loading for hydrogen evolution and oxidation using Ru@Pt core-shell nanocatalysts. Sci Rep 2015;5:12220.
[43] Wei G-F, Liu Z-P. Restructuring and hydrogen evolution on Pt nanoparticle. Chem Sci 2015;6:1485–90.
[44] Esposito DV, Hunt ST, Stottlemyer AL, Dobson KD, McCandless BE, Birkmire RW, et al. Low-cost hydrogen-evolution catalysts based on monolayer platinum on tungsten monocarbide substrates. Angew Chem Int Ed 2010;49:9859–62.
[45] Wang L, Mahoney EG, Zhao S, Yang B, Chen JG. Low loadings of platinum on transition metal carbides for hydrogen oxidation and evolution reactions in alkaline electrolytes. Chem Commun 2016;52:3697–700.
[46] Esposito DV, Chen JG. Monolayer platinum supported on tungsten carbides as low-cost electrocatalysts: opportunities and limitations. Energy Environ Sci 2011;4:3900–12.
[47] Wu M, Shen PK, Wei Z, Song S, Nie M. High activity PtPd-WC/C electrocatalyst for hydrogen evolution reaction. J Power Sources 2007;166:310–6.
[48] Esposito DV, Hunt ST, Kimmel YC, Chen JG. A new class of electrocatalysts for hydrogen production from water electrolysis: metal monolayers supported on low-cost transition metal carbides. J Am Chem Soc 2012;134:3025–33.
[49] Greeley J, Norskov JK, Kibler LA, El-Aziz AM, Kolb DM. Hydrogen evolution over bimetallic systems: understanding the trends. ChemPhysChem 2006;7:1032–5.
[50] Greeley J, Jaramillo TF, Bonde J, Chorkendorff IB, Norskov JK. Computational high-throughput screening of electrocatalytic materials for hydrogen evolution. Nat Mater 2006;5:909–13.
[51] Stephens IEL, Chorkendorff I. Minimizing the use of platinum in hydrogen-evolving electrodes. Angew Chem Int Ed 2011;50:1476–7.
[52] Yang XF, Koel BE, Wang H, Chen WH, Bartynski RA. Nanofaceted C/Re(1121): fabrication, structure, and template for synthesizing nanostructured model Pt electrocatalyst for hydrogen evolution reaction. ACS Nano 2012;6:1404–9.
[53] Cheng N, Stambula S, Wang D, Banis MN, Liu J, Riese A, et al. Platinum single-atom and cluster catalysis of the hydrogen evolution reaction. Nat Commun 2016;7:13638.
[54] Mi Y, Wen L, Wang Z, Cao D, Zhao H, Zhou Y, et al. Ultra-low mass loading of platinum nanoparticles on bacterial cellulose derived carbon nanofibers for efficient hydrogen evolution. Catal Today 2016;262:141–5.
[55] Xu G-R, Hui J-J, Huang T, Chen Y, Lee J-M. Platinum nanocuboids supported on reduced graphene oxide as efficient electrocatalyst for the hydrogen evolution reaction. J Power Sources 2015;285:393–9.
[56] Zeng ZY, Tan CL, Huang X, Bao SY, Zhang H. Growth of noble metal nanoparticles on single-layer TiS_2 and TaS_2 nanosheets for hydrogen evolution reaction. Energy Environ Sci 2014;7:797–803.
[57] Kye J, Shin M, Lim B, Jang J-W, Oh I, Hwang S. Platinum monolayer electrocatalyst on gold nanostructures on silicon for photoelectrochemical hydrogen evolution. ACS Nano 2013;7:6017–23.
[58] Lu J, Zhou W, Wang L, Jia J, Ke Y, Yang L, et al. Core-shell nanocomposites based on gold nanoparticle@zinc-iron-embedded porous carbons derived from metal-organic frameworks as efficient dual catalysts for oxygen reduction and hydrogen evolution reactions. ACS Catal 2016;6:1045–53.
[59] Zhou W, Xiong T, Shi C, Zhou J, Zhou K, Zhu N, et al. Bioreduction of precious metals by microorganism: efficient gold@N-doped carbon electrocatalysts for the hydrogen evolution reaction. Angew Chem Int Ed 2016;55:8416–20.
[60] Ray C, Dutta S, Negishi Y, Pal T. A new stable Pd-Mn_3O_4 nanocomposite as an efficient electrocatalyst for the hydrogen evolution reaction. Chem Commun 2016;52:6095–8.
[61] Pierozynski B. Hydrogen evolution reaction at Pd-modified carbon fibre and nickel-coated carbon fibre materials. Int J Hydrogen Energy 2013;38:7733–40.
[62] Xu Y. The hydrogen evolution reaction on single crystal gold electrode. Int J Hydrogen Energy 2009;34:77–83.
[63] Mech K, Zabinski P, Kowalik R, Tokarski T, Fitzner K. Electrodeposition of Co-Pd alloys from ammonia solutions and their catalytic activity for hydrogen evolution reaction. J Appl Electrochem 2014;44:97–103.
[64] Qin Y, Dai X, Zhang X, Huang X, Sun H, Gao D, et al. Microwave-assisted synthesis of multiply-twinned Au-Ag nanocrystals on reduced graphene oxide for high catalytic performance towards hydrogen evolution reaction. J Mater Chem A 2016;4:3865–71.
[65] Fan Z, Luo Z, Huang X, Li B, Chen Y, Wang J, et al. Synthesis of 4H/fcc noble multimetallic nanoribbons for electrocatalytic hydrogen evolution reaction. J Am Chem Soc 2016;138:1414–9.
[66] Lv H, Xi Z, Chen Z, Guo S, Yu Y, Zhu W, et al. A new core/shell NiAu/Au nanoparticle catalyst with Pt-like activity for hydrogen evolution reaction. J Am Chem Soc 2015;137:5859–62.
[67] Zheng Y, Jiao Y, Zhu Y, Li LH, Han Y, Chen Y, et al. High electrocatalytic hydrogen evolution activity of an anomalous ruthenium catalyst. J Am Chem Soc 2016;138:16174–81.
[68] Zhu L, Lin H, Li Y, Liao F, Lifshitz Y, Sheng M, et al. A rhodium/silicon co-electrocatalyst design concept to surpass platinum hydrogen evolution activity at high overpotentials. Nat Commun 2016;7:12272.
[69] Basu M, Nazir R, Fageria P, Pande S. Construction of CuS/Au heterostructure through a simple photoreduction route for enhanced electrochemical hydrogen evolution and photocatalysis. Sci Rep 2016;6:34738.
[70] Hinnemann B, Moses PG, Bonde J, Jorgensen KP, Nielsen JH, Horch S, et al. Biornimetic hydrogen evolution: MoS_2 nanoparticles as catalyst for hydrogen evolution. J Am Chem Soc 2005;127:5308–9.
[71] Jaramillo TF, Jorgensen KP, Bonde J, Nielsen JH, Horch S, Chorkendorff I. Identification of active edge sites for electrochemical H_2 evolution from MoS_2 nanocatalysts. Science 2007;317:100–2.
[72] Morales-Guio CG, Hu XL. Amorphous molybdenum sulfides as hydrogen evolution catalysts. Acc Chem Res 2014;47:2671–81.
[73] Wang DZ, Wang ZP, Wang CL, Zhou P, Wu ZZ, Liu ZH. Distorted MoS_2 nanostructures: an efficient catalyst for the electrochemical hydrogen evolution reaction. Electrochem Commun 2013;34:219–22.
[74] Ma L, Ting LRL, Molinari V, Giordano C, Yeo BS. Efficient hydrogen evolution reaction catalyzed by molybdenum carbide and molybdenum nitride nanocatalysts synthesized via the urea glass route. J Mater Chem A 2015;3:8361–8.
[75] Wang T, Du K, Liu W, Zhu Z, Shao Y, Li M. Enhanced electrocatalytic activity of MoP microparticles for hydrogen evolution by grinding and electrochemical activation. J Mater Chem A 2015;3:4368–73.
[76] Casalongue HGS, Benck JD, Tsai C, Karlsson RKB, Kaya S, Ng ML, et al. Operando characterization of an amorphous molybdenum sulfide nanoparticle catalyst during the hydrogen evolution reaction. J Phys Chem C 2014;118:29252–9.
[77] Tang C, Sun A, Xu Y, Wu Z, Wang D. High specific surface area Mo_2C nanoparticles as an efficient electrocatalyst for hydrogen evolution. J Power Sources 2015;296:18–22.

[78] Hatay I, Ge PY, Vrubel H, Hu X, Girault HH. Hydrogen evolution at polarised liquid/liquid interfaces catalyzed by molybdenum disulfide. Energy Environ Sci 2011;4:4246–51.
[79] Vrubel H, Hu X. Molybdenum boride and carbide catalyze hydrogen evolution in both acidic and basic solutions. Angew Chem Int Ed 2012;51:12703–6.
[80] Zhao X, Ma X, Sun J, Li D, Yang X. Enhanced catalytic activities of surfactant-assisted exfoliated WS_2 nanodots for hydrogen evolution. ACS Nano 2016;10:2159–66.
[81] Xu J, Cui J, Guo C, Zhao Z, Jiang R, Xu S, et al. Ultrasmall Cu_7S_4@MoS_2 hetero-nanoframes with abundant active edge sites for ultrahigh-performance hydrogen evolution. Angew Chem Int Ed 2016;55:6502–5.
[82] Lin J, Peng ZW, Wang G, Zakhidov D, Larios E, Yacaman MJ, et al. Enhanced electrocatalysis for hydrogen evolution reactions from WS_2 nanoribbons. Adv Energy Mater 2014;4:1301875.
[83] Murugesan S, Akkineni A, Chou BP, Glaz MS, Bout DAV, Stevenson KJ. Room temperature electrodeposition of molybdenum sulfide for catalytic and photoluminescence applications. ACS Nano 2013;7:8199–205.
[84] Shin S, Jin Z, Kwon DH, Bose R, Min Y-S. High turnover frequency of hydrogen evolution reaction on amorphous MoS_2 thin film directly grown by atomic layer deposition. Langmuir 2015;31:1196–202.
[85] Ting LRL, Deng Y, Ma L, Zhang Y-J, Peterson AA, Yeo BS. Catalytic activities of sulfur atoms in amorphous molybdenum sulfide for the electrochemical hydrogen evolution reaction. ACS Catal 2016;6:861–7.
[86] Lee SC, Benck JD, Tsai C, Park J, Koh AL, Abild-Pedersen F, et al. Chemical and phase evolution of amorphous molybdenum sulfide catalysts for electrochemical hydrogen production. ACS Nano 2016;10:624–32.
[87] Vrubel H, Moehl T, Gratzel M, Hu XL. Revealing and accelerating slow electron transport in amorphous molybdenum sulphide particles for hydrogen evolution reaction. Chem Commun 2013;49:8985–7.
[88] Vrubel H, Merki D, Hu XL. Hydrogen evolution catalyzed by MoS_3 and MoS_2 particles. Energy Environ Sci 2012;5:6136–44.
[89] Benck JD, Chen Z, Kuritzky LY, Forman AJ, Jaramillo TF. Amorphous molybdenum sulfide catalysts for electrochemical hydrogen production: insights into the origin of their catalytic activity. ACS Catal 2012;2:1916–23.
[90] Vrubel H, Hu X. Growth and activation of an amorphous molybdenum sulfide hydrogen evolving catalyst. ACS Catal 2013;3:2002–11.
[91] Merki D, Fierro S, Vrubel H, Hu X. Amorphous molybdenum sulfide films as catalysts for electrochemical hydrogen production in water. Chem Sci 2011;2:1262–7.
[92] Tran PD, Tran TV, Orio M, Torelli S, Truong QD, Nayuki K, et al. Coordination polymer structure and revisited hydrogen evolution catalytic mechanism for amorphous molybdenum sulfide. Nat Mater 2016;15:640–6.
[93] Wan C, Regmi YN, Leonard BM. Multiple phases of molybdenum carbide as electrocatalysts for the hydrogen evolution reaction. Angew Chem Int Ed 2014;53:6407–10.
[94] Liao L, Wang SN, Xiao JJ, Bian XJ, Zhang YH, Scanlon MD, et al. A nanoporous molybdenum carbide nanowire as an electrocatalyst for hydrogen evolution reaction. Energy Environ Sci 2014;7:387–92.
[95] Xiao P, Ge X, Wang H, Liu Z, Fisher A, Wang X. Novel molybdenum carbide-tungsten carbide composite nanowires and their electrochemical activation for efficient and stable hydrogen evolution. Adv Funct Mater 2015;25:1520–6.
[96] Chen Z, Cummins D, Reinecke BN, Clark E, Sunkara MK, Jaramillo TF. Core-shell MoO_3-MoS_2 nanowires for hydrogen evolution: a functional design for electrocatalytic materials. Nano Lett 2011;11:4168–75.
[97] Lin H, Shi Z, He S, Yu X, Wang S, Gao Q, et al. Heteronanowires of MoC-Mo_2C as efficient electrocatalysts for hydrogen evolution reaction. Chem Sci 2016;7:3399–405.
[98] Cummins DR, Martinez U, Sherehiy A, Kappera R, Martinez-Garcia A, Schulze RK, et al. Efficient hydrogen evolution in transition metal dichalcogenides via a simple one-step hydrazine reaction. Nat Commun 2016;7:11857.
[99] Ma FX, Wu HB, Xia BY, Xu CY, Lou XW. Hierarchical β-Mo_2C nanotubes organized by ultrathin nanosheets as a highly efficient electrocatalyst for hydrogen production. Angew Chem Int Ed 2015;54:15395–9.
[100] Luo Z, Miao R, Huan TD, Mosa IM, Poyraz AS, Zhong W, et al. Mesoporous MoO_{3-x} material as an efficient electrocatalyst for hydrogen evolution reactions. Adv Energy Mater 2016;6:1600528.
[101] Chen XB, Wang DZ, Wang ZP, Zhou P, Wu ZZ, Jiang F. Molybdenum phosphide: a new highly efficient catalyst for the electrochemical hydrogen evolution reaction. Chem Commun 2014;50:11683–5.
[102] Xiao P, Sk MA, Thia L, Ge XM, Lim RJ, Wang JY, et al. Molybdenum phosphide as an efficient electrocatalyst for the hydrogen evolution reaction. Energy Environ Sci 2014;7:2624–9.
[103] Xing Z, Liu Q, Asiri AM, Sun X. High-efficiency electrochemical hydrogen evolution catalyzed by tungsten phosphide submicroparticles. ACS Catal 2015;5:145–9.
[104] Wen Y, Xia Y, Zhang S. Tungsten disulphide nanorattle: a new type of high performance electrocatalyst for hydrogen evolution reaction. J Power Sources 2016;307:593–8.
[105] Zhao Y, Kamiya K, Hashimoto K, Nakanishi S. In situ CO_2-emission assisted synthesis of molybdenum carbonitride nanomaterial as hydrogen evolution electrocatalyst. J Am Chem Soc 2015;137:110–3.
[106] Wu A, Tian C, Yan H, Jiao Y, Yan Q, Yang G, et al. Hierarchical MoS_2@MoP core-shell heterojunction electrocatalysts for efficient hydrogen evolution reaction over a broad pH range. Nanoscale 2016;8:11052–9.
[107] Zhang J, Wu M-H, Shi Z-T, Jiang M, Jian W-J, Xiao Z, et al. Composition and interface engineering of alloyed $MoS_{2x}Se_{2(1-x)}$ nanotubes for enhanced hydrogen evolution reaction activity. Small 2016;12:4379–85.
[108] Zheng Y, Jiao Y, Jaroniec M, Qiao SZ. Advancing the electrochemistry of the hydrogen-evolution reaction through combining experiment and theory. Angew Chem Int Ed 2015;54:52–65.
[109] Ye R, del Angel-Vicente P, Liu Y, Arellano-Jimenez MJ, Peng Z, Wang T, et al. High-performance hydrogen evolution from $MoS_{2(1-x)}P_x$ solid solution. Adv Mater 2016;28:1427–32.
[110] Tang C, Wang W, Sun A, Qi C, Zhang D, Wu Z, et al. Sulfur-decorated molybdenum carbide catalysts for enhanced hydrogen evolution. ACS Catal 2015;5:6956–63.
[111] Zhao Y, Kamiya K, Hashimoto K, Nakanishi S. Hydrogen evolution by tungsten carbonitride nanoelectrocatalysts synthesized by the formation of a tungsten acid/polymer hybrid in situ. Angew Chem Int Ed 2013;52:13638–41.
[112] Escalera-Lopez D, Niu Y, Yin J, Cooke K, Rees NV, Palmer RE. Enhancement of the hydrogen evolution reaction from Ni-MoS_2 hybrid nanoclusters. ACS Catal 2016;6:6008–17.
[113] Lin H, Liu N, Shi Z, Guo Y, Tang Y, Gao Q. Cobalt-doping in molybdenum-carbide nanowires toward efficient electrocatalytic hydrogen evolution. Adv Funct Mater 2016;26:5590–8.
[114] Merki D, Vrubel H, Rovelli L, Fierro S, Hu X. Fe Co, and Ni ions promote the catalytic activity of amorphous molybdenum sulfide films for hydrogen evolution. Chem Sci 2012;3:2515–25.
[115] Wan C, Leonard BM. Iron-doped molybdenum carbide catalyst with high activity and stability for the hydrogen evolution reaction. Chem Mater 2015;27:4281–8.
[116] Tran PD, Chiam SY, Boix PP, Ren Y, Pramana SS, Fize J, et al. Novel cobalt/nickel-tungsten-sulfide catalysts for electrocatalytic hydrogen generation from water. Energy Environ Sci 2013;6:2452–9.
[117] Yu L, Xia BY, Wang X, Lou XW. General formation of M-MoS_3 (M = Co, Ni) hollow structures with enhanced electrocatalytic activity for hydrogen evolution. Adv Mater 2016;28:92–7.

[118] Wang T, Wang X, Liu Y, Zheng J, Li X. A highly efficient and stable biphasic nanocrystalline Ni-Mo-N catalyst for hydrogen evolution in both acidic and alkaline electrolytes. Nano Energy 2016;22:111–9.
[119] Staszak-Jirkovsky J, Malliakas CD, Lopes PP, Danilovic N, Kota SS, Chang K-C, et al. Design of active and stable Co-Mo-S_x chalcogels as pH-universal catalysts for the hydrogen evolution reaction. Nat Mater 2016;15:197–203.
[120] Xiong K, Li L, Zhang L, Ding W, Peng L, Wang Y, et al. Ni-doped Mo_2C nanowires supported on Ni foam as a binder-free electrode for enhancing the hydrogen evolution performance. J Mater Chem A 2015;3:1863–7.
[121] Fan X, Zhou H, Guo X. WC nanocrystals grown on vertically aligned carbon nanotubes: an efficient and stable electrocatalyst for hydrogen evolution reaction. ACS Nano 2015;9:5125–34.
[122] Hu W-H, Shang X, Han G-Q, Dong B, Liu Y-R, Li X, et al. MoS_x supported graphene oxides with different degree of oxidation as efficient electrocatalysts for hydrogen evolution. Carbon 2016;100:236–42.
[123] He C, Tao J. Synthesis of nanostructured clean surface molybdenum carbides on graphene sheets as efficient and stable hydrogen evolution reaction catalysts. Chem Commun 2015;51:8323–5.
[124] Yan H, Jiao Y, Wu A, Tian C, Zhang X, Wang L, et al. Cluster-like molybdenum phosphide anchored on reduced graphene oxide for efficient hydrogen evolution over a broad pH range. Chem Commun 2016;52:9530–3.
[125] Li F, Li J, Cao Z, Lin X, Li X, Fang Y, et al. MoS_2 quantum dot decorated RGO: a designed electrocatalyst with high active site density for the hydrogen evolution reaction. J Mater Chem A 2015;3:21772–8.
[126] Lin J-F, Pitkanen O, Maklin J, Puskas R, Kukovecz A, Dombovari A, et al. Synthesis of tungsten carbide and tungsten disulfide on vertically aligned multi-walled carbon nanotube forests and their application as non-Pt electrocatalysts for the hydrogen evolution reaction. J Mater Chem A 2015;3:14609–16.
[127] Shi Z, Wang Y, Lin H, Zhang H, Shen M, Xie S, et al. Porous nano MoC@graphite shell derived from a MOFs-directed strategy: an efficient electrocatalyst for the hydrogen evolution reaction. J Mater Chem A 2016;4:6006–13.
[128] Sljukic B, Vujkovic M, Amaral L, Santos DMF, Rocha RP, Sequeira CAC, et al. Carbon-supported Mo_2C electrocatalysts for hydrogen evolution reaction. J Mater Chem A 2015;3:15505–12.
[129] Yang X, Feng X, Tan H, Zang H, Wang X, Wang Y, et al. N-Doped graphene-coated molybdenum carbide nanoparticles as highly efficient electrocatalysts for the hydrogen evolution reaction. J Mater Chem A 2016;4:3947–54.
[130] Li F, Li J, Lin X, Li X, Fang Y, Jiao L, et al. Designed synthesis of multi-walled carbon nanotubes@Cu@MoS_2 hybrid as advanced electrocatalyst for highly efficient hydrogen evolution reaction. J Power Sources 2015;300:301–8.
[131] Pu Z, Liu Q, Asiri AM, Obaid AY, Sun X. Graphene film-confined molybdenum sulfide nanoparticles: facile one-step electrodeposition preparation and application as a highly active hydrogen evolution reaction electrocatalyst. J Power Sources 2014;263:181–5.
[132] Jaramillo TF, Bonde J, Zhang J, Ooi B-L, Andersson K, Ulstrup J, et al. Hydrogen evolution on supported incomplete cubane-type $Mo_3S_4^{4+}$ electrocatalysts. J Phys Chem C 2008;112:17492–8.
[133] Li YG, Wang HL, Xie LM, Liang YY, Hong GS, Dai HJ. MoS_2 nanoparticles grown on graphene: an advanced catalyst for the hydrogen evolution reaction. J Am Chem Soc 2011;133:7296–9.
[134] Liao L, Zhu J, Bian X, Zhu L, Scanlon MD, Girault HH, et al. MoS_2 formed on mesoporous graphene as a highly active catalyst for hydrogen evolution. Adv Funct Mater 2013;23:5326–33.
[135] Yan H, Tian C, Wang L, Wu A, Meng M, Zhao L, et al. Phosphorus-modified tungsten nitride/reduced graphene oxide as a high-performance, non-noble-metal electrocatalyst for the hydrogen evolution reaction. Angew Chem Int Ed 2015;54:6325–9.
[136] Tang Y-J, Gao M-R, Liu C-H, Li S-L, Jiang H-L, Lan Y-Q, et al. Porous molybdenum-based hybrid catalysts for highly efficient hydrogen evolution. Angew Chem Int Ed 2015;54:12928–32.
[137] Wu R, Zhang J, Shi Y, Liu D, Zhang B. Metallic WO_2-carbon mesoporous nanowires as highly efficient electrocatalysts for hydrogen evolution reaction. J Am Chem Soc 2015;137:6983–6.
[138] Cui W, Cheng N, Liu Q, Ge C, Asiri AM, Sun X. Mo_2C nanoparticles decorated graphitic carbon sheets: biopolymer-derived solid-state synthesis and application as an efficient electrocatalyst for hydrogen generation. ACS Catal 2014;4:2658–61.
[139] Huang Y, Gong Q, Song X, Feng K, Nie K, Zhao F, et al. Mo_2C nanoparticles dispersed on hierarchical carbon microflowers for efficient electrocatalytic hydrogen evolution. ACS Nano 2016;10:11337–43.
[140] Pan LF, Li YH, Yang S, Liu PF, Yu MQ, Yang HG. Molybdenum carbide stabilized on graphene with high electrocatalytic activity for hydrogen evolution reaction. Chem Commun 2014;50:13135–7.
[141] Chen WF, Wang CH, Sasaki K, Marinkovic N, Xu W, Muckerman JT, et al. Highly active and durable nanostructured molybdenum carbide electrocatalysts for hydrogen production. Energy Environ Sci 2013;6:943–51.
[142] Youn DH, Han S, Kim JY, Kim JY, Park H, Choi SH, et al. Highly active and stable hydrogen evolution electrocatalysts based on molybdenum compounds on carbon nanotube-graphene hybrid support. ACS Nano 2014;8:5164–73.
[143] Chen W-F, Schneider JM, Sasaki K, Wang C-H, Schneider J, Iyer S, et al. Tungsten carbide-nitride on graphene nanoplatelets as a durable hydrogen evolution electrocatalyst. ChemSusChem 2014;7:2414–8.
[144] Hunt ST, Nimmanwudipong T, Roman-Leshkov Y. Engineering non-sintered, metal-terminated tungsten carbide nanoparticles for catalysis. Angew Chem Int Ed 2014;53:5131–6.
[145] Ma R, Zhou Y, Chen Y, Li P, Liu Q, Wang J. Ultrafine molybdenum carbide nanoparticles composited with carbon as a highly active hydrogen-evolution electrocatalyst. Angew Chem Int Ed 2015;54:14723–7.
[146] Li J-S, Wang Y, Liu C-H, Li S-L, Wang Y-G, Dong L-Z, et al. Coupled molybdenum carbide and reduced graphene oxide electrocatalysts for efficient hydrogen evolution. Nat Commun 2016;7:11204.
[147] Zhu J, Sakaushi K, Clavel G, Shalom M, Antonietti M, Fellinger T-P. A general salt-templating method to fabricate vertically aligned graphitic carbon nanosheets and their metal carbide hybrids for superior lithium ion batteries and water splitting. J Am Chem Soc 2015;137:5480–5.
[148] Wang S, Wang J, Zhu M, Bao X, Xiao B, Su D, et al. Molybdenum-carbide-modified nitrogen-doped carbon vesicle encapsulating nickel nanoparticles: a highly efficient, low-cost catalyst for hydrogen evolution reaction. J Am Chem Soc 2015;137:15753–9.
[149] Chen Y-Y, Zhang Y, Jiang W-J, Zhang X, Dai Z, Wan L-J, et al. Pomegranate-like N, P-doped Mo2 C@C nanospheres as highly active electrocatalysts for alkaline hydrogen evolution. ACS Nano 2016;10:8851–60.
[150] Wu HB, Xia BY, Yu L, Yu X-Y, Lou XW. Porous molybdenum carbide nano-octahedrons synthesized via confined carburization in metal-organic frameworks for efficient hydrogen production. Nat Commun 2015;6:6512.
[151] Yang J, Zhang F, Wang X, He D, Wu G, Yang Q, et al. Porous molybdenum phosphide nano-octahedrons derived from confined phosphorization in UIO-66 for efficient hydrogen evolution. Angew Chem Int Ed 2016;55:12854–8.
[152] Zhang X, Xie Y. Recent advances in free-standing two-dimensional crystals with atomic thickness: design, assembly and transfer strategies. Chem Soc Rev 2013;42:8187–99.
[153] Tan C, Zhang H. Wet-chemical synthesis and applications of non-layer structured two-dimensional nanomaterials. Nat Commun 2015;6:7873.
[154] Gupta A, Sakthivel T, Seal S. Recent development in 2D materials beyond graphene. Progr Mater Sci 2015;73:44–126.
[155] Wu ZZ, Fang BZ, Wang ZP, Wang CL, Liu ZH, Liu FY, et al. MoS_2 nanosheets: a designed structure with high active site density for the hydrogen evolution reaction. ACS Catal 2013;3:2101–7.
[156] Geng X, Sun W, Wu W, Chen B, Al-Hilo A, Benamara M, et al. Pure and stable metallic phase molybdenum disulfide nanosheets for hydrogen evolution reaction. Nat Commun 2016;7:10672.
[157] Zhang S, Chowdari BVR, Wen Z, Jin J, Yang J. Constructing highly oriented configuration by few-layer MoS_2: toward high-performance lithium-ion batteries and hydrogen evolution reactions. ACS Nano 2015;9:12464–72.

[158] Xie J, Zhang H, Li S, Wang R, Sun X, Zhou M, et al. Defect-rich MoS_2 ultrathin nanosheets with additional active edge sites for enhanced electrocatalytic hydrogen evolution. Adv Mater 2013;25:5807–13.
[159] Ye G, Gong Y, Lin J, Li B, He Y, Pantelides ST, et al. Defects engineered monolayer MoS_2 for improved hydrogen evolution reaction. Nano Lett 2016;16:1097–103.
[160] Chung DY, Park SK, Chung YH, Yu SH, Lim DH, Jung N, et al. Edge-exposed MoS_2 nano-assembled structures as efficient electrocatalysts for hydrogen evolution reaction. Nanoscale 2014;6:2131–6.
[161] Xie J, Li S, Zhang X, Zhang J, Wang R, Zhang H, et al. Atomically-thin molybdenum nitride nanosheets with exposed active surface sites for efficient hydrogen evolution. Chem Sci 2014;5:4615–20.
[162] Cao BF, Veith GM, Neuefeind JC, Adzic RR, Khalifah PG. Mixed close-packed cobalt molybdenum nitrides as non-noble metal electrocatalysts for the hydrogen evolution reaction. J Am Chem Soc 2013;135:19186–92.
[163] Deng J, Yuan W, Ren P, Wang Y, Deng D, Zhang Z, et al. High-performance hydrogen evolution electrocatalysis by layer-controlled MoS_2 nanosheets. RSC Adv 2014;4:34733–8.
[164] Voiry D, Yamaguchi H, Li J, Silva R, Alves DCB, Fujita T, et al. Enhanced catalytic activity in strained chemically exfoliated WS_2 nanosheets for hydrogen evolution. Nat Mater 2013;12:850–5.
[165] Voiry D, Salehi M, Silva R, Fujita T, Chen MW, Asefa T, et al. Conducting MoS_2 nanosheets as catalysts for hydrogen evolution reaction. Nano Lett 2013;13:6222–7.
[166] Chang K, Hai X, Pang H, Zhang H, Shi L, Liu G, et al. Targeted synthesis of 2H- and 1T-phase MoS_2 monolayers for catalytic hydrogen evolution. Adv Mater 2016;28:10033–41.
[167] Lin L, Miao N, Wen Y, Zhang S, Ghosez P, Sun Z, et al. Sulfur-depleted monolayered molybdenum disulfide nanocrystals for superelectrochemical hydrogen evolution reaction. ACS Nano 2016;10:8929–37.
[168] Li H, Tsai C, Koh AL, Cai L, Contryman AW, Fragapane AH, et al. Activating and optimizing MoS_2 basal planes for hydrogen evolution through the formation of strained sulphur vacancies. Nat Mater 2016;15:48–53.
[169] Li H, Du M, Mleczko MJ, Koh AL, Nishi Y, Pop E, et al. Kinetic study of hydrogen evolution reaction over strained MoS_2 with sulfur vacancies using scanning electrochemical microscopy. J Am Chem Soc 2016;138:5123–9.
[170] Wang J, Yan M, Zhao K, Liao X, Wang P, Pan X, et al. Field effect enhanced hydrogen evolution reaction of MoS_2 nanosheets. Adv Mater 2016;29:1604464.
[171] Li G, Zhang D, Qiao Q, Yu Y, Peterson D, Zafar A, et al. All the catalytic active sites of MoS_2 for hydrogen evolution. J Am Chem Soc 2016;138:16632–8.
[172] Yin Y, Han J, Zhang Y, Zhang X, Xu P, Yuan Q, et al. Contributions of phase, sulfur vacancies, and edges to the hydrogen evolution reaction catalytic activity of porous molybdenum disulfide nanosheets. J Am Chem Soc 2016;138:7965–72.
[173] Xie J, Zhang J, Li S, Grote F, Zhang X, Zhang H, et al. Controllable disorder engineering in oxygen-incorporated MoS_2 ultrathin nanosheets for efficient hydrogen evolution. J Am Chem Soc 2013;135:17881–8.
[174] Xiao W, Liu P, Zhang J, Song W, Feng YP, Gao D, et al. Dual-functional N dopants in edges and basal plane of MoS_2 nanosheets toward efficient and durable hydrogen evolution. Adv Energy Mater 2016:1602086.
[175] Ren X, Ma Q, Fan H, Pang L, Zhang Y, Yao Y, et al. A Se-doped MoS_2 nanosheet for improved hydrogen evolution reaction. Chem Commun 2015;51:15997–6000.
[176] Sun C, Zhang J, Ma J, Liu P, Gao D, Tao K, et al. N-doped WS_2 nanosheets: a high-performance electrocatalyst for the hydrogen evolution reaction. J Mater Chem A 2016;4:11234–8.
[177] Xu C, Peng S, Tan C, Ang H, Tan H, Zhang H, et al. Ultrathin S-doped $MoSe_2$ nanosheets for efficient hydrogen evolution. J Mater Chem A 2014;2:5597–601.
[178] Deng J, Li H, Xiao J, Tu Y, Deng D, Yang H, et al. Triggering the electrocatalytic hydrogen evolution activity of the inert two-dimensional MoS_2 surface via single-atom metal doping. Energy Environ Sci 2015;8:1594–601.
[179] Sun X, Dai J, Guo Y, Wu C, Hu F, Zhao J, et al. Semimetallic molybdenum disulfide ultrathin nanosheets as an efficient electrocatalyst for hydrogen evolution. Nanoscale 2014;6:8359–67.
[180] Lv X-J, She G-W, Zhou S-X, Li Y-M. Highly efficient electrocatalytic hydrogen production by nickel promoted molybdenum sulfide microspheres catalysts. RSC Adv 2013;3:21231–6.
[181] Gopalakrishnan D, Damien D, Shaijumon MM. MoS_2 quantum dot-interspersed exfoliated MoS_2 nanosheets. ACS Nano 2014;8:5297–303.
[182] Yan Y, Ge XM, Liu ZL, Wang JY, Lee JM, Wang X. Facile synthesis of low crystalline MoS_2 nanosheet-coated CNTs for enhanced hydrogen evolution reaction. Nanoscale 2013;5:7768–71.
[183] Zheng XL, Xu JB, Yan KY, Wang H, Wang ZL, Yang SH. Space-confined growth of MoS_2 nanosheets within graphite: the layered hybrid of MoS_2 and graphene as an active catalyst for hydrogen evolution reaction. Chem Mater 2014;26:2344–53.
[184] Deng ZH, Li L, Ding W, Xiong K, Wei ZD. Synthesized ultrathin MoS_2 nanosheets perpendicular to graphene for catalysis of hydrogen evolution reaction. Chem Commun 2015;51:1893–6.
[185] Firmiano EGS, Cordeiro MAL, Rabelo AC, Dalmaschio CJ, Pinheiro AN, Pereira EC, et al. Graphene oxide as a highly selective substrate to synthesize a layered MoS_2 hybrid electrocatalyst. Chem Commun 2012;48:7687–9.
[186] Huang G, Liu H, Wang S, Yang X, Liu B, Chen H, et al. Hierarchical architecture of WS_2 nanosheets on graphene frameworks with enhanced electrochemical properties for lithium storage and hydrogen evolution. J Mater Chem A 2015;3:24128–38.
[187] Liu Z, Li N, Zhao H, Du Y. Colloidally synthesized $MoSe_2$/graphene hybrid nanostructures as efficient electrocatalysts for hydrogen evolution. J Mater Chem A 2015;3:19706–10.
[188] Xu S, Lei Z, Wu P. Facile preparation of 3D MoS_2/$MoSe_2$ nanosheet-graphene networks as efficient electrocatalysts for the hydrogen evolution reaction. J Mater Chem A 2015;3:16337–47.
[189] Liu N, Yang L, Wang S, Zhong Z, He S, Yang X, et al. Ultrathin MoS_2 nanosheets growing within an in-situ-formed template as efficient electrocatalysts for hydrogen evolution. J Power Sources 2015;275:588–94.
[190] Yang L, Zhou W, Lu J, Hou D, Ke Y, Li G, et al. Hierarchical spheres constructed by defect-rich MoS_2/carbon nanosheets for efficient electrocatalytic hydrogen evolution. Nano Energy 2016;22:490–8.
[191] Huang Y, Lu H, Gu H, Fu J, Mo S, Wei C, et al. A CNT@$MoSe_2$ hybrid catalyst for efficient and stable hydrogen evolution. Nanoscale 2015;7:18595–602.
[192] Shifa TA, Wang F, Cheng Z, Zhan X, Wang Z, Liu K, et al. A vertical-oriented WS_2 nanosheet sensitized by graphene: an advanced electrocatalyst for hydrogen evolution reaction. Nanoscale 2015;7:14760–5.
[193] Zhang J, Wang Q, Wang L, Li Xa, Huang W. Layer-controllable WS2-reduced graphene oxide hybrid nanosheets with high electrocatalytic activity for hydrogen evolution. Nanoscale 2015;7:10391–7.
[194] Kumar TN, Chandrasekaran N, Phani KL. Structural and electronic modification of MoS_2 nanosheets using S-doped carbon for efficient electrocatalysis of the hydrogen evolution reaction. Chem Commun 2015;51:5052–5.
[195] Guo Y, Zhang X, Zhang X, You T. Defect-and S-rich ultrathin MoS_2 nanosheet embedded N-doped carbon nanofibers for efficient hydrogen evolution. J Mater Chem A 2015;3:15927–34.
[196] Du C, Huang H, Wu Y, Wu S, Song W. Ultra-efficient electrocatalytic hydrogen evolution at one-step carbonization generated molybdenum carbide nanosheets/N-doped carbon. Nanoscale 2016;8:16251–8.
[197] Tang Y-J, Wang Y, Wang X-L, Li S-L, Huang W, Dong L-Z, et al. Molybdenum disulfide/nitrogen-doped reduced graphene oxide nanocomposite with enlarged interlayer spacing for electrocatalytic hydrogen evolution. Adv Energy Mater 2016;6:1600116.
[198] Li DJ, Maiti UN, Lim J, Choi DS, Lee WJ, Oh Y, et al. Molybdenum sulfide/N-doped CNT forest hybrid catalysts for high-performance hydrogen evolution reaction. Nano Lett 2014;14:1228–33.

[199] Zhu H, Du M, Zhang M, Zou M, Yang T, Wang S, et al. S-rich single-layered MoS_2 nanoplates embedded in N-doped carbon nanofibers: efficient co-electrocatalysts for the hydrogen evolution reaction. Chem Commun 2014;50:15435–8.
[200] Chen W-F, Sasaki K, Ma C, Frenkel AI, Marinkovic N, Muckerman JT, et al. Hydrogen-evolution catalysts based on non-noble metal nickel-molybdenum nitride nanosheets. Angew Chem Int Ed 2012;51:6131–5.
[201] Zhou WJ, Hou DM, Sang YH, Yao SH, Zhou J, Li GQ, et al. MoO_2 nanobelts@nitrogen self-doped MoS_2 nanosheets as effective electrocatalysts for hydrogen evolution reaction. J Mater Chem A 2014;2:11358–64.
[202] Huang Y, Miao Y-E, Fu J, Mo S, Wei C, Liu T. Perpendicularly oriented few-layer $MoSe_2$ on SnO_2 nanotubes for efficient hydrogen evolution reaction. J Mater Chem A 2015;3:16263–71.
[203] Huang Y, Miao Y-E, Zhang L, Tjiu WW, Pan J, Liu T. Synthesis of few-layered MoS_2 nanosheet-coated electrospun SnO_2 nanotube heterostructures for enhanced hydrogen evolution reaction. Nanoscale 2014;6:10673–9.
[204] Tiwari AP, Kim D, Kim Y, Prakash O, Lee H. Highly active and stable layered ternary transition metal chalcogenide for hydrogen evolution reaction. Nano Energy 2016;28:366–72.
[205] Yan Y, Xia B, Qi X, Wang H, Xu R, Wang J-Y, et al. Nano-tungsten carbide decorated graphene as co-catalysts for enhanced hydrogen evolution on molybdenum disulfide. Chem Commun 2013;49:4884–6.
[206] Shi J, Ma D, Han G-F, Zhang Y, Ji Q, Gao T, et al. Controllable growth and transfer of mono layer MoS_2 on Au foils and its potential application in hydrogen evolution reaction. ACS Nano 2014;8:10196–204.
[207] Lu Z, Zhang H, Zhu W, Yu X, Kuang Y, Chang Z, et al. In situ fabrication of porous MoS_2 thin-films as high-performance catalysts for electrochemical hydrogen evolution. Chem Commun 2013;49:7516–8.
[208] Yu YF, Huang SY, Li YP, Steinmann SN, Yang WT, Cao LY. Layer-dependent electrocatalysis of MoS_2 for hydrogen evolution. Nano Lett 2014;14:553–8.
[209] Chen S, Duan J, Tang Y, Jin B, Qiao SZ. Molybdenum sulfide clusters-nitrogen-doped graphene hybrid hydrogel film as an efficient three-dimensional hydrogen evolution electrocatalyst. Nano Energy 2015;11:11–8.
[210] Yang Y, Fei H, Ruan G, Xiang C, Tour JM. Edge-oriented MoS_2 nanoporous films as flexible electrodes for hydrogen evolution reactions and supercapacitor devices. Adv Mater 2014;26:8163–8.
[211] Tao L, Duan X, Wang C, Duan X, Wang S. Plasma-engineered MoS_2 thin-film as an efficient electrocatalyst for hydrogen evolution reaction. Chem Commun 2015;51:7470–3.
[212] Kibsgaard J, Chen Z, Reinecke BN, Jaramillo TF. Engineering the surface structure of MoS_2 to preferentially expose active edge sites for electrocatalysis. Nat Mater 2012;11:963–9.
[213] Kong D, Wang H, Cha JJ, Pasta M, Koski KJ, Yao J, et al. Synthesis of MoS_2 and $MoSe_2$ films with vertically aligned layers. Nano Lett 2013;13:1341–7.
[214] Wang H, Kong D, Johanes P, Cha JJ, Zheng G, Yan K, et al. $MoSe_2$ and WSe_2 nanofilms with vertically aligned molecular layers on curved and rough surfaces. Nano Lett 2013;13:3426–33.
[215] Wang HT, Lu ZY, Xu SC, Kong DS, Cha JJ, Zheng GY, et al. Electrochemical tuning of vertically aligned MoS_2 nanofilms and its application in improving hydrogen evolution reaction. Proc Natl Acad Sci USA 2013;110:19701–6.
[216] Saadi FH, Carim AI, Velazquez JM, Baricuatro JH, McCrory CCL, Soriaga MP, et al. Operand synthesis of macroporous molybdenum diselenide films for electrocatalysis of the hydrogen-evolution reaction. ACS Catal 2014;4:2866–73.
[217] Wang T, Zhuo J, Du K, Chen B, Zhu Z, Shao Y, et al. Electrochemically fabricated polypyrrole and MoS_x copolymer films as a highly active hydrogen evolution electrocatalyst. Adv Mater 2014;26:3761–6.
[218] Lu Z, Zhu W, Yu X, Zhang H, Li Y, Sun X, et al. Ultrahigh hydrogen evolution performance of under-water "superaerophobic" MoS_2 nanostructured electrodes. Adv Mater 2014;26:2683–7.
[219] Xie X, Yu R, Xue N, Bin Yousaf A, Du H, Liang K, et al. P doped molybdenum dioxide on Mo foil with high electrocatalytic activity for the hydrogen evolution reaction. J Mater Chem A 2016;4:1647–52.
[220] Kibsgaard J, Jaramillo TF. Molybdenum phosphosulfide: an active, acid-stable, earth-abundant catalyst for the hydrogen evolution reaction. Angew Chem Int Ed 2014;53:14433–7.
[221] Wang DZ, Pan Z, Wu ZZ, Wang ZP, Liu ZH. Hydrothermal synthesis of MoS_2 nanoflowers as highly efficient hydrogen evolution reaction catalysts. J Power Sources 2014;264:229–34.
[222] Guo XN, Tong XL, Wang YW, Chen CM, Jin GQ, Guo XY. High photoelectrocatalytic performance of a MoS_2-SiC hybrid structure for hydrogen evolution reaction. J Mater Chem A 2013;1:4657–61.
[223] Cheng L, Huang WJ, Gong QF, Liu CH, Liu Z, Li YG, et al. Ultrathin WS_2 nanoflakes as a high-performance electrocatalyst for the hydrogen evolution reaction. Angew Chem Int Ed 2014;53:7860–3.
[224] Zhang L, Wu HB, Yan Y, Wang X, Lou XW. Hierarchical MoS_2 microboxes constructed by nanosheets with enhanced electrochemical properties for lithium storage and water splitting. Energy Environ Sci 2014;7:3302–6.
[225] Ekspong J, Sharifi T, Shchukarev A, Klechikov A, Wagberg T, Gracia-Espino E. Stabilizing active edge sites in semicrystalline molybdenum sulfide by anchorage on nitrogen-doped carbon nanotubes for hydrogen evolution reaction. Adv Funct Mater 2016;36:6766–76.
[226] Xiang Z, Zhang Z, Xu X, Zhang Q, Yuan C. MoS_2 nanosheets array on carbon cloth as a 3D electrode for highly efficient electrochemical hydrogen evolution. Carbon 2016;98:84–9.
[227] Hou Y, Zhang B, Wen Z, Cui S, Guo X, He Z, et al. A 3D hybrid of layered MoS_2/nitrogen-doped graphene nanosheet aerogels: an effective catalyst for hydrogen evolution in microbial electrolysis cells. J Mater Chem A 2014;2:13795–800.
[228] Park S-K, Chung DY, Ko D, Sung Y-E, Piao Y. Three-dimensional carbon foam/N-doped graphene@MoS_2 hybrid nanostructures as effective electrocatalysts for the hydrogen evolution reaction. J Mater Chem A 2016;4:12720–5.
[229] Zhang X, Zhang Y, Yu B-B, Yin X-L, Jiang W-J, Jiang Y, et al. Physical vapor deposition of amorphous MoS_2 nanosheet arrays on carbon cloth for highly reproducible large-area electrocatalysts for the hydrogen evolution reaction. J Mater Chem A 2015;3:19277–81.
[230] Kwon DH, Jin Z, Shin S, Lee W-S, Min Y-S. A comprehensive study on atomic layer deposition of molybdenum sulfide for electrochemical hydrogen evolution. Nanoscale 2016;8:7180–8.
[231] Dou S, Wu J, Tao L, Shen A, Huo J, Wang S. Carbon-coated MoS_2 nanosheets as highly efficient electrocatalysts for the hydrogen evolution reaction. Nanotechnology 2016;27:045402.
[232] Shi J, Pu Z, Liu Q, Asiri AM, Hu J, Sun X. Tungsten nitride nanorods array grown on carbon cloth as an efficient hydrogen evolution cathode at all pH values. Electrochim Acta 2015;154:345–51.
[233] Deng C, Ding F, Li X, Guo Y, Ni W, Yan H, et al. Templated-preparation of a three-dimensional molybdenum phosphide sponge as a high performance electrode for hydrogen evolution. J Mater Chem A 2016;4:59–66.
[234] Zhou H, Yu F, Sun J, He R, Wang Y, Guo CF, et al. Highly active and durable self-standing WS_2/graphene hybrid catalysts for the hydrogen evolution reaction. J Mater Chem A 2016;4:9472–6.
[235] Zhu W, Tang C, Liu D, Wang J, Asiri AM, Sun X. A self-standing nanoporous MoP_2 nanosheet array: an advanced pH-universal catalytic electrode for the hydrogen evolution reaction. J Mater Chem A 2016;4:7169–73.
[236] Wu T, Pi M, Zhang D, Chen S. Three-dimensional porous structural MoP_2 nanoparticles as a novel and superior catalyst for electrochemical hydrogen evolution. J Power Sources 2016;328:551–7.
[237] Liu Y, Ren L, Zhang Z, Qi X, Li H, Zhong J. 3D binder-free $MoSe_2$ nanosheets/carbon cloth electrodes for efficient and stable hydrogen evolution prepared by simple electrophoresis deposition strategy. Sci Rep 2016;6:22516.
[238] Ang H, Wang H, Li B, Zong Y, Wang X, Yan Q. 3D hierarchical porous Mo_2C for efficient hydrogen evolution. Small 2016;12:2859–65.
[239] Wang X-D, Xu Y-F, Rao H-S, Xu W-J, Chen H-Y, Zhang W-X, et al. Novel porous molybdenum tungsten phosphide hybrid nanosheets on carbon cloth for efficient hydrogen evolution. Energy Environ Sci 2016;9:1468–75.

[240] Zhang Y, Ouyang B, Xu J, Chen S, Rawat RS, Fan HJ. 3D porous hierarchical nickel-molybdenum nitrides synthesized by RF plasma as highly active and stable hydrogen-evolution-reaction electrocatalysts. Adv Energy Mater 2016;6:1600221.
[241] Tan Y, Liu P, Chen L, Cong W, Ito Y, Han J, et al. Monolayer MoS_2 films supported by 3D nanoporous metals for high-efficiency electrocatalytic hydrogen production. Adv Mater 2014;26:8023–8.
[242] Ma CB, Qi XY, Chen B, Bao SY, Yin ZY, Wu XJ, et al. MoS_2 nanoflower-decorated reduced graphene oxide paper for high-performance hydrogen evolution reaction. Nanoscale 2014;6:5624–9.
[243] Jin Y, Shen PK. Nanoflower-like metallic conductive MoO_2 as a high-performance non-precious metal electrocatalyst for the hydrogen evolution reaction. J Mater Chem A 2015;3:20080–5.
[244] Gong Q, Cheng L, Liu C, Zhang M, Feng Q, Ye H, et al. Ultrathin $MoS_{2(1-x)}Se_{2x}$ alloy nanoflakes for electrocatalytic hydrogen evolution reaction. ACS Catal 2015;5:2213–9.
[245] Zou M, Chen J, Xiao L, Zhu H, Yang T, Zhang M, et al. WSe_2 and $W(Se_xS_{1-x})_2$ nanoflakes grown on carbon nanofibers for the electrocatalytic hydrogen evolution reaction. J Mater Chem A 2015;3:18090–7.
[246] Xu K, Wang FM, Wang ZX, Zhan XY, Wang QS, Cheng ZZ, et al. Component-controllable $WS_{2(1-x)}Se_{2x}$ nanotubes for efficient hydrogen evolution reaction. ACS Nano 2014;8:8468–76.
[247] Kiran V, Mukherjee D, Jenjeti RN, Sampath S. Active guests in the MoS_2/$MoSe_2$ host lattice: efficient hydrogen evolution using few-layer alloys of $MoS_{2(1-x)}Se_{2x}$. Nanoscale 2014;6:12856–63.
[248] Duan J, Chen S, Chambers BA, Andersson GG, Qiao SZ. 3D WS_2 nanolayers@heteroatom-doped graphene films as hydrogen evolution catalyst electrodes. Adv Mater 2015;27:4234–41.
[249] Tian L, Yan X, Chen X. Electrochemical activity of iron phosphide nanoparticles in hydrogen evolution reaction. ACS Catal 2016;6:5441–8.
[250] Callejas JF, McEnaney JM, Read CG, Crompton JC, Biacchi AJ, Popczun EJ, et al. Electrocatalytic and photocatalytic hydrogen production from acidic and neutral-pH aqueous solutions using iron phosphide nanoparticles. ACS Nano 2014;8:11101–7.
[251] Fan X, Peng Z, Ye R, Zhou H, Guo X. M_3C (M: Fe Co, Ni) nanocrystals encased in graphene nanoribbons: an active and stable bifunctional electrocatalyst for oxygen reduction and hydrogen evolution reactions. ACS Nano 2015;9:7407–18.
[252] Zhang Z, Lu B, Hao J, Yang W, Tang J. FeP nanoparticles grown on graphene sheets as highly active non-precious-metal electrocatalysts for hydrogen evolution reaction. Chem Commun 2014;50:11554–7.
[253] Jiang J, Wang C, Zhang J, Wang W, Zhou X, Pan B, et al. Synthesis of FeP_2/C nanohybrids and their performance for hydrogen evolution reaction. J Mater Chem A 2015;3:499–503.
[254] Lv C, Yang Q, Huang Q, Huang Z, Xia H, Zhang C. Phosphorus doped single wall carbon nanotubes loaded with nanoparticles of iron phosphide and iron carbide for efficient hydrogen evolution. J Mater Chem A 2016;4:13336–43.
[255] Zhu X, Liu M, Liu Y, Chen R, Nie Z, Li J, et al. Carbon-coated hollow mesoporous FeP microcubes: an efficient and stable electrocatalyst for hydrogen evolution. J Mater Chem A 2016;4:8974–7.
[256] Zhang Z, Hao J, Yang W, Lu B, Tang J. Modifying candle soot with FeP nanoparticles into high-performance and cost-effective catalysts for the electrocatalytic hydrogen evolution reaction. Nanoscale 2015;7:4400–5.
[257] Tavakkoli M, Kallio T, Reynaud O, Nasibulin AG, Johans C, Sainio J, et al. Single-shell carbon-encapsulated iron nanoparticles: synthesis and high electrocatalytic activity for hydrogen evolution reaction. Angew Chem Int Ed 2015;54:4535–8.
[258] Deng J, Ren P, Deng D, Yu L, Yang F, Bao X. Highly active and durable non-precious-metal catalysts encapsulated in carbon nanotubes for hydrogen evolution reaction. Energy Environ Sci 2014;7:1919–23.
[259] Xu Y, Wu R, Zhang JF, Shi YM, Zhang B. Anion-exchange synthesis of nanoporous FeP nanosheets as electrocatalysts for hydrogen evolution reaction. Chem Commun 2013;49:6656–8.
[260] Liang Y, Liu Q, Asiri AM, Sun X, Luo Y. Self-supported FeP nanorod arrays: a cost-effective 3D hydrogen evolution cathode with high catalytic activity. ACS Catal 2014;4:4065–9.
[261] Yan Y, Thia L, Xia BY, Ge X, Liu Z, Fisher A, et al. Construction of efficient 3D gas evolution electrocatalyst for hydrogen evolution: porous FeP nanowire arrays on graphene sheets. Adv Sci 2015;2:1500120.
[262] Jiang P, Liu Q, Liang Y, Tian J, Asiri AM, Sun X. A cost-effective 3D hydrogen evolution cathode with high catalytic activity: FeP nanowire array as the active phase. Angew Chem Int Ed 2014;53:12855–9.
[263] Son CY, Kwak IH, Lim YR, Park J. FeP and FeP_2 nanowires for efficient electrocatalytic hydrogen evolution reaction. Chem Commun 2016;52:2819–22.
[264] Yang X, Lu A-Y, Zhu Y, Min S, Hedhili MN, Han Y, et al. Rugae-like FeP nanocrystal assembly on a carbon cloth: an exceptionally efficient and stable cathode for hydrogen evolution. Nanoscale 2015;7:10974–81.
[265] Jasion D, Barforoush JM, Qiao Q, Zhu Y, Ren S, Leonard KC. Low-dimensional hyperthin FeS_2 nanostructures for efficient and stable hydrogen evolution electrocatalysis. ACS Catal 2015;5:6653–7.
[266] Guo Y, Shang C, Zhang X, Wang E. Electrocatalytic hydrogen evolution using the MS_2@MoS_2/rGO (M = Fe or Ni) hybrid catalyst. Chem Commun 2016;52:11795–8.
[267] Kong DS, Cha JJ, Wang HT, Lee HR, Cui Y. First-row transition metal dichalcogenide catalysts for hydrogen evolution reaction. Energy Environ Sci 2013;6:3553–8.
[268] Sun YJ, Liu C, Grauer DC, Yano JK, Long JR, Yang PD, et al. Electrodeposited cobalt-sulfide catalyst for electrochemical and photoelectrochemical hydrogen generation from water. J Am Chem Soc 2013;135:17699–702.
[269] Faber MS, Dziedzic R, Lukowski MA, Kaiser NS, Ding Q, Jin S. High-performance electrocatalysis using metallic cobalt pyrite (CoS_2) micro- and nanostructures. J Am Chem Soc 2014;136:10053–61.
[270] Kornienko N, Resasco J, Becknell N, Jian C-M, Liu Y-S, Nie K, et al. Operando spectroscopic analysis of an amorphous cobalt sulfide hydrogen evolution electrocatalyst. J Am Chem Soc 2015;137:7448–55.
[271] Caban-Acevedo M, Stone ML, Schmidt JR, Thomas JG, Ding Q, Chang H-C, et al. Efficient hydrogen evolution catalysis using ternary pyrite-type cobalt phosphosulphide. Nat Mater 2015;14:1245–51.
[272] Liu W, Hu E, Jiang H, Xiang Y, Weng Z, Li M, et al. A highly active and stable hydrogen evolution catalyst based on pyrite-structured cobalt phosphosulfide. Nat Commun 2016;7:10771.
[273] Peng S, Li L, Han X, Sun W, Srinivasan M, Mhaisalkar SG, et al. Cobalt sulfide nanosheet/graphene/carbon nanotube nanocomposites as flexible electrodes for hydrogen evolution. Angew Chem Int Ed 2014;53:12594–9.
[274] Feng L-L, Fan M, Wu Y, Liu Y, Li G-D, Chen H, et al. Metallic Co_9S_8 nanosheets grown on carbon cloth as efficient binder-free electrocatalysts for the hydrogen evolution reaction in neutral media. J Mater Chem A 2016;4:6860–7.
[275] Ouyang C, Wang X, Wang S. Phosphorus-doped CoS_2 nanosheet arrays as ultra-efficient electrocatalysts for the hydrogen evolution reaction. Chem Commun 2015;51:14160–3.
[276] Zhang H, Lei L, Zhang X. One-step synthesis of cubic pyrite-type $CoSe_2$ at low temperature for efficient hydrogen evolution reaction. RSC Adv 2014;4:54344–8.
[277] Zhang H, Yang B, Wu X, Li Z, Lei L, Zhang X. Polymorphic $CoSe_2$ with mixed orthorhombic and cubic phases for highly efficient hydrogen evolution reaction. ACS Appl Mater Inter 2015;7:1772–9.
[278] Chen P, Xu K, Tao S, Zhou T, Tong Y, Ding H, et al. Phase-transformation engineering in cobalt diselenide realizing enhanced catalytic activity for hydrogen evolution in an alkaline medium. Adv Mater 2016;28:7527–32.
[279] Kong DS, Wang HT, Lu ZY, Cui Y. $CoSe_2$ nanoparticles grown on carbon fiber paper: an efficient and stable electrocatalyst for hydrogen evolution reaction. J Am Chem Soc 2014;136:4897–900.

[280] Liu Q, Shi J, Hu J, Asiri AM, Luo Y, Sun X. $CoSe_2$ nanowires array as a 3D electrode for highly efficient electrochemical hydrogen evolution. ACS Appl Mater Inter 2015;7:3877–81.
[281] Lee C-P, Chen W-F, Billo T, Lin Y-G, Fu F-Y, Samireddi S, et al. Beaded stream-like $CoSe_2$ nanoneedle array for efficient hydrogen evolution electrocatalysis. J Mater Chem A 2016;4:4553–61.
[282] Wang K, Zhou C, Xi D, Shi Z, He C, Xia H, et al. Component-controllable synthesis of $Co(S_xSe_{1-x})_2$ nanowires supported by carbon fiber paper as high-performance electrode for hydrogen evolution reaction. Nano Energy 2015;18:1–11.
[283] Liu K, Wang F, Xu K, Shifa TA, Cheng Z, Zhan X, et al. $CoS_{2x}Se_{2(1-x)}$ nanowire array: an efficient ternary electrocatalyst for the hydrogen evolution reaction. Nanoscale 2016;8:4699–704.
[284] Tian L, Yan X, Chen X, Liu L, Chen X. One-pot, large-scale, simple synthesis of Co_xP nanocatalysts for electrochemical hydrogen evolution. J Mater Chem A 2016;4:13011–6.
[285] Jiang P, Liu Q, Ge C, Cui W, Pu Z, Asiri AM, et al. CoP nanostructures with different morphologies: synthesis, characterization and a study of their electrocatalytic performance toward the hydrogen evolution reaction. J Mater Chem A 2014;2:14634–40.
[286] Liu Q, Tian J, Cui W, Jiang P, Cheng N, Asiri AM, et al. Carbon nanotubes decorated with CoP nanocrystals: a highly active non-noble-metal nanohybrid electrocatalyst for hydrogen evolution. Angew Chem Int Ed 2014;53:6710–4.
[287] Pan Y, Lin Y, Chen Y, Liu Y, Liu C. Cobalt phosphide-based electrocatalysts: synthesis and phase catalytic activity comparison for hydrogen evolution. J Mater Chem A 2016;4:4745–54.
[288] Li M, Liu X, Xiong Y, Bo X, Zhang Y, Han C, et al. Facile synthesis of various highly dispersive CoP nanocrystal embedded carbon matrices as efficient electrocatalysts for the hydrogen evolution reaction. J Mater Chem A 2015;3:4255–65.
[289] Popczun EJ, Read CG, Roske CW, Lewis NS, Schaak RE. Highly active electrocatalysis of the hydrogen evolution reaction by cobalt phosphide nanoparticles. Angew Chem Int Ed 2014;53:5427–30.
[290] Zhou D, He L, Zhu W, Hou X, Wang K, Du G, et al. Interconnected urchin-like cobalt phosphide microspheres film for highly efficient electrochemical hydrogen evolution in both acidic and basic media. J Mater Chem A 2016;4:10114–7.
[291] Tian JQ, Liu Q, Asiri AM, Sun XP. Self-supported nanoporous cobalt phosphide nanowire arrays: an efficient 3D hydrogen-evolving cathode over the wide range of pH 0–14. J Am Chem Soc 2014;136:7587–90.
[292] Saadi FH, Carim AI, Verlage E, Hemminger JC, Lewis NS, Soriaga MP. CoP as an acid-stable active electrocatalyst for the hydrogen-evolution reaction: electrochemical synthesis, interfacial characterization and performance evaluation. J Phys Chem C 2014;118:29294–300.
[293] Zhou W, Zhou Y, Yang L, Huang J, Ke Y, Zhou K, et al. N-doped carbon-coated cobalt nanorod arrays supported on a titanium mesh as highly active electrocatalysts for the hydrogen evolution reaction. J Mater Chem A 2015;3:1915–9.
[294] Zou XC, Huang XC, Goswami A, Silva R, Sathe BR, Mikmekova E, et al. Cobalt-embedded nitrogen-rich carbon nanotubes efficiently catalyze hydrogen evolution reaction at all pH values. Angew Chem Int Ed 2014;53:4372–6.
[295] Zhang X, Liu R, Zang Y, Liu G, Wang G, Zhang Y, et al. Co/CoO nanoparticles immobilized on Co-N-doped carbon as trifunctional electrocatalysts for oxygen reduction, oxygen evolution and hydrogen evolution reactions. Chem Commun 2016;52:5946–9.
[296] Wang Z-L, Hao X-F, Jiang Z, Sun X-P, Xu D, Wang J, et al. C and N hybrid coordination derived Co-C-N complex as a highly efficient electrocatalyst for hydrogen evolution reaction. J Am Chem Soc 2015;137:15070–3.
[297] Liang H-W, Brueller S, Dong R, Zhang J, Feng X, Muellen K. Molecular metal-N-x centres in porous carbon for electrocatalytic hydrogen evolution. Nat Commun 2015;6:7992.
[298] Masa J, Weide P, Peeters D, Sinev I, Xia W, Sun Z, et al. Amorphous cobalt boride (Co_2B) as a highly efficient nonprecious catalyst for electrochemical water splitting: oxygen and hydrogen evolution. Adv Energy Mater 2016;6:1502313.
[299] Gupta S, Patel N, Miotello A, Kothari DC. Cobalt-boride: an efficient and robust electrocatalyst for hydrogen evolution reaction. J Power Sources 2015;279:620–5.
[300] Ahn SH, Hwang SJ, Yoo SJ, Choi I, Kim HJ, Jang JH, et al. Electrodeposited Ni dendrites with high activity and durability for hydrogen evolution reaction in alkaline water electrolysis. J Mater Chem 2012;22:15153–9.
[301] Chen Z, Ma Z, Song J, Wang L, Shao G. Novel one-step synthesis of wool-ball-like Ni-carbon nanotubes composite cathodes with favorable electrocatalytic activity for hydrogen evolution reaction in alkaline solution. J Power Sources 2016;324:86–96.
[302] Fan L, Liu PF, Yan X, Gu L, Yang ZZ, Yang HG, et al. Atomically isolated nickel species anchored on graphitized carbon for efficient hydrogen evolution electrocatalysis. Nat Commun 2016;7:10667.
[303] Popczun EJ, McKone JR, Read CG, Biacchi AJ, Wiltrout AM, Lewis NS, et al. Nanostructured nickel phosphide as an electrocatalyst for the hydrogen evolution reaction. J Am Chem Soc 2013;135:9267–70.
[304] Feng L, Vrubel H, Bensimon M, Hu X. Easily-prepared dinickel phosphide (Ni_2P) nanoparticles as an efficient and robust electrocatalyst for hydrogen evolution. Phys Chem Chem Phys 2014;16:5917–21.
[305] Chang J, Li S, Li G, Ge J, Liu C, Xing W. Monocrystalline $Ni_{12}P_5$ hollow spheres with ultrahigh specific surface areas as advanced electrocatalysts for the hydrogen evolution reaction. J Mater Chem A 2016;4:9755–9.
[306] Chung DY, Han JW, Lim D-H, Jo J-H, Yoo SJ, Lee H, et al. Structure dependent active sites of Ni_xS_y as electrocatalysts for hydrogen evolution reaction. Nanoscale 2015;7:5157–63.
[307] Jiang P, Liu Q, Sun X. NiP_2 nanosheet arrays supported on carbon cloth: an efficient 3D hydrogen evolution cathode in both acidic and alkaline solutions. Nanoscale 2014;6:13440–5.
[308] Pu Z, Liu Q, Tang C, Asiri AM, Sun X. Ni_2P nanoparticle films supported on a Ti plate as an efficient hydrogen evolution cathode. Nanoscale 2014;6:11031–4.
[309] Huang Z, Chen Z, Chen Z, Lv C, Meng H, Zhang C. $Ni_{12}P_5$ nanoparticles as an efficient catalyst for hydrogen generation via electrolysis and photoelectrolysis. ACS Nano 2014;8:8121–9.
[310] Tang C, Cheng N, Pu Z, Xing W, Sun X. NiSe nanowire film supported on nickel foam: an efficient and stable 3D bifunctional electrode for full water splitting. Angew Chem Int Ed 2015;54:9351–5.
[311] Zhou H, Wang Y, He R, Yu F, Sun J, Wang F, et al. One-step synthesis of self-supported porous $NiSe_2$/Ni hybrid foam: an efficient 3D electrode for hydrogen evolution reaction. Nano Energy 2016;20:29–36.
[312] Tang C, Xie L, Sun X, Asiri AM, He Y. Highly efficient electrochemical hydrogen evolution based on nickel diselenide nanowall film. Nanotechnology 2016;27:20LT02.
[313] Liu P, Rodriguez JA. Catalysts for hydrogen evolution from the NiFe hydrogenase to the $Ni_2P(001)$ surface: the importance of ensemble effect. J Am Chem Soc 2005;127:14871–8.
[314] Wang D-Y, Gong M, Chou H-L, Pan C-J, Chen H-A, Wu Y, et al. Highly active and stable hybrid catalyst of cobalt-doped FeS_2 nanosheets-carbon nanotubes for hydrogen evolution reaction. J Am Chem Soc 2015;137:1587–92.
[315] Huang Z-F, Song J, Li K, Tahir M, Wang Y-T, Pan L, et al. Hollow cobalt-based bimetallic sulfide polyhedra for efficient all-pH-value electrochemical and photocatalytic hydrogen evolution. J Am Chem Soc 2016;138:1359–65.
[316] Long X, Li G, Wang Z, Zhu H, Zhang T, Xiao S, et al. Metallic Iron-nickel sulfide ultrathin nanosheets as a highly active electrocatalyst for hydrogen evolution reaction in acidic media. J Am Chem Soc 2015;137:11900–3.
[317] Xu YF, Gao MR, Zheng YR, Jiang J, Yu SH. Nickel/Nickel(II) oxide nanoparticles anchored onto cobalt(IV) diselenide nanobelts for the electrochemical production of hydrogen. Angew Chem Int Ed 2013;52:8546–50.
[318] Feng Y, Yu X-Y, Paik U. Nickel cobalt phosphides quasi-hollow nanocubes as an efficient electrocatalyst for hydrogen evolution in alkaline solution. Chem Commun 2016;52:1633–6.

[319] Li Q, Xing Z, Wang D, Sun X, Yang X. In situ electrochemically activated CoMn-S@NiO/CC nanosheets array for enhanced hydrogen evolution. ACS Catal 2016;6:2797–801.
[320] Liu T, Ma X, Liu D, Hao S, Du G, Ma Y, et al. Mn doping of CoP nanosheets array: an efficient electrocatalyst for hydrogen evolution reaction with enhanced activity at all pH values. ACS Catal 2016:98–102.
[321] Ansovini D, Lee CJJ, Chua CS, Ong LT, Tan HR, Webb WR, et al. A highly active hydrogen evolution electrocatalyst based on a cobalt-nickel sulfide composite electrode. J Mater Chem A 2016;4:9744–9.
[322] Li Y, Zhang H, Jiang M, Kuang Y, Wang H, Sun X. Amorphous Co-Mo-S ultrathin films with low-temperature sulfurization as high-performance electrocatalysts for the hydrogen evolution reaction. J Mater Chem A 2016;4:13731–5.
[323] Ma L, Hu Y, Chen R, Zhu G, Chen T, Lv H, et al. Self-assembled ultrathin $NiCo_2S_4$ nanoflakes grown on Ni foam as high-performance flexible electrodes for hydrogen evolution reaction in alkaline solution. Nano Energy 2016;24:139–47.
[324] Duan J, Chen S, Vasileff A, Qiao SZ. Anion and cation modulation in metal compounds for bifunctional overall water splitting. ACS Nano 2016;10:8738–45.
[325] Wang J, Zhong H-X, Wang Z-L, Meng F-L, Zhang X-B. Integrated three-dimensional carbon paper/carbon tubes/cobalt-sulfide sheets as an efficient electrode for overall water splitting. ACS Nano 2016;10:2342–8.
[326] Qu K, Zheng Y, Jiao Y, Zhang X, Dai S, Qiao S-Z. Polydopamine-inspired, dual heteroatom-doped carbon nanotubes for highly efficient overall water splitting. Adv Energy Mater 2017;7:1602068.
[327] Chen G-F, Ma TY, Liu Z-Q, Li N, Su Y-Z, Davey K, et al. Efficient and stable bifunctional electrocatalysts Ni/Ni_xM_y(M = P, S) for overall water splitting. Adv Funct Mater 2016;26:3314–23.
[328] Li J, Yan M, Zhou X, Huang Z-Q, Xia Z, Chang C-R, et al. Mechanistic insights on ternary $Ni_{2-x}Co_xP$ for hydrogen evolution and their hybrids with graphene as highly efficient and robust catalysts for overall water splitting. Adv Funct Mater 2016;36:6785–96.
[329] Sivanantham A, Ganesan P, Shanmugam S. Hierarchical $NiCo_2S_4$ nanowire arrays supported on Ni foam: an efficient and durable bifunctional electrocatalyst for oxygen and hydrogen evolution reactions. Adv Funct Mater 2016;26:4661–72.
[330] Zhu Y, Ma TY, Jaroniec M, Qiao SZ. Self-templating synthesis of hollow Co_3O_4 microtube arrays for highly efficient water electrolysis. Angew Chem Int Ed 2017;56:1324–8.
[331] Yan Y, Xia BY, Ge X, Liu Z, Fisher A, Wang X. A flexible electrode based on iron phosphide nanotubes for overall water splitting. Chemistry 2015;21:18062–7.
[332] Jin H, Wang J, Su D, Wei Z, Pang Z, Wang Y. In situ cobalt-cobalt oxide/N-doped carbon hybrids as superior bifunctional electrocatalysts for hydrogen and oxygen evolution. J Am Chem Soc 2015;137:2688–94.
[333] Bayatsarmadi B, Zheng Y, Tang Y, Jaroniec M, Qiao SZ. Significant enhancement of water splitting activity of N-carbon electrocatalyst by trace level Co doping. Small 2016;12:3703–11.
[334] Tian J, Liu Q, Cheng N, Asiri AM, Sun X. Self-supported Cu_3P nanowire arrays as an integrated high-performance three-dimensional cathode for generating hydrogen from water. Angew Chem Int Ed 2014;53:9577–81.
[335] Shinde SS, Sami A, Kim D-H, Lee J-H. Nanostructured SnS-N-doped graphene as an advanced electrocatalyst for the hydrogen evolution reaction. Chem Commun 2015;51:15716–9.
[336] Han Y, Yue X, Jin Y, Huang X, Shen PK. Hydrogen evolution reaction in acidic media on single-crystalline titanium nitride nanowires as an efficient non-noble metal electrocatalyst. J Mater Chem A 2016;4:3673–7.
[337] Kumar B, Saha S, Basu M, Ganguli AK. Enhanced hydrogen/oxygen evolution and stability of nanocrystalline (4–6 nm) copper particles. J Mater Chem A 2013;1:4728–35.
[338] Peng X, Hu L, Wang L, Zhang X, Fu J, Huo K, et al. Vanadium carbide nanoparticles encapsulated in graphitic carbon network nanosheets: a high-efficiency electrocatalyst for hydrogen evolution reaction. Nano Energy 2016;26:603–9.
[339] Zhou Y, Zhou W, Hou D, Li G, Wan J, Feng C, et al. Metal-carbon hybrid electrocatalysts derived from ion-exchange resin containing heavy metals for efficient hydrogen evolution reaction. Small 2016;12:2768–74.
[340] Shalom M, Gimenez S, Schipper F, Herraiz-Cardona I, Bisquert J, Antonietti M. Controlled carbon nitride growth on surfaces for hydrogen evolution electrodes. Angew Chem Int Ed 2014;53:3654–8.
[341] Zheng Y, Jiao Y, Zhu Y, Li LH, Han Y, Chen Y, et al. Hydrogen evolution by a metal-free electrocatalyst. Nat Commun 2014;5:3783.
[342] Das RK, Wang Y, Vasilyeva SV, Donoghue E, Pucher I, Kamenov G, et al. Extraordinary hydrogen evolution and oxidation reaction activity from carbon nanotubes and graphitic carbons. ACS Nano 2014;8:8447–56.
[343] Cui W, Liu Q, Cheng NY, Asiri AM, Sun XP. Activated carbon nanotubes: a highly-active metal-free electrocatalyst for hydrogen evolution reaction. Chem Commun 2014;50:9340–2.
[344] Zhuo JQ, Wang TY, Zhang G, Liu L, Gan LB, Li MX. Salts of $C_{60}(OH)_8$ electrodeposited onto a glassy carbon electrode: surprising catalytic performance in the hydrogen evolution reaction. Angew Chem Int Ed 2013;52:10867–70.
[345] Geng D, Chen Y, Chen Y, Li Y, Li R, Sun X, et al. High oxygen-reduction activity and durability of nitrogen-doped graphene. Energy Environ Sci 2011;4:760–4.
[346] Liu Z-W, Peng F, Wang H-J, Yu H, Zheng W-X, Yang J. Phosphorus-doped graphite layers with high electrocatalytic activity for the O_2 reduction in an alkaline medium. Angew Chem Int Ed 2011;50:3257–61.
[347] Sathe BR, Zou XX, Asefa T. Metal-free B-doped graphene with efficient electrocatalytic activity for hydrogen evolution reaction. Catal Sci Technol 2014;4:2023–30.
[348] Chhetri M, Maitra S, Chakraborty H, Waghmare UV, Rao CNR. Superior performance of borocarbonitrides, $B_xC_yN_z$, as stable, low-cost metal-free electrocatalysts for the hydrogen evolution reaction. Energy Environ Sci 2016;9:95–101.
[349] Duan J, Chen S, Jaroniec M, Qiao SZ. Heteroatom-doped graphene-based materials for energy-relevant electrocatalytic processes. ACS Catal 2015;5:5207–34.
[350] Zheng Y, Jiao Y, Qiao SZ. Engineering of carbon-based electrocatalysts for emerging energy conversion: from fundamentality to functionality. Adv Mater 2015;27:5372–8.
[351] Jiao Y, Zheng Y, Davey K, Qiao S-Z. Activity origin and catalyst design principles for electrocatalytic hydrogen evolution on heteroatom-doped graphene. Nature Energy 2016;1:16130.
[352] Zheng Y, Jiao Y, Li LH, Xing T, Chen Y, Jaroniec M, et al. Toward design of synergistically active carbon-based catalysts for electrocatalytic hydrogen evolution. ACS Nano 2014;8:5290–6.
[353] Duan J, Chen S, Jaroniec M, Qiao SZ. Porous C_3N_4 nanolayers@N-graphene films as catalyst electrodes for highly efficient hydrogen evolution. ACS Nano 2015;9:931–40.
[354] Zhang J, Qu L, Shi G, Liu J, Chen J, Dai L. N, P-codoped carbon networks as efficient metal-free bifunctional catalysts for oxygen reduction and hydrogen evolution reactions. Angew Chem Int Ed 2016;55:2230–4.
[355] Yan D, Dou S, Tao L, Liu Z, Liu Z, Huo J, et al. Electropolymerized supermolecule derived N, P co-doped carbon nanofiber networks as a highly efficient metal-free electrocatalyst for the hydrogen evolution reaction. J Mater Chem A 2016;4:13726–30.
[356] Ito Y, Cong W, Fujita T, Tang Z, Chen M. High catalytic activity of nitrogen and sulfur Co-doped nanoporous graphene in the hydrogen evolution reaction. Angew Chem Int Ed 2015;54:2131–6.
[357] Liu X, Zhou W, Yang L, Li L, Zhang Z, Ke Y, et al. Nitrogen and sulfur co-doped porous carbon derived from human hair as highly efficient metal-free electrocatalysts for hydrogen evolution reactions. J Mater Chem A 2015;3:8840–6.
[358] Johnson TC, Morris DJ, Wills M. Hydrogen generation from formic acid and alcohols using homogeneous catalysts. Chem Soc Rev 2010;39:81–8.

[359] Zhang Z-W, Li J-C, Jiang Q. Density functional theory calculations of the metal-doped carbon nanostructures as hydrogen storage systems under electric fields: a review. Front Phys 2011;6:162–76.
[360] Ao ZM, Jiang Q, Zhang RQ, Tan TT, Li S. Al doped graphene: a promising material for hydrogen storage at room temperature. J Appl Phys 2009;105:074307.
[361] Liu W, Zhao YH, Li Y, Jiang Q, Lavernia EJ. Enhanced hydrogen storage on li-dispersed carbon nanotubes. J Phys Chem C 2009;113:2028–33.
[362] Liu W, Zhao YH, Nguyen J, Li Y, Jiang Q, Lavernia EJ. Electric field induced reversible switch in hydrogen storage based on single-layer and bilayer graphenes. Carbon 2009;47:3452–60.
[363] Song EH, Yoo SH, Kim JJ, Lai SW, Jiang Q, Cho SO. External electric field induced hydrogen storage/release on calcium-decorated single-layer and bilayer silicene. Phys Chem Chem Phys 2014;16:23985–92.
[364] Zhang Z-W, Zheng W-T, Jiang Q. Hydrogen adsorption on Ce/BNNT systems: a DFT study. Int J Hydrogen Energy 2012;37:5090–9.
[365] Zhang ZW, Zheng WT, Jiang Q. Hydrogen adsorption on Ce/SWCNT systems: a DFT study. Phys Chem Chem Phys 2011;13:9483–9.
[366] Zhang ZW, Li JC, Jiang Q. Hydrogen adsorption on Eu/SWCNT systems: a DFT study. J Phys Chem C 2010;114:7733–7.
[367] Ao Z, Dou S, Xu Z, Jiang Q, Wang G. Hydrogen storage in porous graphene with Al decoration. Int J Hydrogen Energy 2014;39:16244–51.
[368] Ao ZM, Peeters FM. High-capacity hydrogen storage in Al-adsorbed graphene. Phys Rev B 2010;81:205406.
[369] Ao ZM, Tan TT, Li S, Jiang Q. Molecular hydrogen storage in Al-doped bulk graphite with wider layer distances. Solid State Commun 2009;149:1363–7.
[370] Parambhath VB, Nagar R, Sethupathi K, Ramaprabhu S. Investigation of spillover mechanism in palladium decorated hydrogen exfoliated functionalized graphene. J Phys Chem C 2011;115:15679–85.
[371] Ao ZM, Peeters FM. Electric field activated hydrogen dissociative adsorption to nitrogen-doped graphene. J Phys Chem C 2010;114:14503–9.
[372] Wu W, Ao Z, Wang T, Li C, Li S. Electric field induced hydrogenation of silicene. Phys Chem Chem Phys 2014;16:16588–94.
[373] Ao ZM, Hernandez-Nieves AD, Peeters FM, Li S. The electric field as a novel switch for uptake/release of hydrogen for storage in nitrogen doped graphene. Phys Chem Chem Phys 2012;14:1463–7.
[374] Li Z, Xu Q. Metal-nanoparticle-catalyzed hydrogen generation from formic acid. Acc Chem Res 2017;50:1449–58.
[375] Yadav M, Xu Q. Liquid-phase chemical hydrogen storage materials. Energy Environ Sci 2012;5:9698–725.
[376] Wiener H, Sasson Y, Blum J. Palladium-catalyzed decomposition of aqueous alkali-metal formate solutions. J Mol Catal 1986;35:277–84.
[377] Eley DD, Luetic P. The formic acid decomposition on palladium-gold alloys. Trans Faraday Soc 1957;53:1483–7.
[378] Ojeda M, Iglesia E. Formic acid dehydrogenation on Au-based catalysts at near-ambient temperatures. Angew Chem Int Ed 2009;48:4800–3.
[379] Yadav M, Akita T, Tsumori N, Xu Q. Strong metal-molecular support interaction (SMMSI): amine-functionalized gold nanoparticles encapsulated in silica nanospheres highly active for catalytic decomposition of formic acid. J Mater Chem 2012;22:12582–6.
[380] Bi Q-Y, Du X-L, Liu Y-M, Cao Y, He H-Y, Fan K-N. Efficient subnanometric gold-catalyzed hydrogen generation via formic acid decomposition under ambient conditions. J Am Chem Soc 2012;134:8926–33.
[381] Bulushev DA, Zacharska M, Guo Y, Beloshapkin S, Simakov A. CO-free hydrogen production from decomposition of formic acid over Au/Al_2O_3 catalysts doped with potassium ions. Catal Commun 2017;92:86–9.
[382] Jiang K, Xu K, Zou S, Cai W-B. B-doped Pd catalyst: boosting room-temperature hydrogen production from formic acid-formate solutions. J Am Chem Soc 2014;136:4861–4.
[383] Wang Z-L, Yan J-M, Wang H-L, Ping Y, Jiang Q. Pd/C synthesized with citric acid: an efficient catalyst for hydrogen generation from formic acid/sodium formate. Sci Rep 2012;2:598.
[384] Ji X, Lee KT, Holden R, Zhang L, Zhang J, Botton GA, et al. Nanocrystalline intermetallics on mesoporous carbon for direct formic acid fuel cell anodes. Nat Chem 2010;2:286–93.
[385] Zhu Q-L, Tsumori N, Xu Q. Sodium hydroxide-assisted growth of uniform Pd nanoparticles on nanoporous carbon MSC-30 for efficient and complete dehydrogenation of formic acid under ambient conditions. Chem Sci 2014;5:195–9.
[386] Lee JH, Ryu J, Kim JY, Nam S-W, Han JH, Lim T-H, et al. Carbon dioxide mediated, reversible chemical hydrogen storage using a Pd nanocatalyst supported on mesoporous graphitic carbon nitride. J Mater Chem A 2014;2:9490–5.
[387] Song F-Z, Zhu Q-L, Tsumori N, Xu Q. Diamine-alkalized reduced graphene oxide: immobilization of Sub-2 nm palladium nanoparticles and optimization of catalytic activity for dehydrogenation of formic acid. ACS Catal 2015;5:5141–4.
[388] Bi Q-Y, Lin J-D, Liu Y-M, He H-Y, Huang F-Q, Cao Y. Dehydrogenation of formic acid at room temperature: boosting palladium nanoparticle efficiency by coupling with pyridinic-nitrogen-doped carbon. Angew Chem Int Ed 2016;55:11849–53.
[389] Wang Z-L, Yan J-M, Zhang Y-F, Ping Y, Wang H-L, Jiang Q. Facile synthesis of nitrogen-doped graphene supported AuPd-CeO_2 nanocomposites with high-performance for hydrogen generation from formic acid at room temperature. Nanoscale 2014;6:3073–7.
[390] Wang Z-L, Yan J-M, Wang H-L, Ping Y, Jiang Q. Au@Pd core-shell nanoclusters growing on nitrogen-doped mildly reduced graphene oxide with enhanced catalytic performance for hydrogen generation from formic acid. J Mater Chem A 2013;1:12721–5.
[391] Ping Y, Yan J-M, Wang Z-L, Wang H-L, Jiang Q. $Ag_{0.1}Pd_{0.9}$/rGO: an efficient catalyst for hydrogen generation from formic acid/sodium formate. J Mater Chem A 2013;1:12188–91.
[392] Mori K, Dojo M, Yamashita H. Pd and Pd-Ag nanoparticles within a macroreticular basic resin: an efficient catalyst for hydrogen production from formic acid decomposition. ACS Catal 2013;3:1114–9.
[393] Zhang S, Metin O, Su D, Sun S. Monodisperse AgPd alloy nanoparticles and their superior catalysis for the dehydrogenation of formic acid. Angew Chem Int Ed 2013;52:3681–4.
[394] Ting S-W, Cheng S, Tsang K-Y, van der Laak N, Chan K-Y. Low activation energy dehydrogenation of aqueous formic acid on platinum-ruthenium-bismuth oxide at near ambient temperature and pressure. Chem Commun 2009:7333–5.
[395] Huang Y, Zhou X, Yin M, Liu C, Xing W. Novel PdAu@Au/C core-shell catalyst: superior activity and selectivity in formic acid decomposition for hydrogen generation. Chem Mater 2010;22:5122–8.
[396] Li S-j, Ping Y, Yan J-M, Wang H-L, Wu M, Jiang Q. Facile synthesis of AgAuPd/graphene with high performance for hydrogen generation from formic acid. J Mater Chem A 2015;3:14535–8.
[397] Yurderi M, Bulut A, Caner N, Celebi M, Kaya M, Zahmakiran M. Amine grafted silica supported CrAuPd alloy nanoparticles: superb heterogeneous catalysts for the room temperature dehydrogenation of formic acid. Chem Commun 2015;51:11417–20.
[398] Zhou X, Huang Y, Xing W, Liu C, Liao J, Lu T. High-quality hydrogen from the catalyzed decomposition of formic acid by Pd-Au/C and Pd-Ag/C. Chem Commun 2008:3540–2.
[399] Zhou X, Huang Y, Liu C, Liao J, Lu T, Xing W. Available hydrogen from formic acid decomposed by rare earth elements promoted Pd-Au/C catalysts at low temperature. ChemSusChem 2010;3:1379–82.
[400] Jiang H-L, Xu Q. Porous metal-organic frameworks as platforms for functional applications. Chem Commun 2011;47:3351–70.
[401] Yan J-M, Wang Z-L, Gu L, Li S-J, Wang H-L, Zheng W-T, et al. AuPd-MnO_x/MOF-graphene: an efficient catalyst for hydrogen production from formic acid at room temperature. Adv Energy Mater 2015;5:1500107.
[402] Dai H, Cao N, Yang L, Su J, Luo W, Cheng G. AgPd nanoparticles supported on MIL-101 as high performance catalysts for catalytic dehydrogenation of formic acid. J Mater Chem A 2014;2:11060–4.
[403] Martis M, Mori K, Fujiwara K, Ahn W-S, Yamashita H. Amine-functionalized MIL-125 with imbedded palladium nanoparticles as an efficient catalyst for dehydrogenation of formic acid at ambient temperature. J Phys Chem C 2013;117:22805–10.
[404] Gu X, Lu Z-H, Jiang H-L, Akita T, Xu Q. Synergistic catalysis of metal-organic framework-immobilized Au-Pd nanoparticles in dehydrogenation of formic acid for chemical hydrogen storage. J Am Chem Soc 2011;133:11822–5.
[405] Cheng J, Gu X, Sheng X, Liu P, Su H. Exceptional size-dependent catalytic activity enhancement in the room-temperature hydrogen generation from formic acid over bimetallic nanoparticles supported by porous carbon. J Mater Chem A 2016;4:1887–94.

[406] Qin Y-L, Wang J, Meng F-Z, Wang L-M, Zhang X-B. Efficient PdNi and PdNi@Pd-catalyzed hydrogen generation via formic acid decomposition at room temperature. Chem Commun 2013;49:10028–30.
[407] Chen Y, Zhu Q-L, Tsumori N, Xu Q. Immobilizing highly catalytically active noble metal nanoparticles on reduced graphene oxide: a non-noble metal sacrificial approach. J Am Chem Soc 2015;137:106–9.
[408] Wang Z-L, Wang H-L, Yan J-M, Ping Y, O S-I, Li S-J, et al. DNA-directed growth of ultrafine CoAuPd nanoparticles on graphene as efficient catalysts for formic acid dehydrogenation. Chem Commun 2014;50:2732–4.
[409] Wang Z-L, Yan J-M, Ping Y, Wang H-L, Zheng W-T, Jiang Q. An efficient CoAuPd/C catalyst for hydrogen generation from formic acid at room temperature. Angew Chem Int Ed 2013;52:4406–9.
[410] Zhu DD, Liu JL, Qiao SZ. Recent advances in inorganic heterogeneous electrocatalysts for reduction of carbon dioxide. Adv Mater 2016;28:3423–52.
[411] Qiao J, Liu Y, Hong F, Zhang J. A review of catalysts for the electroreduction of carbon dioxide to produce low-carbon fuels. Chem Soc Rev 2014;43:631–75.
[412] Hori Y, Wakebe H, Tsukamoto T, Koga O. Electrocatalytic process of CO selectivity in electrochemical reduction of CO_2 at metal electrodes in aqueous media. Electrochim Acta 1994;39:1833–9.
[413] Li Y, Sun Q. Recent advances in breaking scaling relations for effective electrochemical conversion of CO_2. Adv Energy Mater 2016;6:1600463.
[414] Kapusta S, Hackerman N. The electroreduction of carbon dioxide and formic acid on tin and indium electrodes. J Electrochem Soc 1983;130:607–13.
[415] Zhao C, Wang J. Electrochemical reduction of CO_2 to formate in aqueous solution using electro-deposited Sn catalysts. Chem Eng J 2016;293:161–70.
[416] Scialdone O, Galia A, Lo Nero G, Proietto F, Sabatino S, Schiavo B. Electrochemical reduction of carbon dioxide to formic acid at a tin cathode in divided and undivided cells: effect of carbon dioxide pressure and other operating parameters. Electrochim Acta 2016;199:332–41.
[417] Wu J, Sharma PP, Harris BH, Zhou X-D. Electrochemical reduction of carbon dioxide: IV dependence of the Faradaic efficiency and current density on the microstructure and thickness of tin electrode. J Power Sources 2014;258:189–94.
[418] Bumroongsakulsawat P, Kelsall GH. Effect of solution pH on CO: formate formation rates during electrochemical reduction of aqueous CO_2 at Sn cathodes. Electrochim Acta 2014;141:216–25.
[419] Lv W, Zhang R, Gao P, Lei L. Studies on the faradaic efficiency for electrochemical reduction of carbon dioxide to formate on tin electrode. J Power Sources 2014;253:276–81.
[420] Anawati, Frankel GS, Agarwal A, Sridhar N. Degradation and deactivation of Sn catalyst used for CO_2 reduction as function of overpotential. Electrochim Acta 2014;133:188–96.
[421] Wu J, Risalvato FG, Ke F-S, Pellechia PJ, Zhou X-D. Electrochemical reduction of carbon dioxide I. effects of the electrolyte on the selectivity and activity with Sn electrode. J Electrochem Soc 2012;159:F353–9.
[422] Irtem E, Andreu T, Parra A, Hernandez-Alonso MD, Garcia-Rodriguez S, Riesco-Garcia JM, et al. Low-energy formate production from CO_2 electroreduction using electrodeposited tin on GDE. J Mater Chem A 2016;4:13582–8.
[423] Kopljar D, Inan A, Vindayer P, Wagner N, Klemm E. Electrochemical reduction of CO_2 to formate at high current density using gas diffusion electrodes. J Appl Electrochem 2014;44:1107–16.
[424] Lei F, Liu W, Sun Y, Xu J, Liu K, Liang L, et al. Metallic tin quantum sheets confined in graphene toward high-efficiency carbon dioxide electroreduction. Nat Commun 2016;7:12697.
[425] Chen Y, Kanan MW. Tin oxide dependence of the CO_2 reduction efficiency on tin electrodes and enhanced activity for tin/tin oxide thin-film catalysts. J Am Chem Soc 2012;134:1986–9.
[426] Quan F, Zhong D, Song H, Jia F, Zhang L. A highly efficient zinc catalyst for selective electroreduction of carbon dioxide in aqueous NaCl solution. J Mater Chem A 2015;3:16409–13.
[427] Wu J, Risalvato FG, Ma S, Zhou X-D. Electrochemical reduction of carbon dioxide III. the role of oxide layer thickness on the performance of Sn electrode in a full electrochemical cell. J Mater Chem A 2014;2:1647–51.
[428] Baruch MF, Pander III JE, White JL, Bocarsly AB. Mechanistic insights into the reduction of CO_2 on tin electrodes using in situ ATR-IR spectroscopy. ACS Catal 2015;5:3148–56.
[429] Dutta A, Kuzume A, Rahaman M, Vesztergom S, Broekmann P. Monitoring the chemical state of catalysts for CO_2 electroreduction: an in operando study. ACS Catal 2015;5:7498–502.
[430] Luc W, Collins C, Wang S, Xin H, He K, Kang Y, et al. Ag-Sn bimetallic catalyst with a core-shell structure for CO_2 reduction. J Am Chem Soc 2017;139:1885–93.
[431] Li F, Chen L, Xue M, Williams T, Zhang Y, MacFarlane DR, et al. Towards a better Sn: efficient electrocatalytic reduction of CO_2 to formate by Sn/SnS_2 derived from SnS_2 nanosheets. Nano Energy 2017;31:270–7.
[432] Zhang S, Kang P, Meyer TJ. Nanostructured tin catalysts for selective electrochemical reduction of carbon dioxide to formate. J Am Chem Soc 2014;136:1734–7.
[433] Li F, Chen L, Knowles GP, MacFarlane DR, Zhang J. Hierarchical mesoporous SnO_2 nanosheets on carbon cloth: a robust and flexible electrocatalyst for CO_2 reduction with high efficiency and selectivity. Angew Chem Int Ed 2016;56:505–9.
[434] Kumar Bijandra, Atla Veerendra, Sudesh K, Quang NT, Sunkara M, et al. Reduced SnO_2 porous nanowires with a high density of grain boundaries as catalysts for efficient electrochemical CO_2-into HCOOH conversion. Angew Chem Int Ed 2017;56:3645–9.
[435] Gao S, Jiao X, Sun Z, Zhang W, Sun Y, Wang C, et al. Ultrathin Co_3O_4 layers realizing optimized CO_2 electroreduction to formate. Angew Chem Int Ed 2016;55:698–702.
[436] Gao S, Sun Z, Liu W, Jiao X, Zu X, Hu Q, et al. Atomic layer confined vacancies for atomic-level insights into carbon dioxide electroreduction. Nat Commun 2017;8:14503.
[437] Gao S, Lin Y, Jiao X, Sun Y, Luo Q, Zhang W, et al. Partially oxidized atomic cobalt layers for carbon dioxide electroreduction to liquid fuel. Nature 2016;529:68–71.
[438] Stalder CJ, Chao S, Wrighton MS. Electrochemical reduction of aqueous bicarbonate to formate with high-current efficiency near the thermodynamic potential at chemically derivatized electrodes. J Am Chem Soc 1984;106:3673–5.
[439] Min X, Kanan MW. Pd-catalyzed electrohydrogenation of carbon dioxide to formate: high mass activity at low overpotential and identification of the deactivation pathway. J Am Chem Soc 2015;137:4701–8.
[440] Klinkova Anna, Luna P De, Dinh Cao-Thang, Voznyy Oleksandr, Larin EM, Kumacheva E, et al. Rational design of efficient palladium catalysts for electroreduction of carbon dioxide to formate. ACS Catal 2016;6:8115–20.
[441] Zhang TT, Zhong HX, Qiu YL, Li XF, Zhang HM. Zn electrode with a layer of nanoparticles for selective electroreduction of CO_2 to formate in aqueous solutions. J Mater Chem A 2016;4:16670–6.
[442] Weng Z, Jiang J, Wu Y, Wu Z, Guo X, Materna KL, et al. Electrochemical CO_2 reduction to hydrocarbons on a heterogeneous molecular Cu catalyst in aqueous solution. J Am Chem Soc 2016;138:8076–9.
[443] Li CW, Kanan MW. CO_2 reduction at low overpotential on Cu electrodes resulting from the reduction of thick Cu_2O films. J Am Chem Soc 2012;134:7231–4.
[444] Kas R, Hummadi KK, Kortlever R, de Wit P, Milbrat A, Luiten-Olieman MWJ, et al. Three-dimensional porous hollow fibre copper electrodes for efficient and high-rate electrochemical carbon dioxide reduction. Nat Commun 2016;7:10748.
[445] Subramanian K, Asokan K, Jeevarathinam D, Chandrasekaran M. Electrochemical membrane reactor for the reduction of carbon dioxide to formate. J Appl Electrochem 2007;37:255–60.
[446] Koleli F, Atilan T, Palamut N, Gizir AM, Aydin R, Hamann CH. Electrochemical reduction of CO_2 at Pb- and Sn-electrodes in a fixed-bed reactor in aqueous K_2CO_3 and $KHCO_3$ media. J Appl Electrochem 2003;33:447–50.

[447] Sekimoto T, Deguchi M, Yotsuhashi S, Yamada Y, Masui T, Kuramata A, et al. Highly selective electrochemical reduction of CO_2 to HCOOH on a gallium oxide cathode. Electrochem Commun 2014;43:95–7.
[448] Chai G-L, Guo Z-X. Highly effective sites and selectivity of nitrogen-doped graphene/CNT catalysts for CO_2 electrochemical reduction. Chem Sci 2016;7:1268–75.
[449] Wu J, Ma S, Sun J, Gold JI, Tiwary C, Kim B, et al. A metal-free electrocatalyst for carbon dioxide reduction to multi-carbon hydrocarbons and oxygenates. Nat Commun 2016;7:13869.
[450] Zhang S, Kang P, Ubnoske S, Brennaman MK, Song N, House RL, et al. Polyethylenimine-enhanced electrocatalytic reduction of CO_2 to formate at nitrogen-doped carbon nanomaterials. J Am Chem Soc 2014;136:7845–8.
[451] Wang H, Chen Y, Hou X, Ma C, Tan T. Nitrogen-doped graphenes as efficient electrocatalysts for the selective reduction of carbon dioxide to formate in aqueous solution. Green Chem 2016;18:3250–6.
[452] Christensen CH, Johannessen T, Sorensen RZ, Norskov JK. Towards an ammonia-mediated hydrogen economy? Catal Today 2006;111:140–4.
[453] Honkala K, Hellman A, Remediakis IN, Logadottir A, Carlsson A, Dahl S, et al. Ammonia synthesis from first-principles calculations. Science 2005;307:555–8.
[454] Furuya N, Yoshiba H. Electroreduction of nitrogen to ammonia on gas-diffusion electrodes modified by metal phthalocyanines. J Electroanal Chem 1989;272:263–6.
[455] Studt F, Tuczek F. Energetics and mechanism of a room-temperature catalytic process for ammonia synthesis (Schrock cycle): comparison with biological nitrogen fixation. Angew Chem Int Ed 2005;44:5639–42.
[456] Yandulov DV, Schrock RR. Catalytic reduction of dinitrogen to ammonia at a single molybdenum center. Science 2003;301:76–8.
[457] Zhang SY, Zhang XY, Zhang ZS, Kong Y, Hua SN. Electroreduction behavior of dinitrogen over ruthenium cathodic catalyst. Chem Lett 2003;32:440–1.
[458] Bao D, Zhang Q, Meng F-L, Zhong H-X, Shi M-M, Zhang Y, et al. Electrochemical reduction of N_2 under ambient conditions for artificial N_2 fixation and renewable energy storage using N_2/NH_3 cycle. Adv Mater 2017;29:1604799.
[459] Li S-J, Bao D, Shi M-M, Wulan B-R, Yan J-M, Jiang Q. Amorphizing of Au nanoparticles by CeO_x-RGO hybrid support towards highly efficient electrocatalyst for N_2 reduction under ambient conditions. Adv Mater 2017;29:1700001.
[460] Shi M-M, Bao D, Wulan B-R, Li Y-H, Zhang Y-F, Yan J-M, et al. Au sub-nanoclusters on TiO_2 toward highly efficient and selective electrocatalyst for N_2 conversion to NH_3 at ambient conditions. Adv Mater 2017;29:1606550.
[461] Wang Y, Gong XG. First-principles study of interaction of cluster Au_{32} with CO, H_2, and O_2. J Chem Phys 2006;125:124703.
[462] Chen S, Perathoner S, Ampelli C, Mebrahtu C, Su D, Centi G. Electrocatalytic synthesis of ammonia at room temperature and atmospheric pressure from water and nitrogen on a carbon-nanotube-based electrocatalyst. Angew Chem Int Ed 2017;56:2699–703.
[463] Chen Shiming, Perathoner Siglinda, Ampelli Claudio, Mebrahtu Chalachew, Su Dangsheng, Centi Gabriele. Room-temperature electrocatalytic synthesis of NH_3 from H_2O and N_2 in a gas-liquid-solid three-phase reactor. ACS Sustainable Chem Eng 2017;5:7393–400.
[464] Chen GF, Cao X, Wu S, Zeng X, Ding LX, Zhu M, et al. Ammonia electrosynthesis with high selectivity under ambient conditions via a Li^+ incorporation strategy. J Am Chem Soc 2017;139:9771–4.
[465] Licht S, Cui B, Wang B, Li F-F, Lau J, Liu S. Ammonia synthesis by N_2 and steam electrolysis in molten hydroxide suspensions of nanoscale Fe_2O_3. Science 2014;345:637–40.
[466] Murakami T, Nishikiori T, Nohira T, Ito Y. Electrolytic synthesis of ammonia in molten salts under atmospheric pressure. J Am Chem Soc 2003;125:334–5.
[467] Marnellos G, Stoukides M. Ammonia synthesis at atmospheric pressure. Science 1998;282:98–100.
[468] Ma J-L, Bao D, Shi M-M, Yan J-M, Zhang X-B. Reversible nitrogen fixation based on a rechargeable lithium-nitrogen battery for energy storage. Chem 2017;2:525–32.